Transformative Science and Engineering for Nuclear Decommissioning

Radiation effects on nuclear waste forms:
How does the crystallinity of glass composite affect radiation tolerance?

Tamás Zagyva – The University of Manchester, Dalton Cumbrian Facility

Theme 1 Integrated Waste Management

2nd November 2022
Glasgow

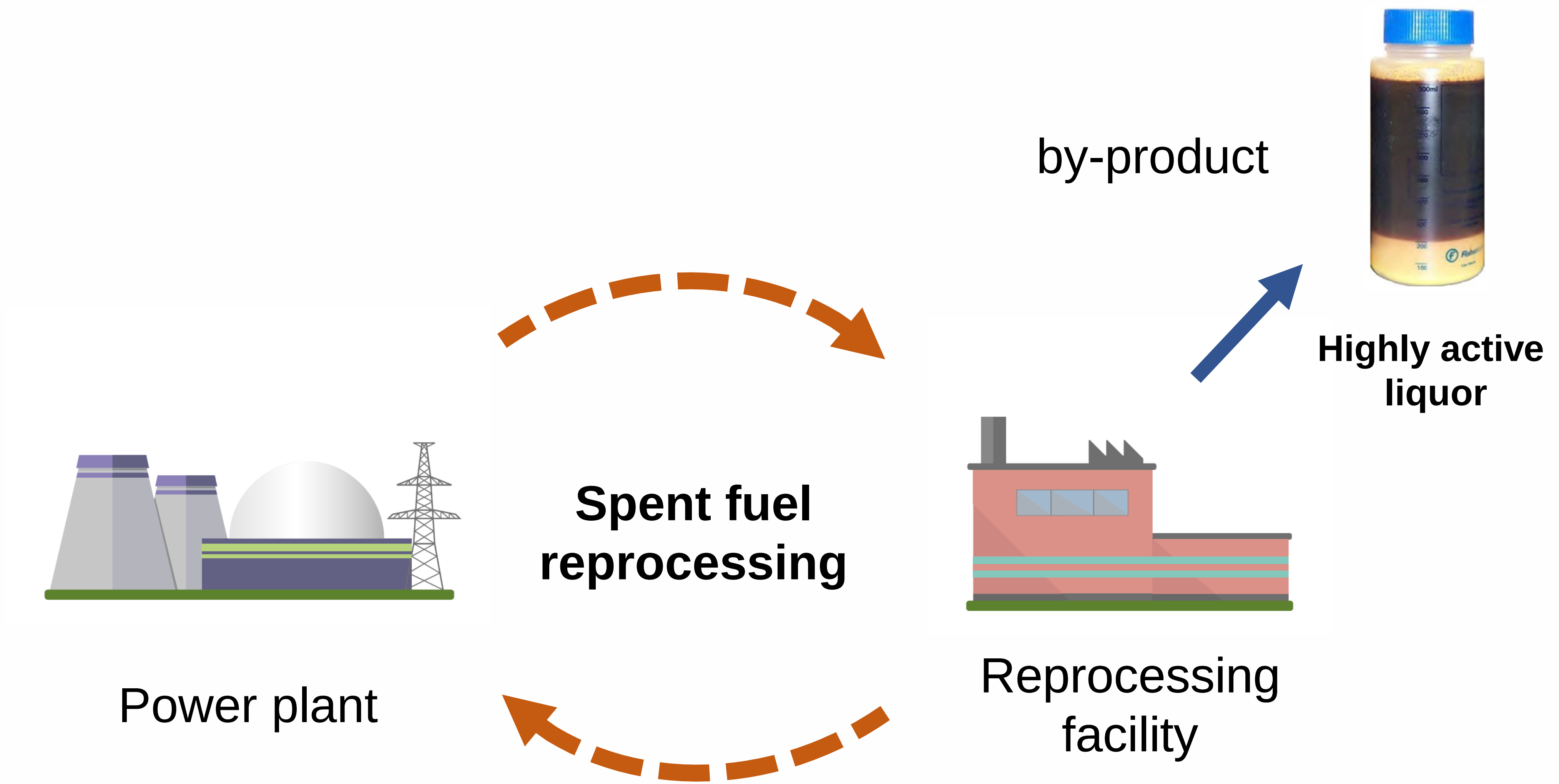
by-product
Highly active liquor
Spent fuel reprocessing
Power plant
Reprocessing facility

Highly active liquor (HAL)

Vitrification

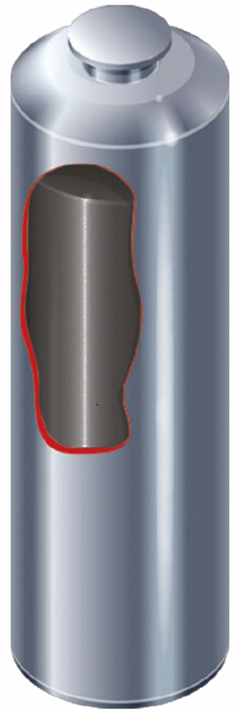

Solid glass wasteform

HAL with high Mo content

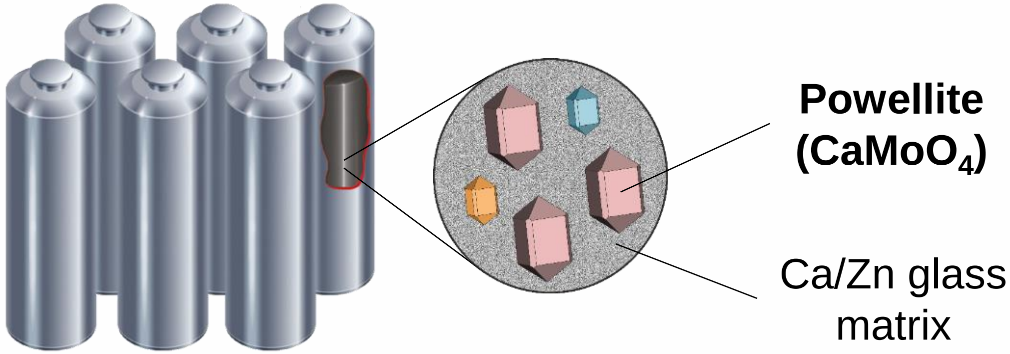

Glass composite high-level waste

Goal of research: evaluate the radiation tolerance of HLW glass composite materials with high Mo content.

α–radiation, β–radiation, γ–radiation

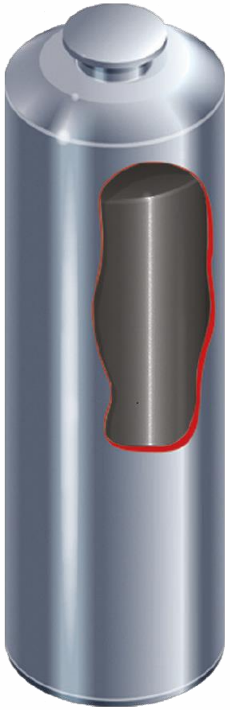

HLW
glass composite

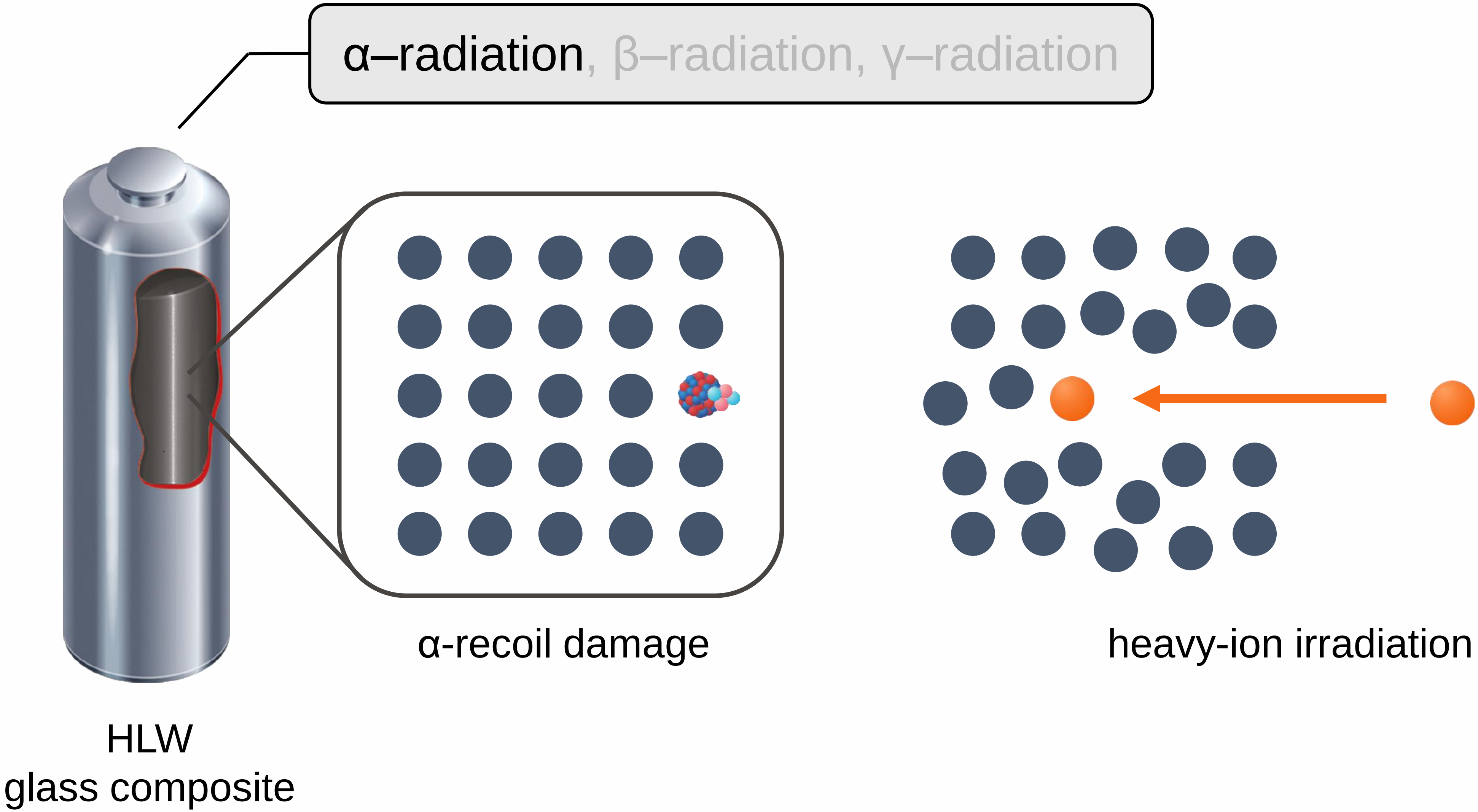
α–radiation, β–radiation, γ–radiation
α-recoil damage
heavy-ion irradiation
HLW
glass composite

Nuclear waste simulant glass composite

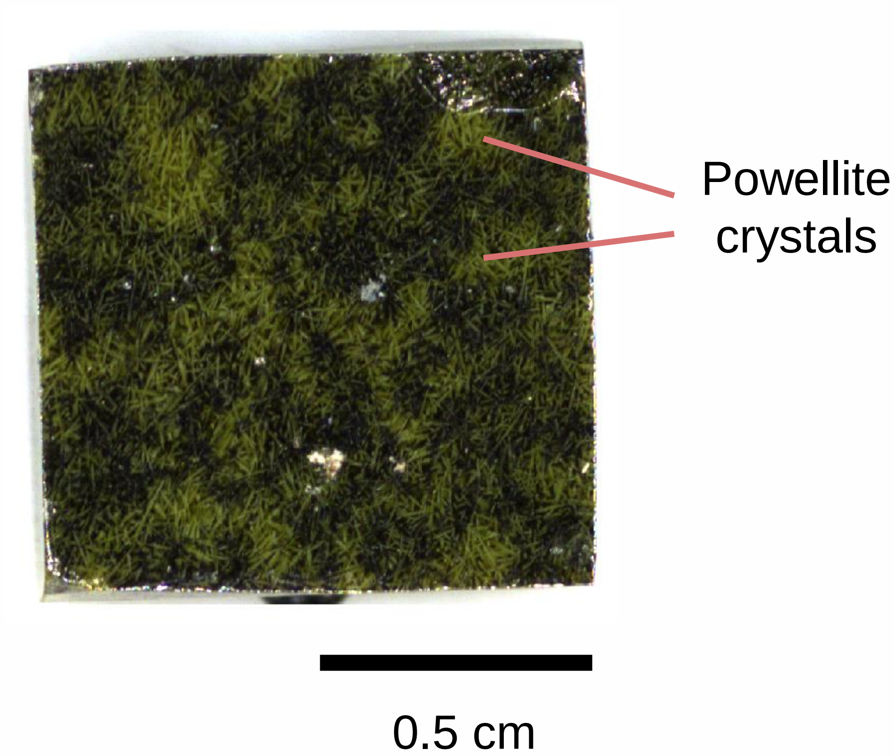

Heavy-ion irradiation experiments

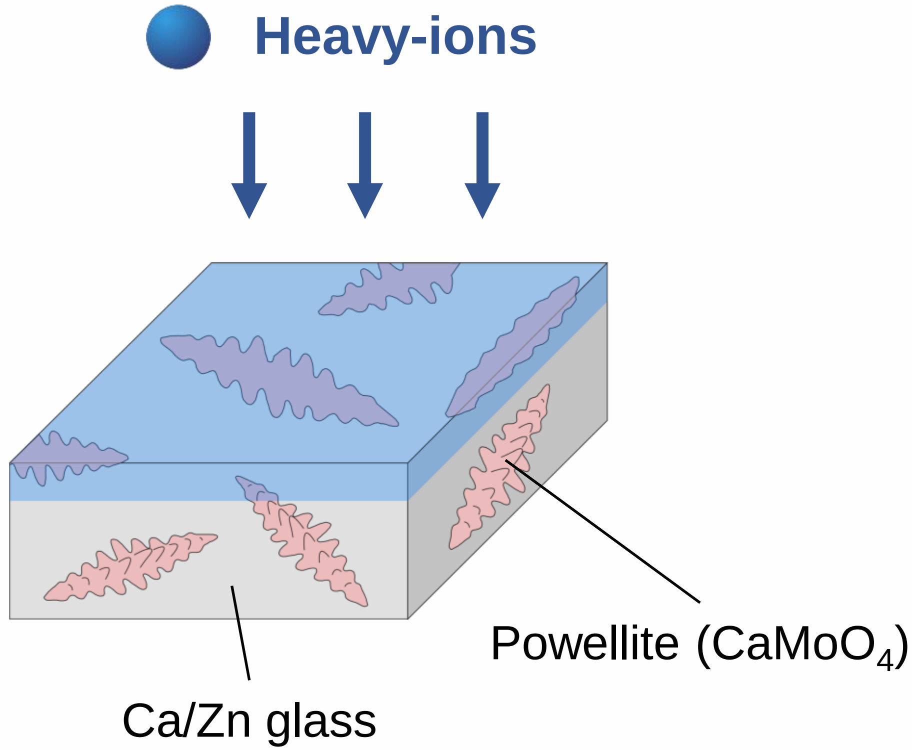

Characterisation of glass composite samples

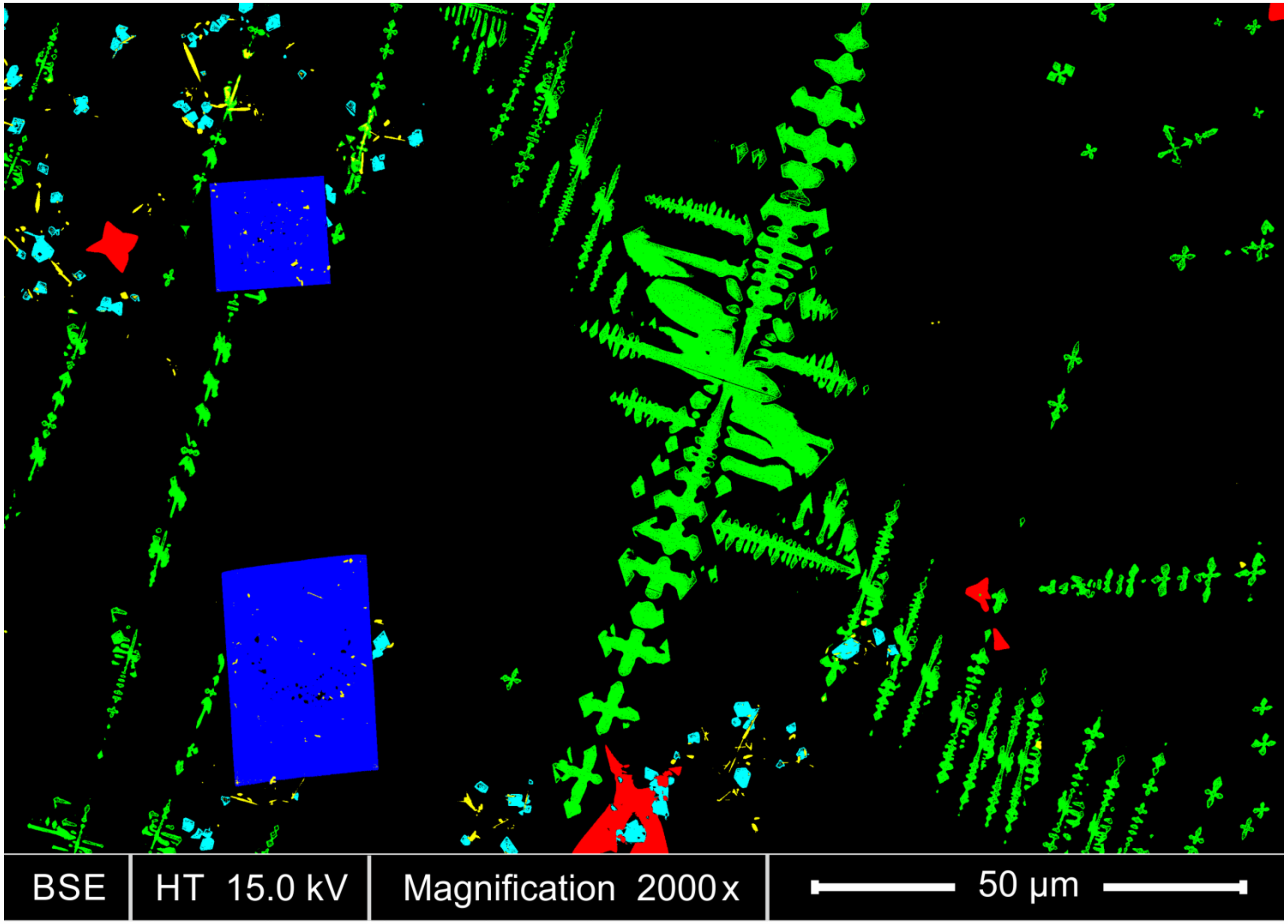

powellite

zircon

cerianite

zincochromite

ruthenium dioxide

crystallinity: 16%

Heavy ion irradiation experiments

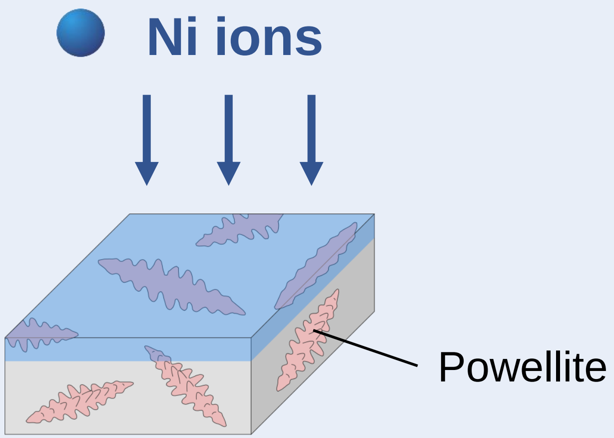

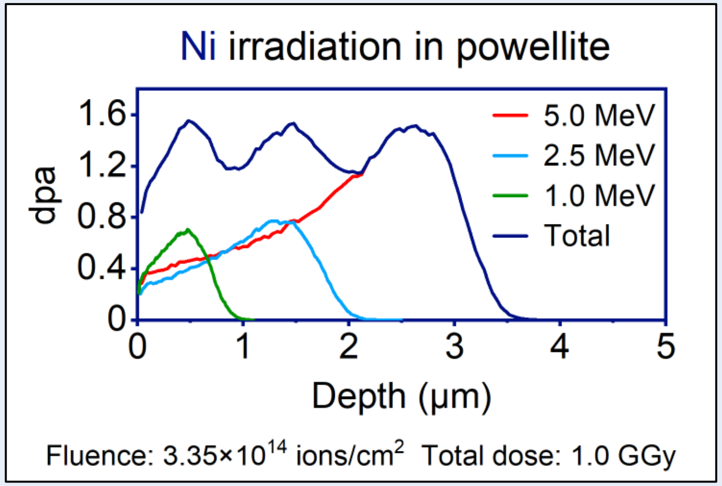

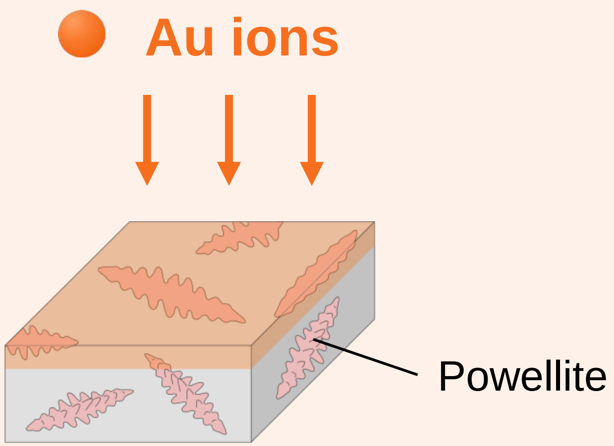

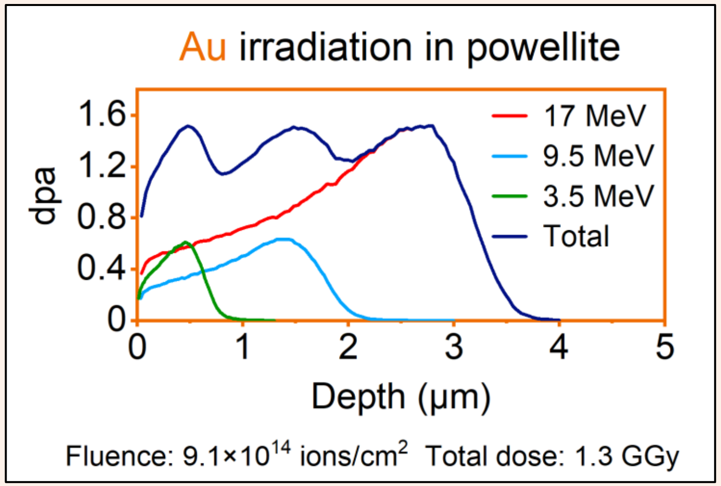

Heavy ion irradiation experiments

BEFORE Au irradiation **AFTER Au irradiation**

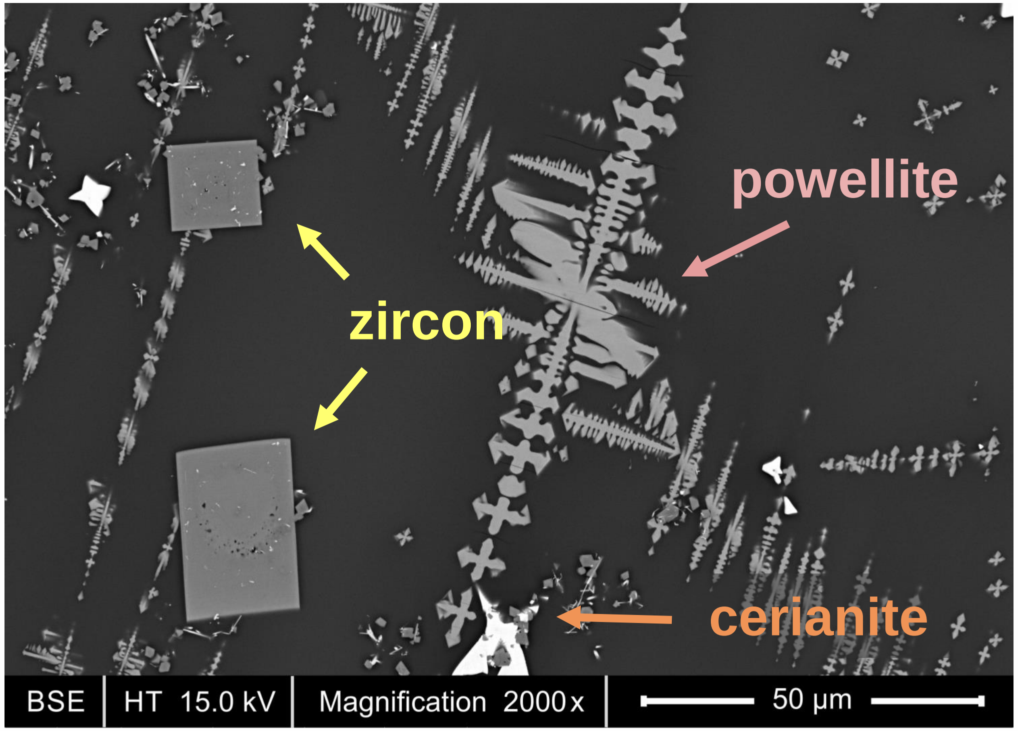

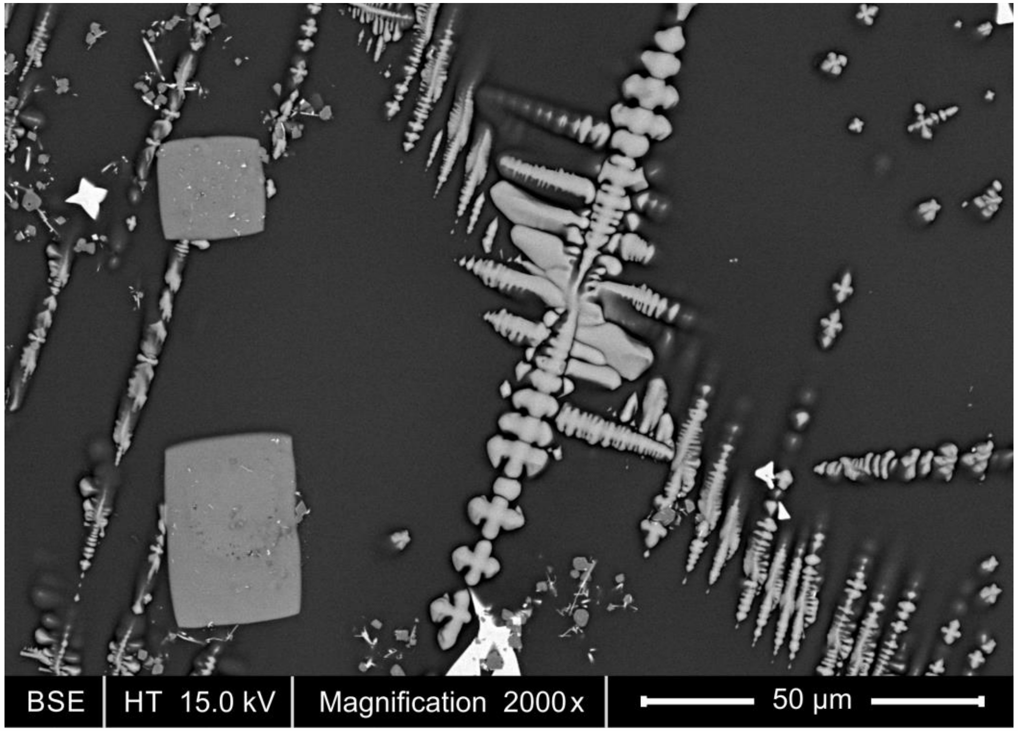

powellite and zircon – swelling

cerianite – no change

Heavy ion irradiation experiments

EBSD analysis

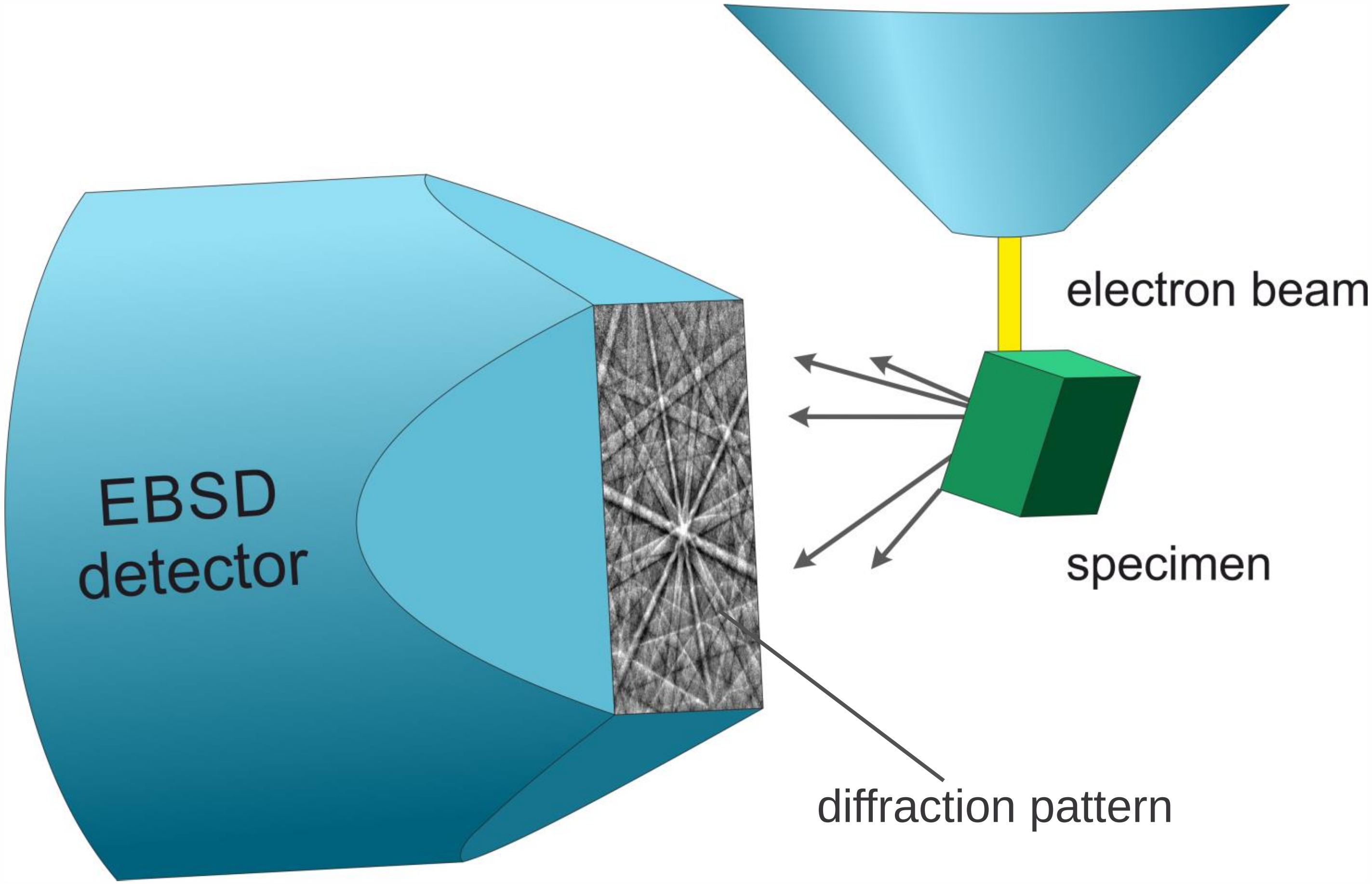

Heavy ion irradiation experiments

EBSD analysis

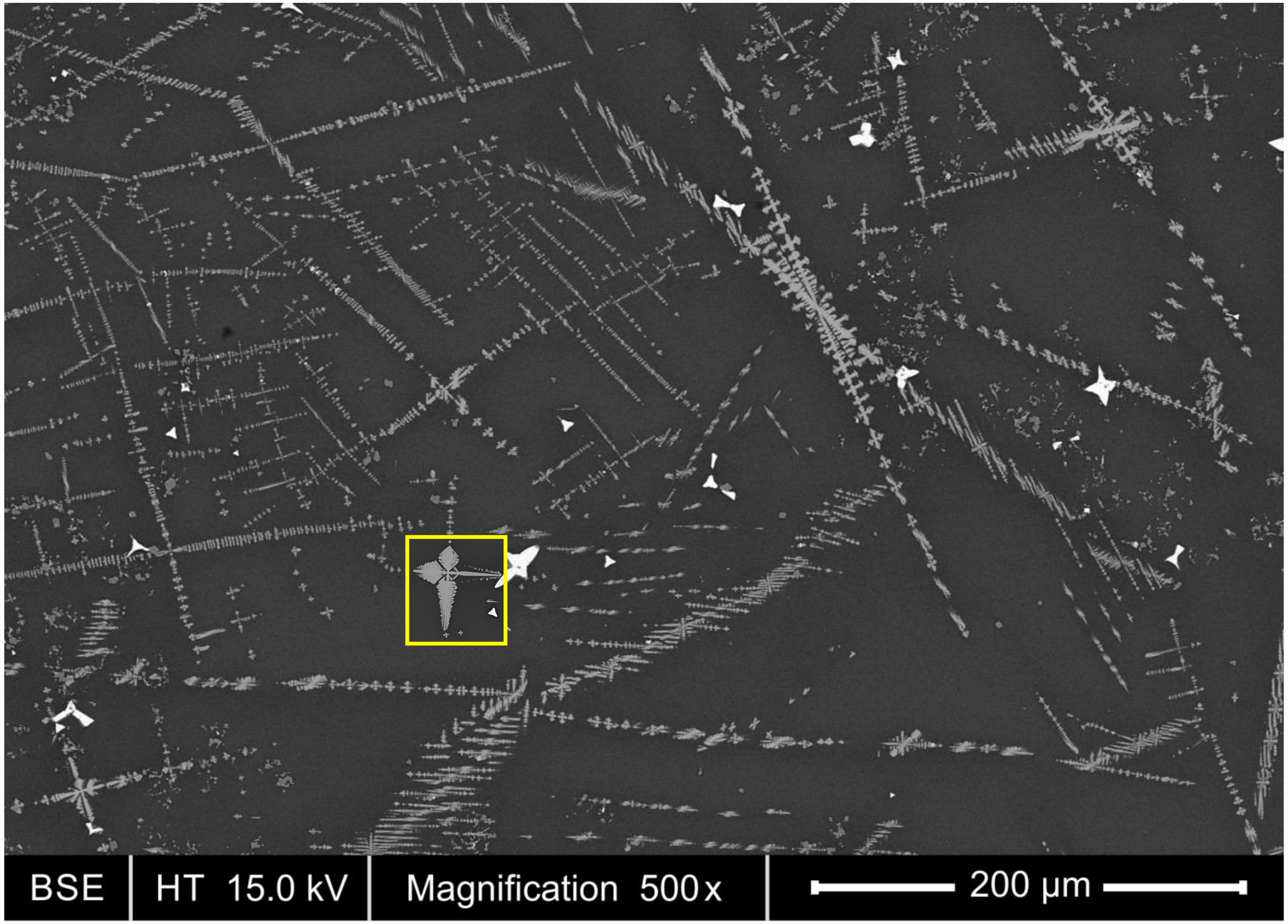

Heavy ion irradiation experiments

EBSD analysis

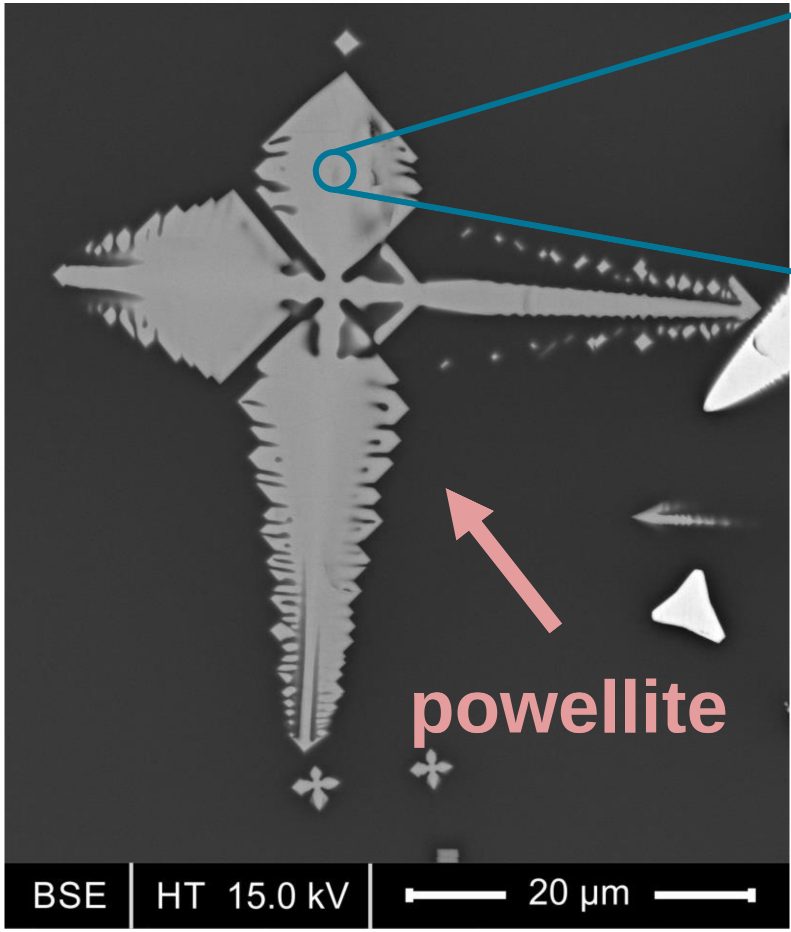

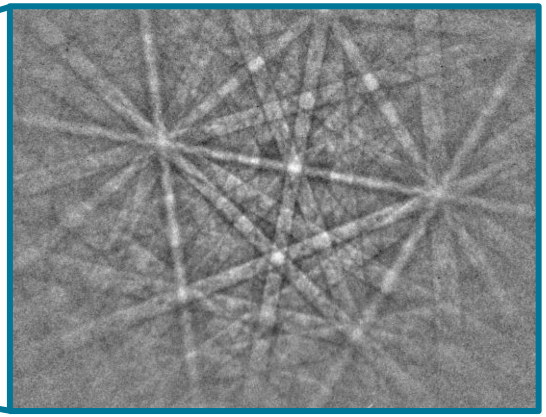

Before **Ni** irradiation

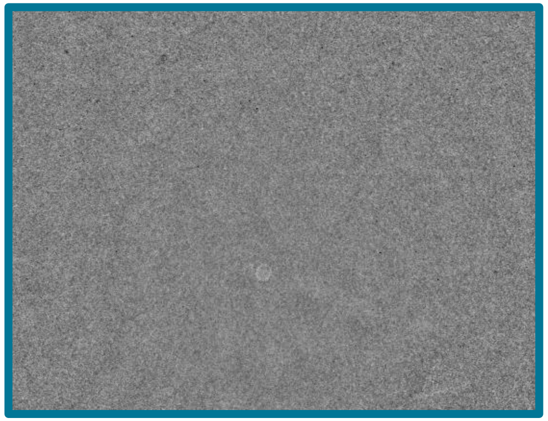

After **Ni** irradiation

Heavy ion irradiation experiments – Ni

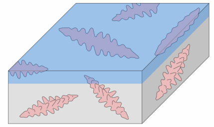

cerianite | zincochromite | ruthenium dioxide | powellite | zircon

before Ni irradiation

after Ni irradiation

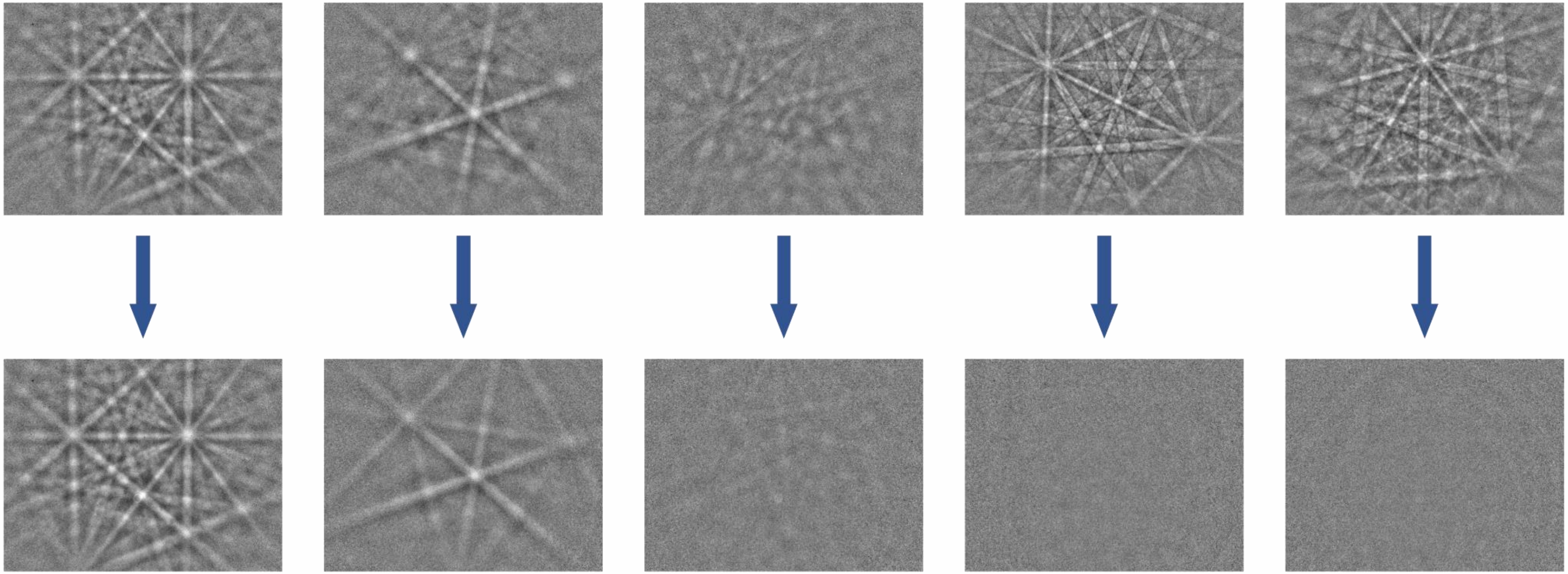

no change | partial amorphisation | complete amorphisation

Heavy ion irradiation experiments – Au

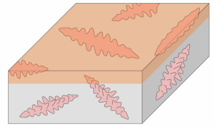

cerianite | zincochromite | ruthenium dioxide | powellite | zircon

before Au irradiation

after Au irradiation

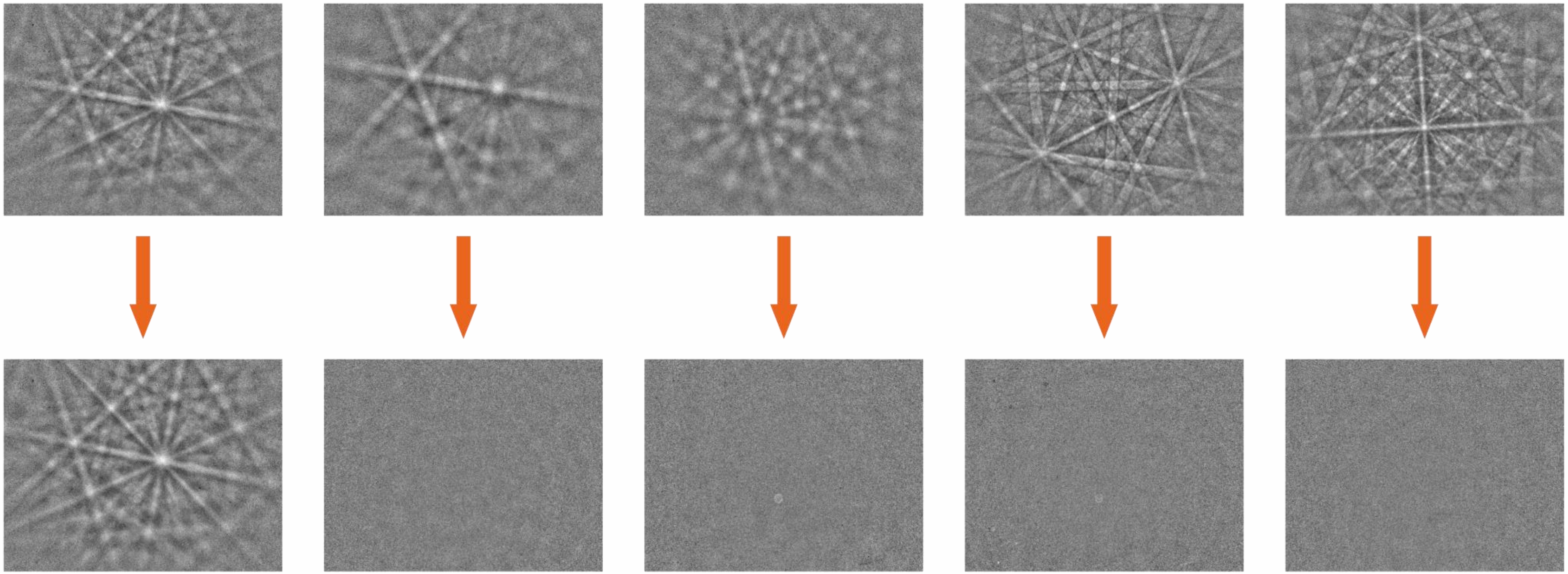

no change | **complete amorphisation** | **complete amorphisation**

Heavy ion irradiation experiments – Ni & Au

GIXRD: incident angle = 1.8°

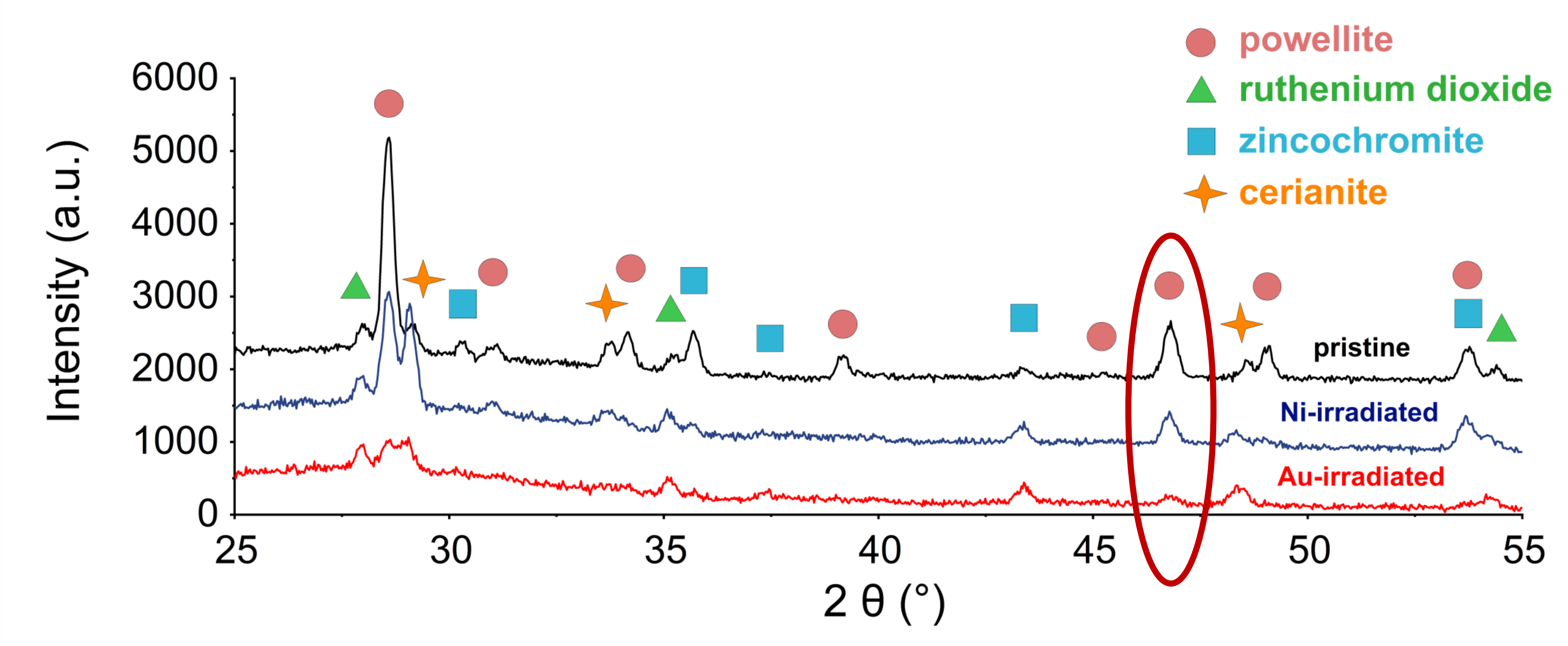

Summary (1)

- relative radiation tolerance of crystals:

high
cerianite
zincochromite ≈ ruthenium dioxide
powellite ≈ zircon
low

- amorphised crystals swelled considerably
- **First evidence of powellite ($CaMoO_4$) amorphisation!**

→ TEM analysis with *in situ* **Ar** and **Xe** ion irradiation

TEM with in situ Ar and Xe ion irradiation

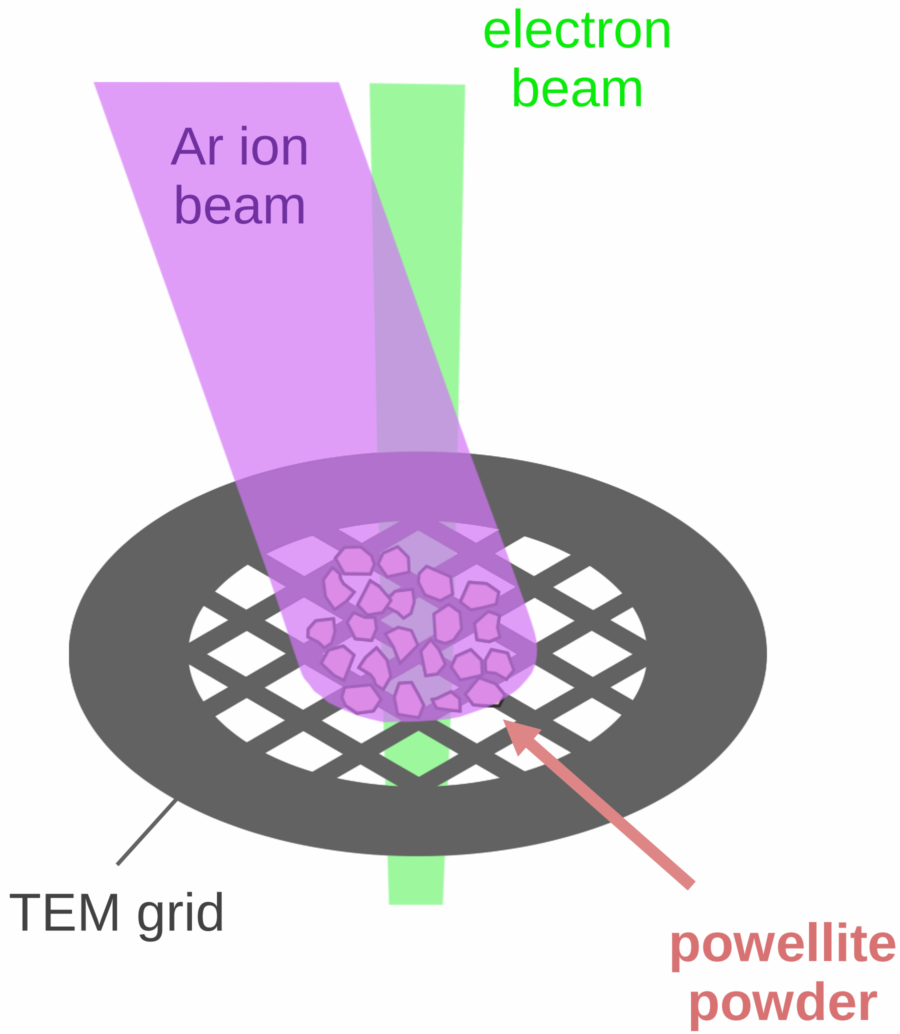

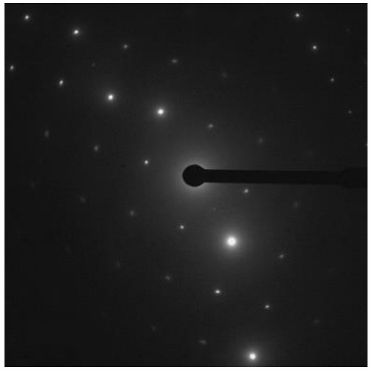

crystalline powellite
before irradiation

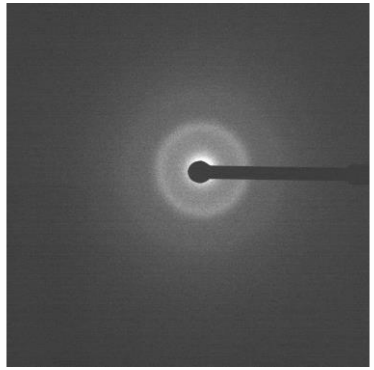

amorphous powellite
after irradiation

TEM with in situ Ar and Xe ion irradiation

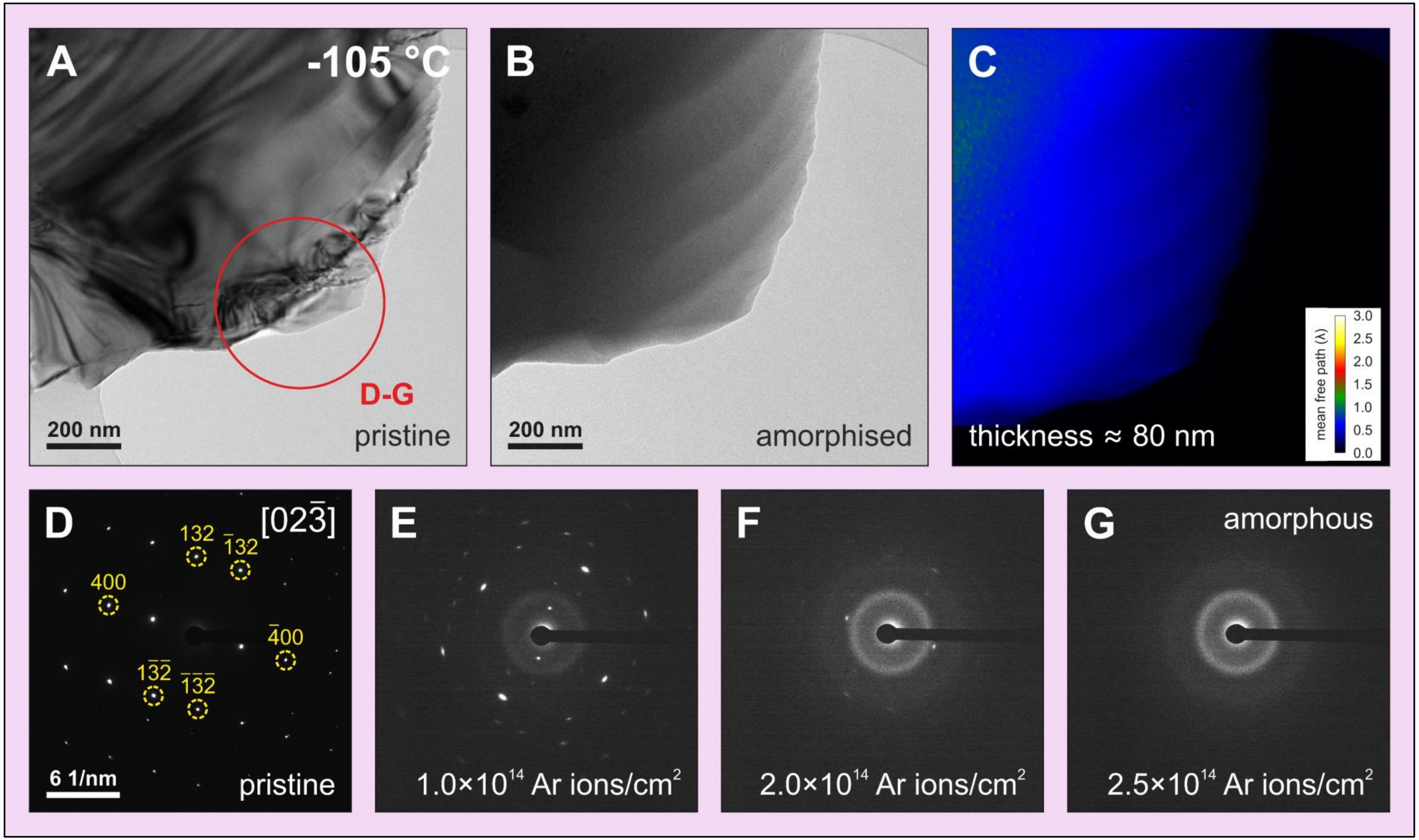

TEM with in situ Ar and Xe ion irradiation

Critical amorphisation doses in powellite

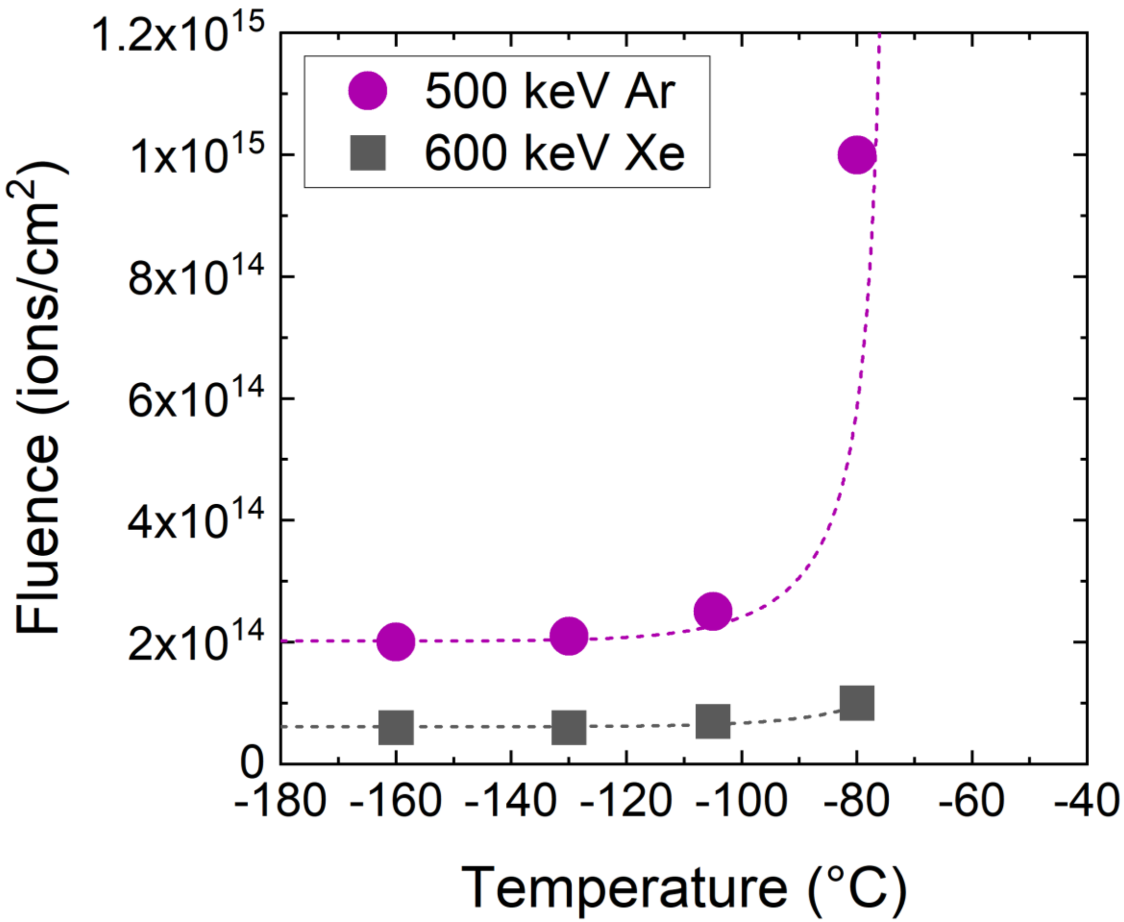

TEM with in situ Ar and Xe ion irradiation

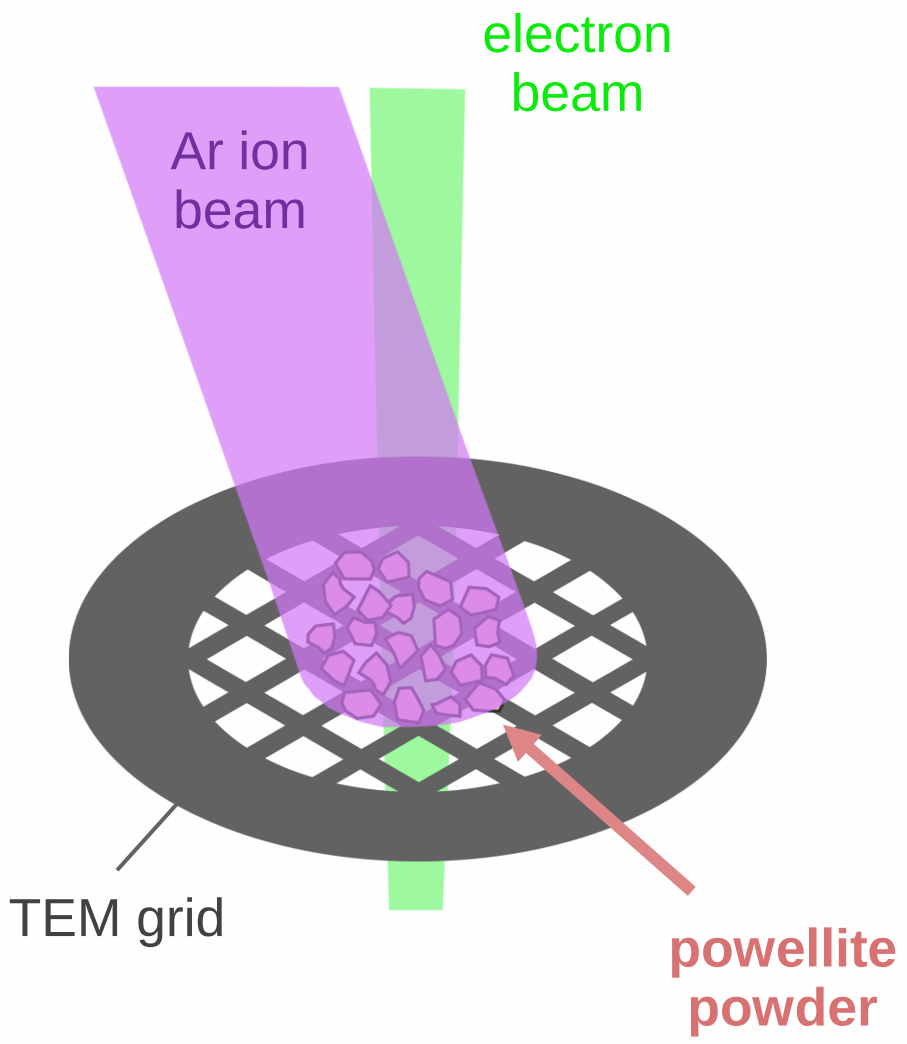

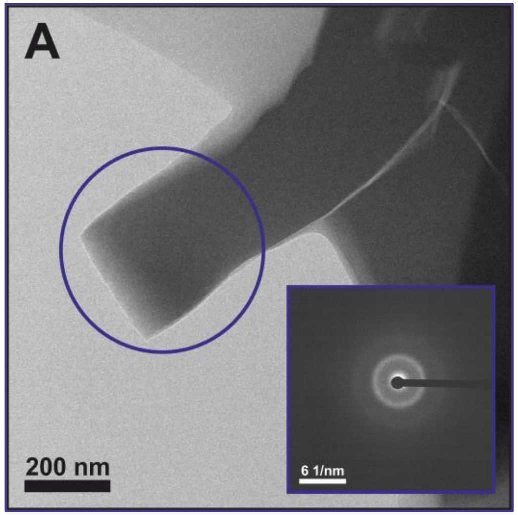

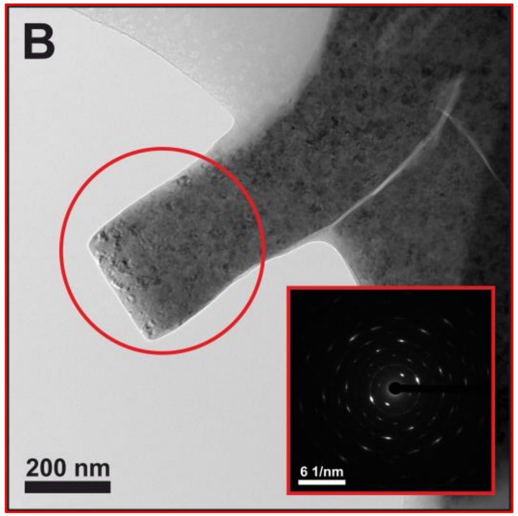

TEM with in situ Ar and Xe ion irradiation

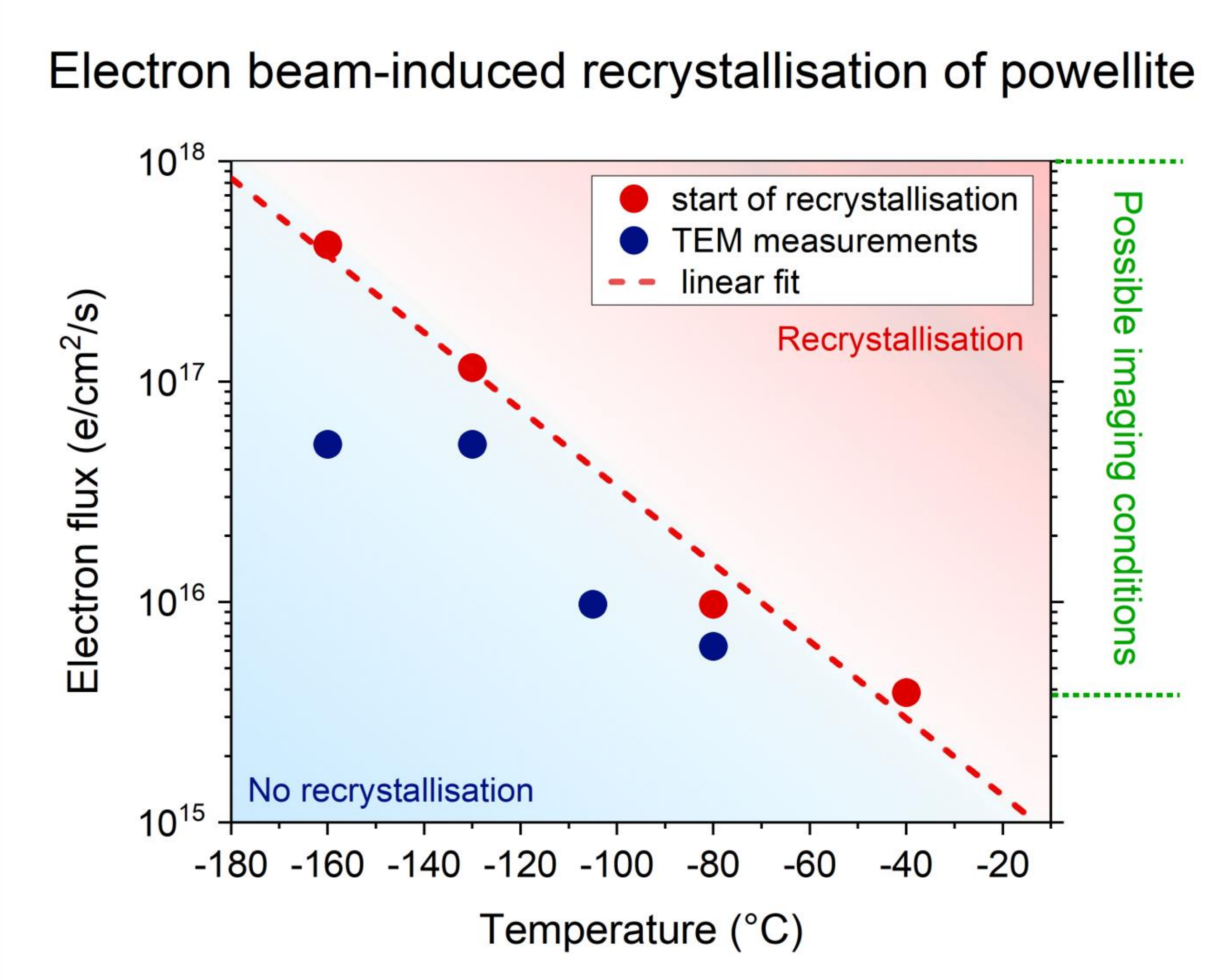

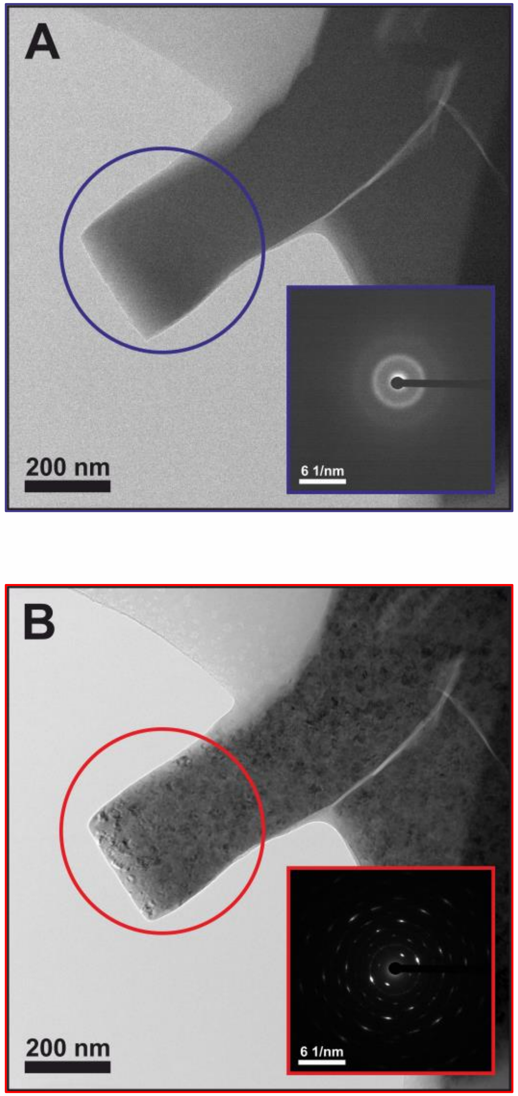

Summary (2)

- 8 irrad. in the literature (He, Ar, Kr, Xe, Au, Pb) – **no amorphisation**
- Ni, Au irrad. (room T) & Ar, Xe irrad. (low T) **– amorphisation**

1. Powellite is sensitive to ionization-induced damage recovery.
2. Temperature effect!
3. Ion type

IATADA

Ionization Activated Thermally Assisted Defect-Annealing

Debelle et al. 2019

Goal of research: evaluate the radiation tolerance of glass composite HLW materials with high Mo content.

Conclusions

- Radiation-induced swelling of powellite and zircon → cracking
- High temperature and high energy alpha particles might suppress the radiation damage.
- Future research should consider:
    - heavy-ion irradiation at high temperature, and He irradiation
    - corrosion tests on amorphous powellite.

TRANSCEND

Transformative Science and Engineering for Nuclear Decommissioning

Thank you for the help!

Robert Harrison
Brian O'Driscoll
Laura Leay

Tracey Taylor
Mike Harrison

NATIONAL NUCLEAR LABORATORY

Anamul Haq Mir
Felix Kaufmann
Paul Bingham
Prince Rautiyal
Györgyi Glodán
Chetna Tyagi
Samir de Moraes Shubeita

Special thanks for the support from National Nuclear Laboratory.

NATIONAL NUCLEAR LABORATORY

Contact Details
tamas.zagyva@postgrad.manchester.ac.uk

Thank you

TRANSCEND

Transformative Science and Engineering for Nuclear Decommissioning

Assessing the strength of biomineral strategies for concrete repairs

Thanos Karampourniotis, University of Strathclyde

Theme 2: Site Decommissioning and Remediation

email: athanasios.karampourniotis@strath.ac.uk

Supervisors:

Professor Rebecca Lunn[1], Dr. Enrico Tubaldi[2], Dr. Grainne El Mountassir[3]

[1,2,3] Department of Civil and Environmental Engineering, Faculty of Engineering, University of Strathclyde, Glasgow, United Kingdom

University of Strathclyde Glasgow

cavendish nuclear

Energy For a Low Carbon Future

LOCATION OF NUCLEAR POWER STATIONS IN THE UK


*Hinkley B power station, **Source:** www.itv.com*


*Heysham 1 power station, **Source**: Lancaster Guardian*

*Hunterston B power station, **Source**: Sky news*


*Dungeness B power station, **Source**: BBC*

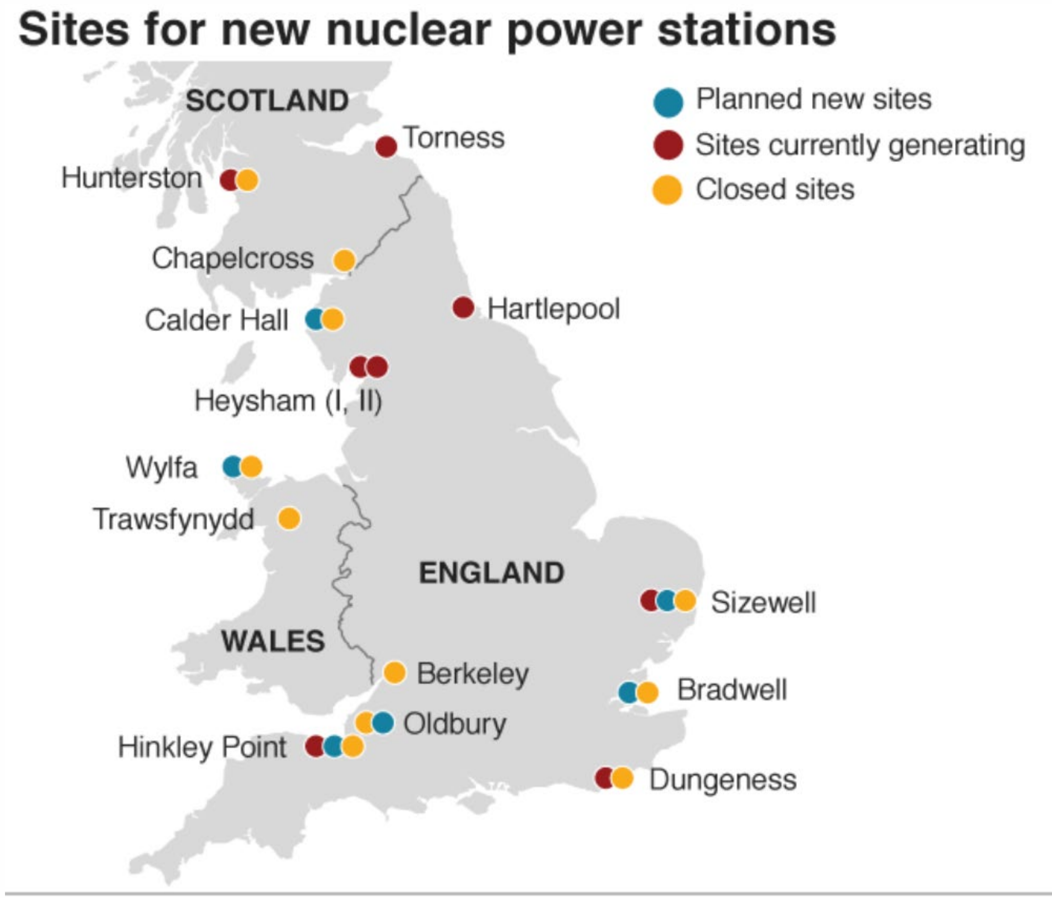

***Source**: BEIS, House of Commons Library*

AGE OF THE NUCLEAR POWER STATIONS IN THE UK

Table of past and present UK nuclear reactors

	Net Capacity (MW)	Number of operating reactors	Published lifetime
Magnox – NDA			
Wylfa	490	1	1971-2015
Advanced Gas Cooled Reactor (AGR) – EDF			
Hinkley Point B	880	2	1976-2023
Hunterson B	890	2	1976-2023
Heysham 1	1,155	2	1983-2019
Dungeness B	1,040	2	1983-2028
Hartlepool	1,180	2	1983-2024
Heysham 2	1,220	2	1988-2023
Torness	1,185	2	1988-2023
Pressurised Water Reactor (PWR) – EDF			
Sizewell B	1,198	1	1995-2035
Total net capacity and number of operating reactors	**9,238**	**16**	

Source*: assets.publishing.service.gov.uk*

TRADITIONAL CONCRETE-REPAIR STRATEGIES

Source: *homedepot.com*

Source: *engineeringdiscoveries.net*

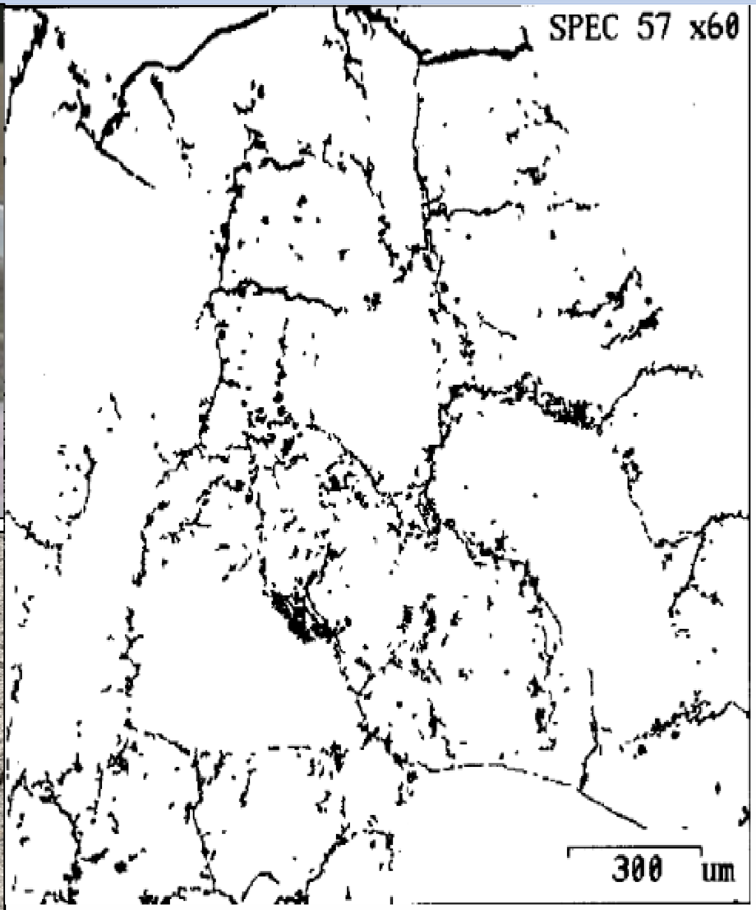

Microcracking network in concrete, Nemati et al. 1998

For repairing concrete microcracking effectively, the strategy used should provide:

- Durability
- Mechanical resistance
- Low viscosity of the solution
- Decreased permeability

MICP VIA UREA HYDROLYSIS

$$CO(NH_2)_2 + H_2O \xrightarrow[\text{S. Pasteurii cell}]{\text{Urea hydrolysis}} 2NH_4^+ + HCO_3^- + OH^-$$

S. Pasteurii cell

1.3 – 4 µm

pH increase

$$HCO_3^- + H_2O^+ + OH^- \leftrightarrow CO_3^{2-} + \cancel{2H_2O} \xrightarrow{\text{Calcium source}} Ca^{2+} + CO_3^{2-} \longrightarrow CaCO_3\ (s)$$

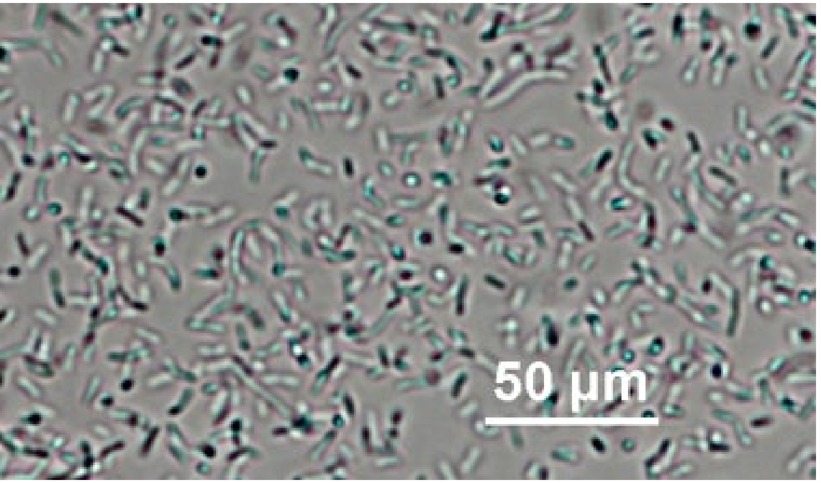

S. Pasteurii under a microscope

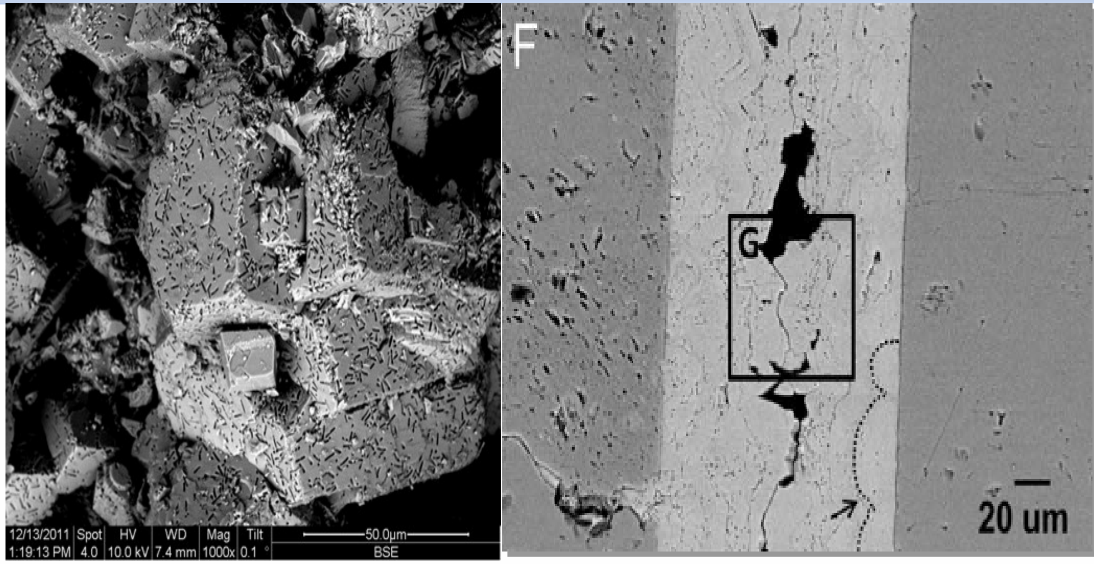

SEM Images showing calcite crystals with encapsulation of bacterial cells.
***Sources**: El Mountassir et al. 2018, Tobler et al. 2018.*

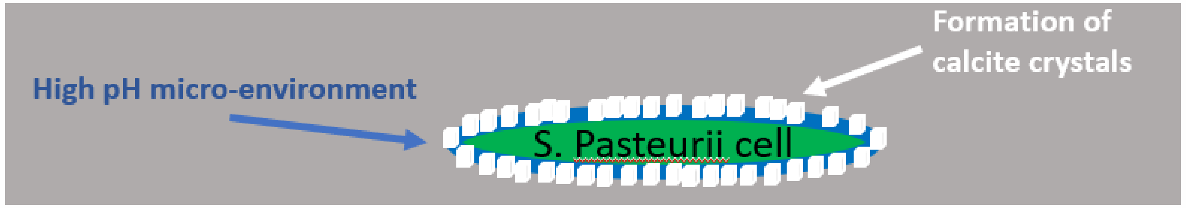

THE AIM AND OBJECTIVES OF THIS PHD ARE:

AIM

- To provide a durable repair for both micro-cracking and large cracks that lasts for decades.

OBJECTIVE

✓ A mesoscale Finite Elements Model has been developed to predict the mechanical behaviour of MICP-treated concrete.

- Experiments are conducted to validate the Finite Elements Model.

Concrete Cores

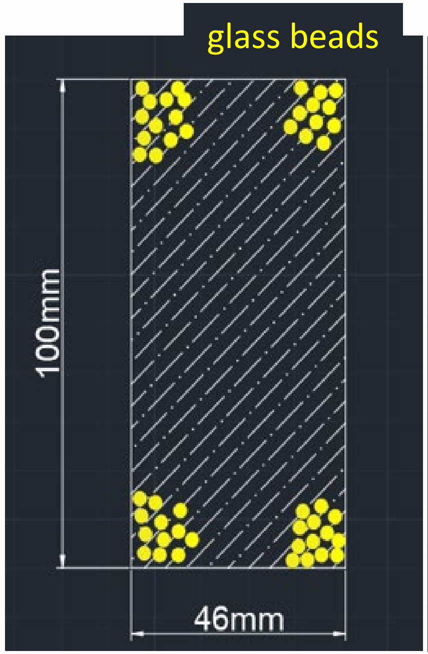

Core 1

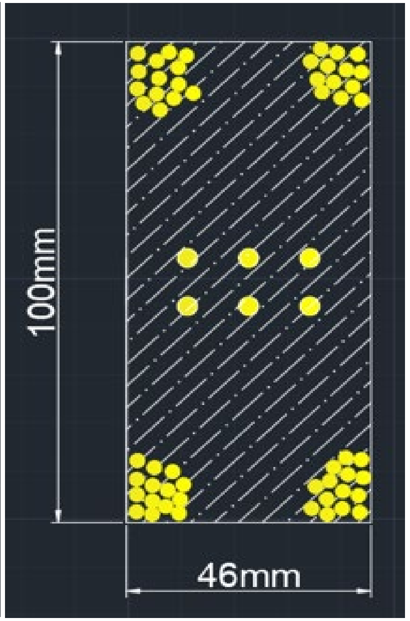

Core 2

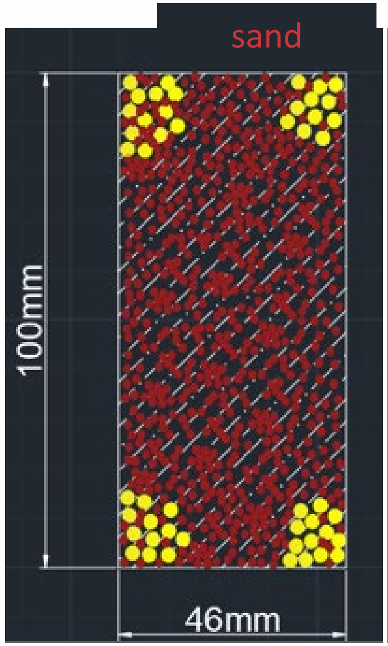

Core 3

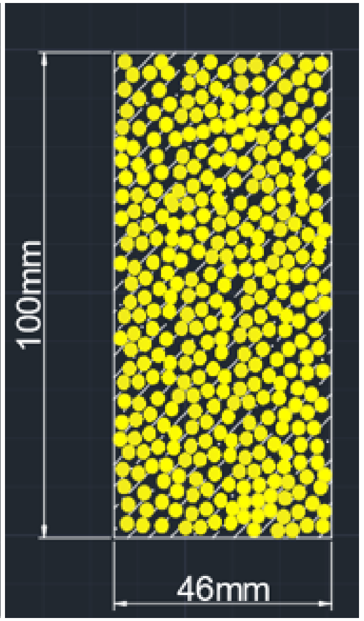

Cores 4 and 5

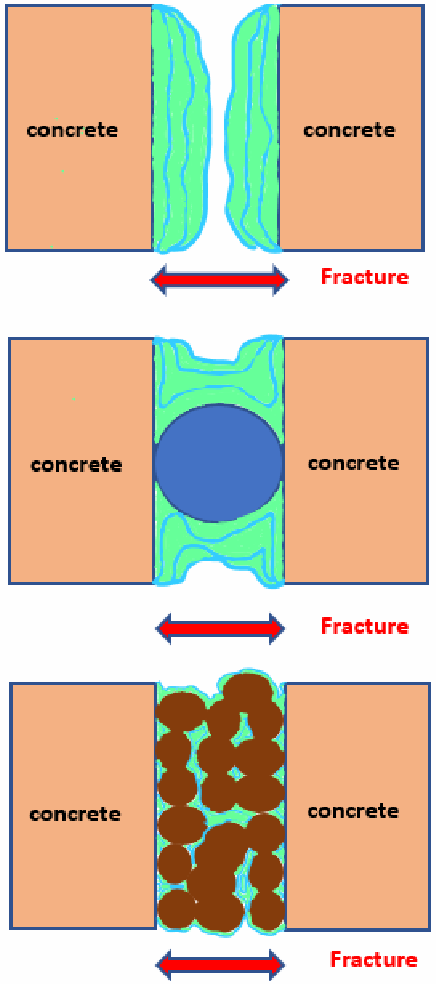

EXPERIMENTAL SETUP

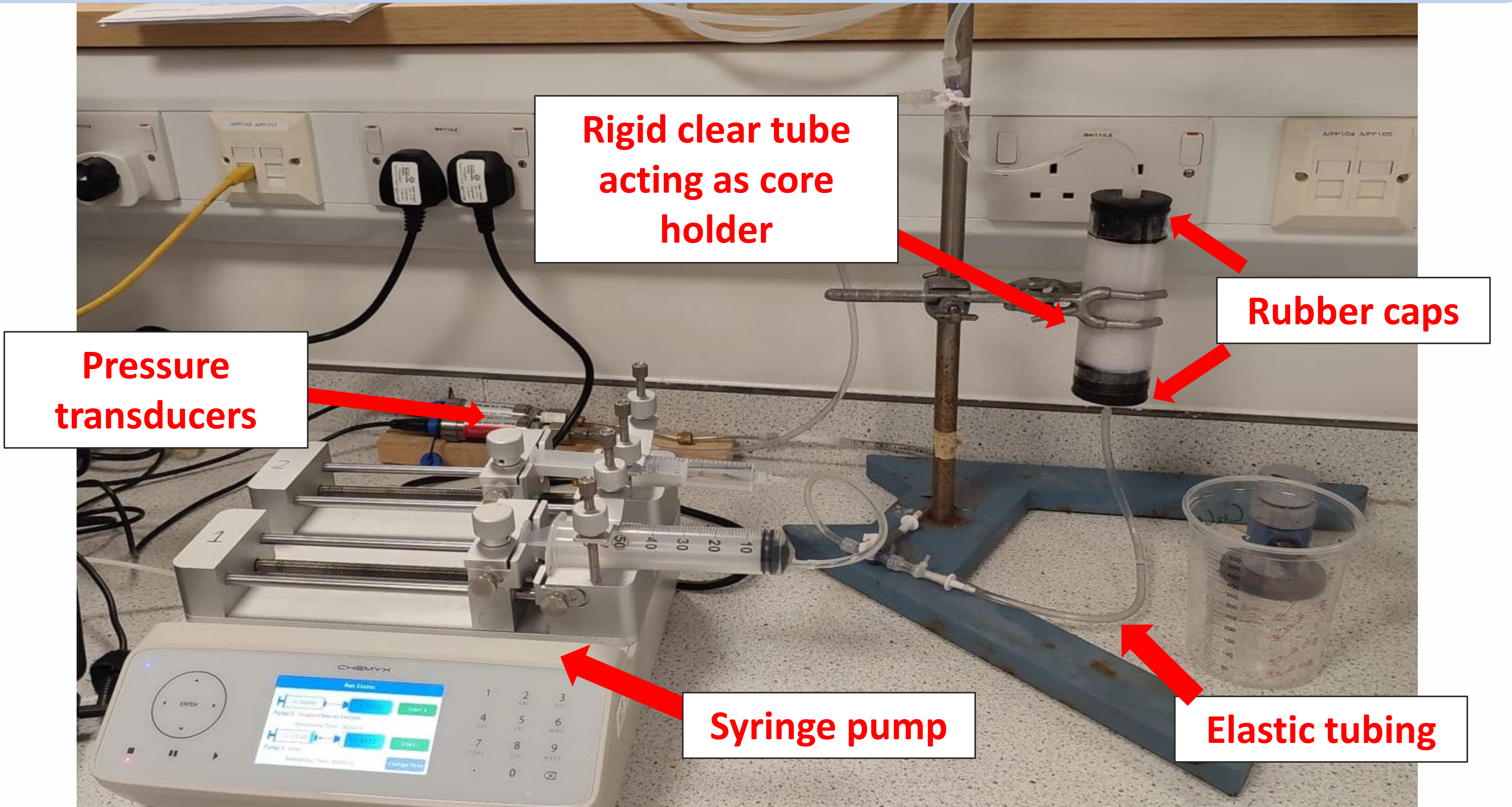

DIFFERENTIAL PRESSURE DURING TREATMENT

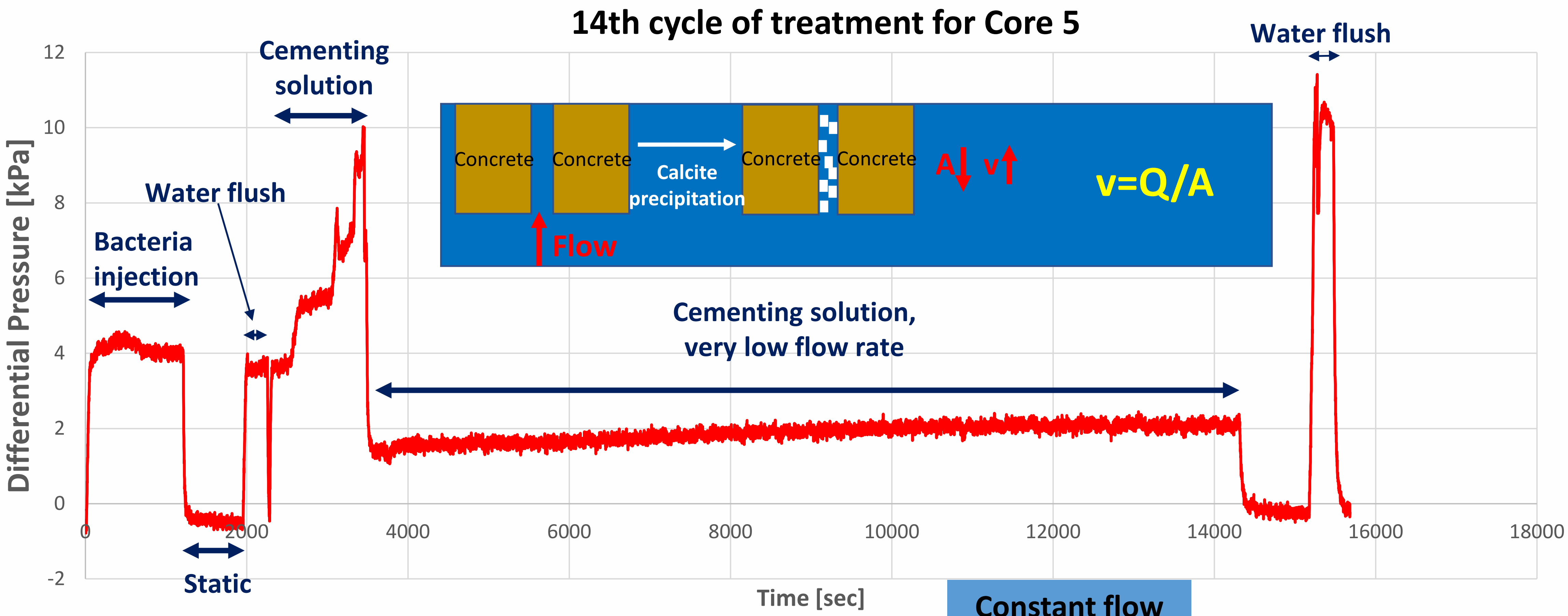

Constant flow rate for each treatment.

TRANSCEND

Transformative Science and Engineering for Nuclear Decommissioning

HYDRAULIC CONDUCTIVITY

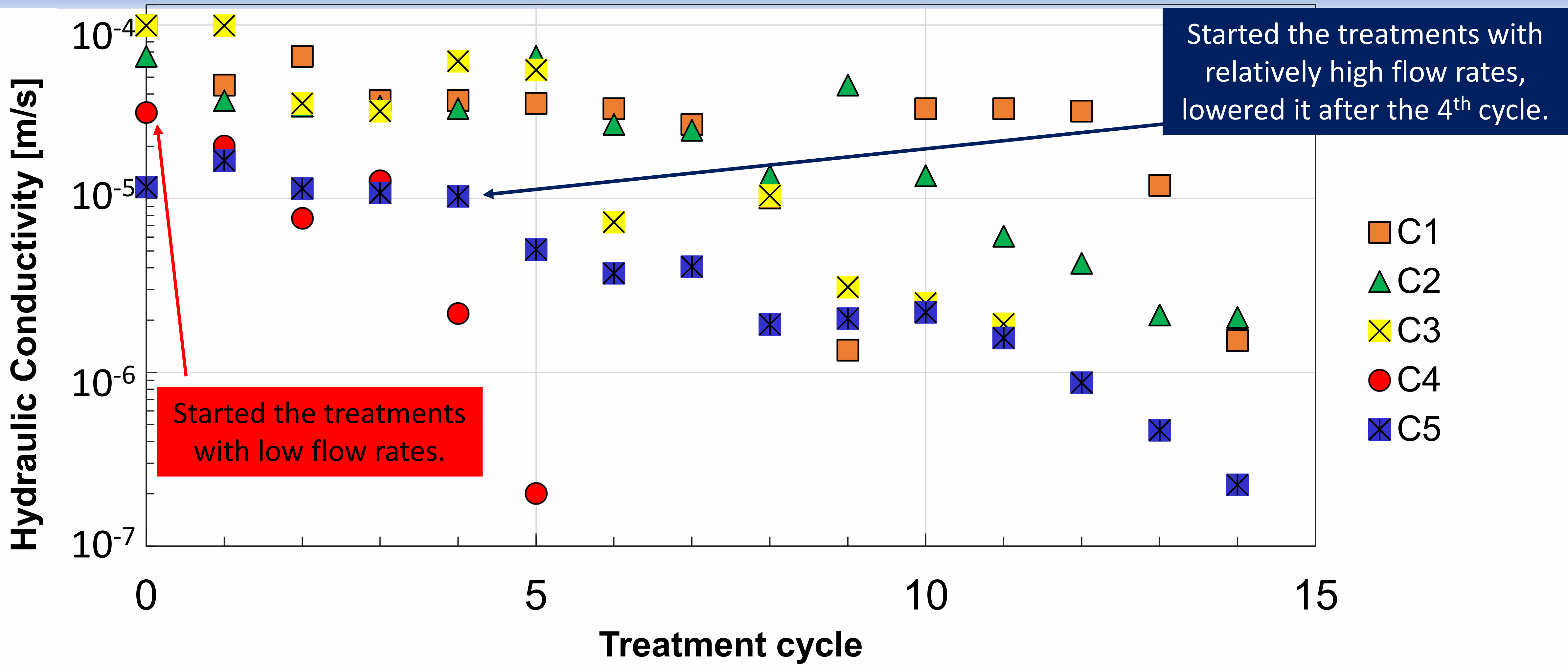

XCT SCANNING

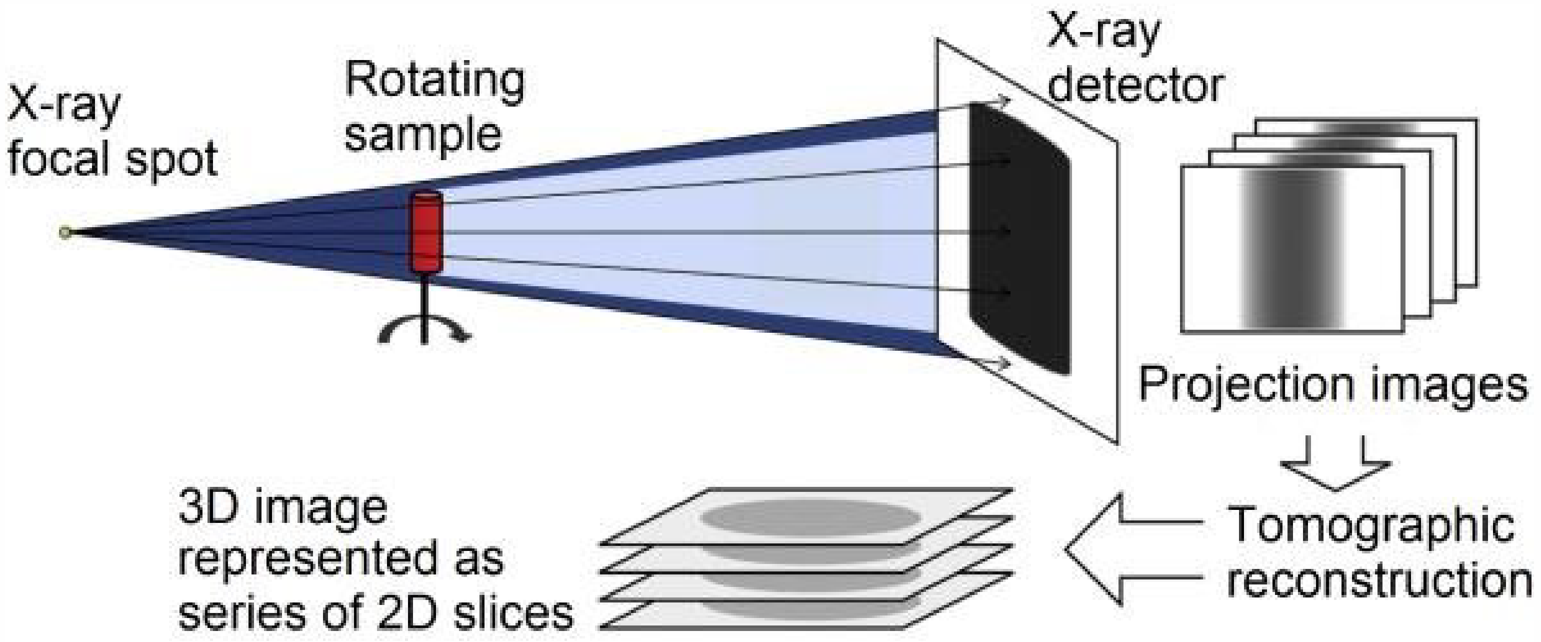

Source: *Fernando Alvarez-Borges et al. 2018*

1) Generate X-rays
2) X-rays pass through the sample
3) Collect images
4) Convert images to 3D model
5) Process and analyze model

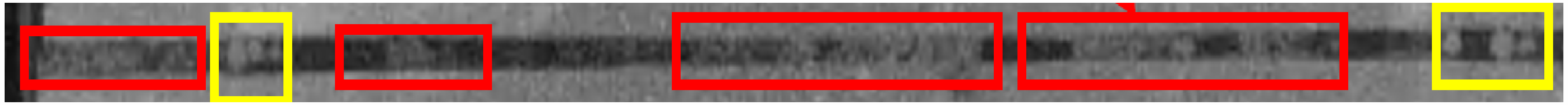

XCT SCANNING C1/IMAGE ANALYSIS

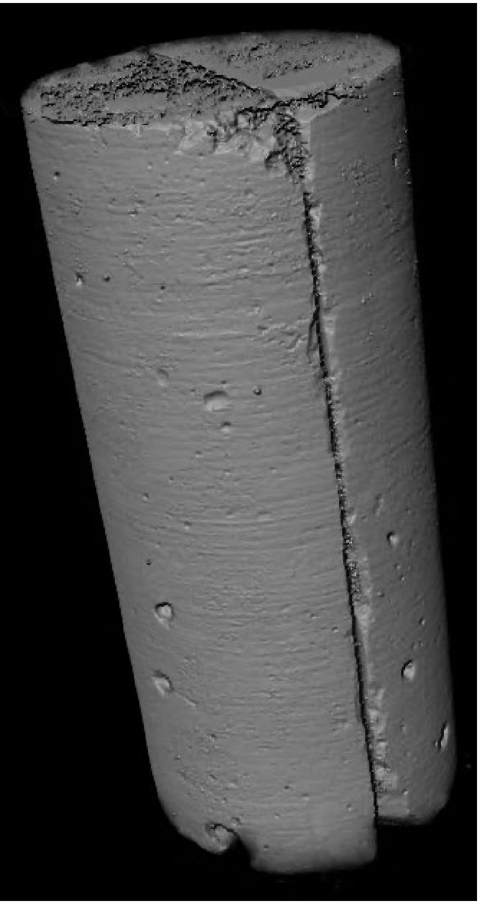

3D model of C1

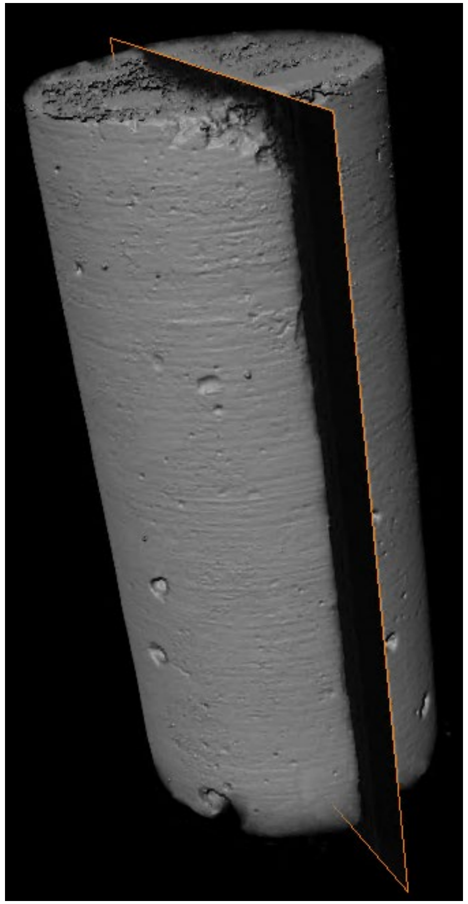

Perpendicular slice in the fracture

The fracture is inclined

Position of a horizontal slice

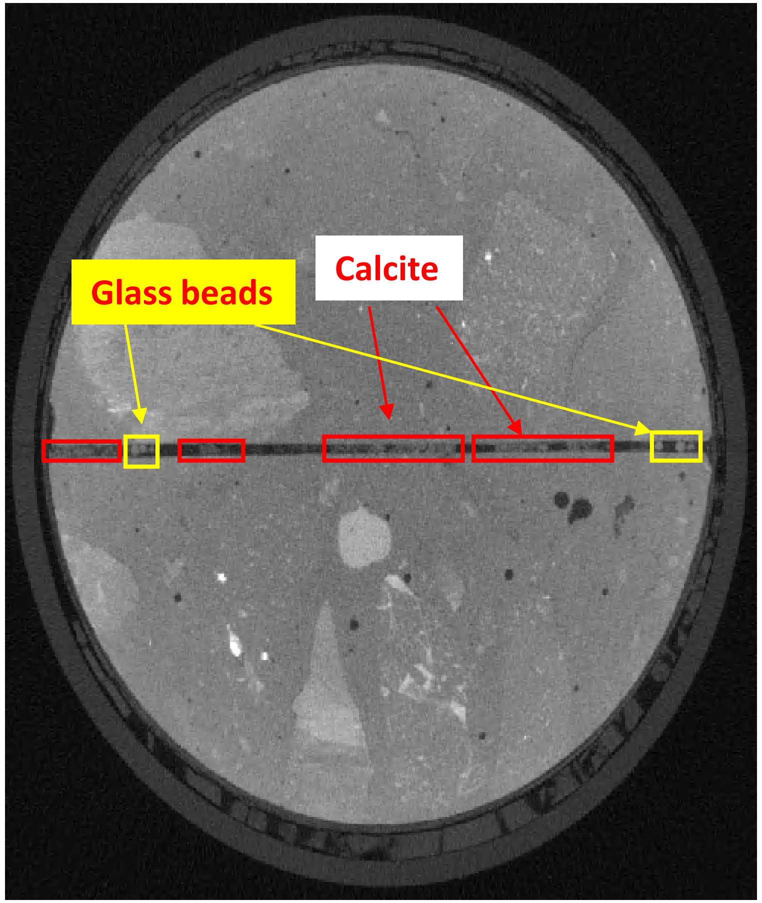

Horizontal slice

XCT SCANNING C1: IMAGE ANALYSIS/SEGMENTATION PROCESS

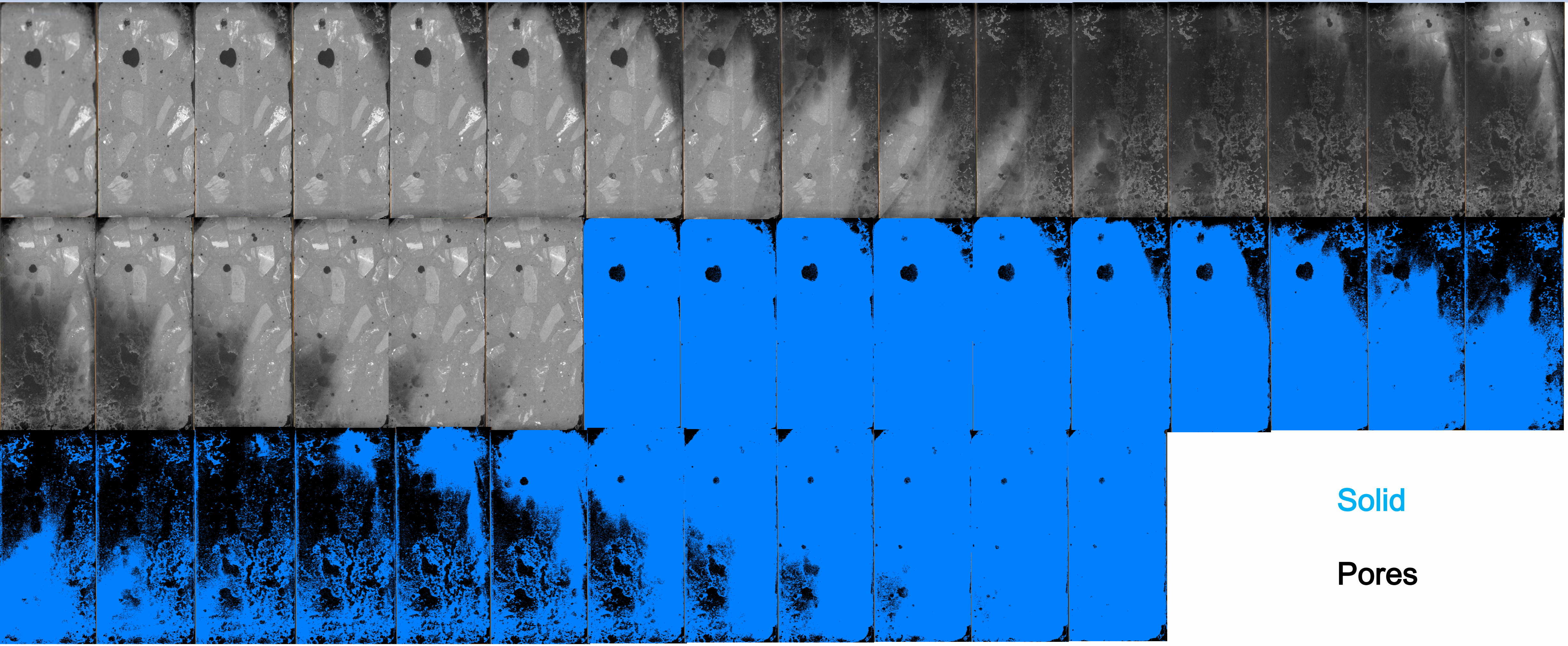

Solid

Pores

FINAL IMAGES

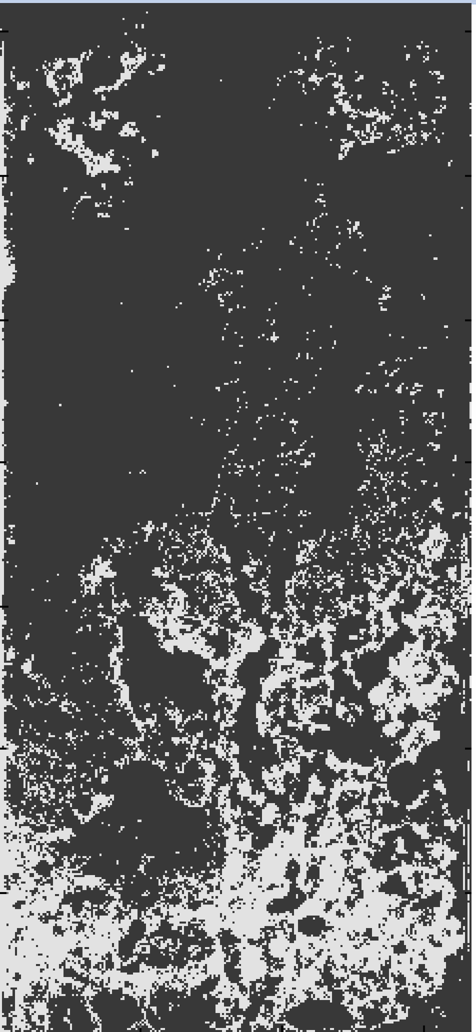

1

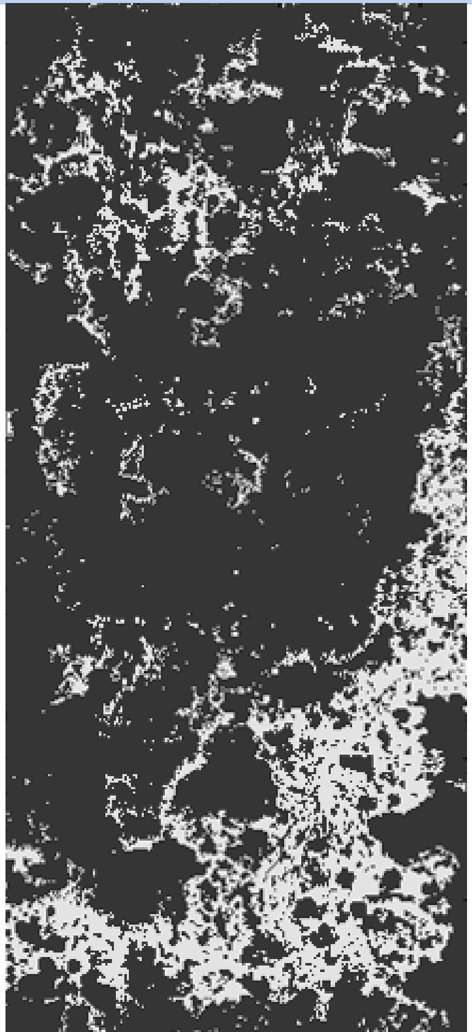

2

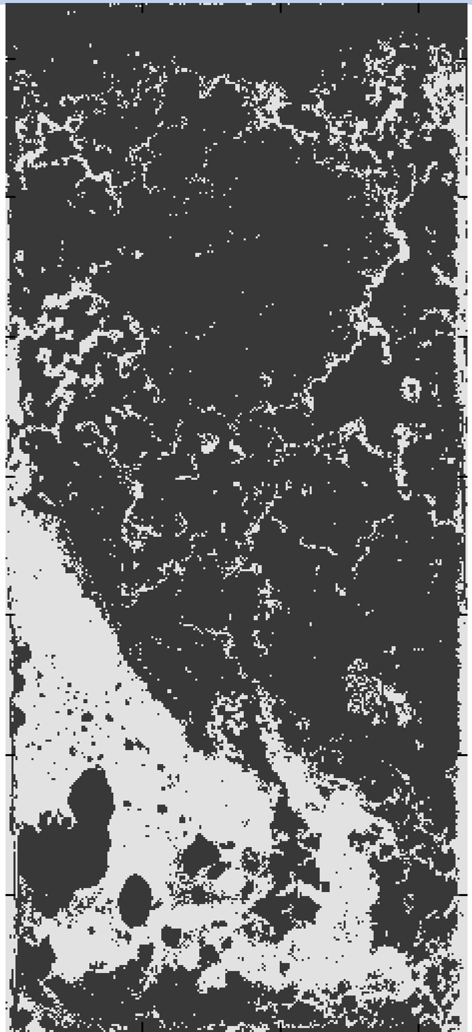

3

1) Contact points bridging the surfaces of the fracture in Concrete Core 1. Cemented area: **20.16%**

2) Contact points bridging the surfaces of the fracture in Concrete Core 2. Cemented area: **22.98%**

3) Contact points bridging the surfaces of the fracture in Concrete Core 3. Cemented area: **26.89%**

White area: Contact points

Black area: No contact points

CEMENTED GLASS BEADS

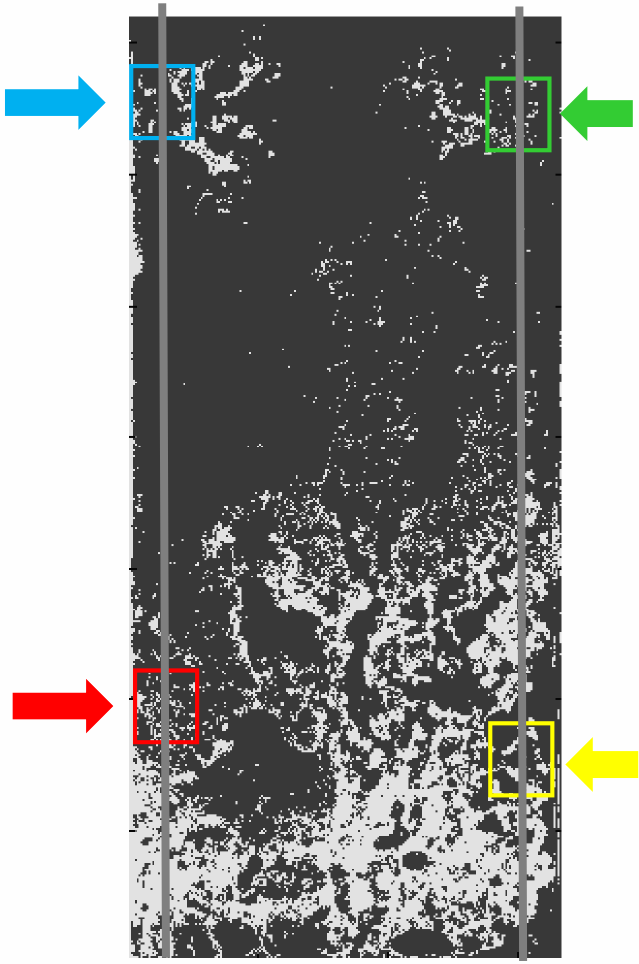

Concrete Core 1 Final Image

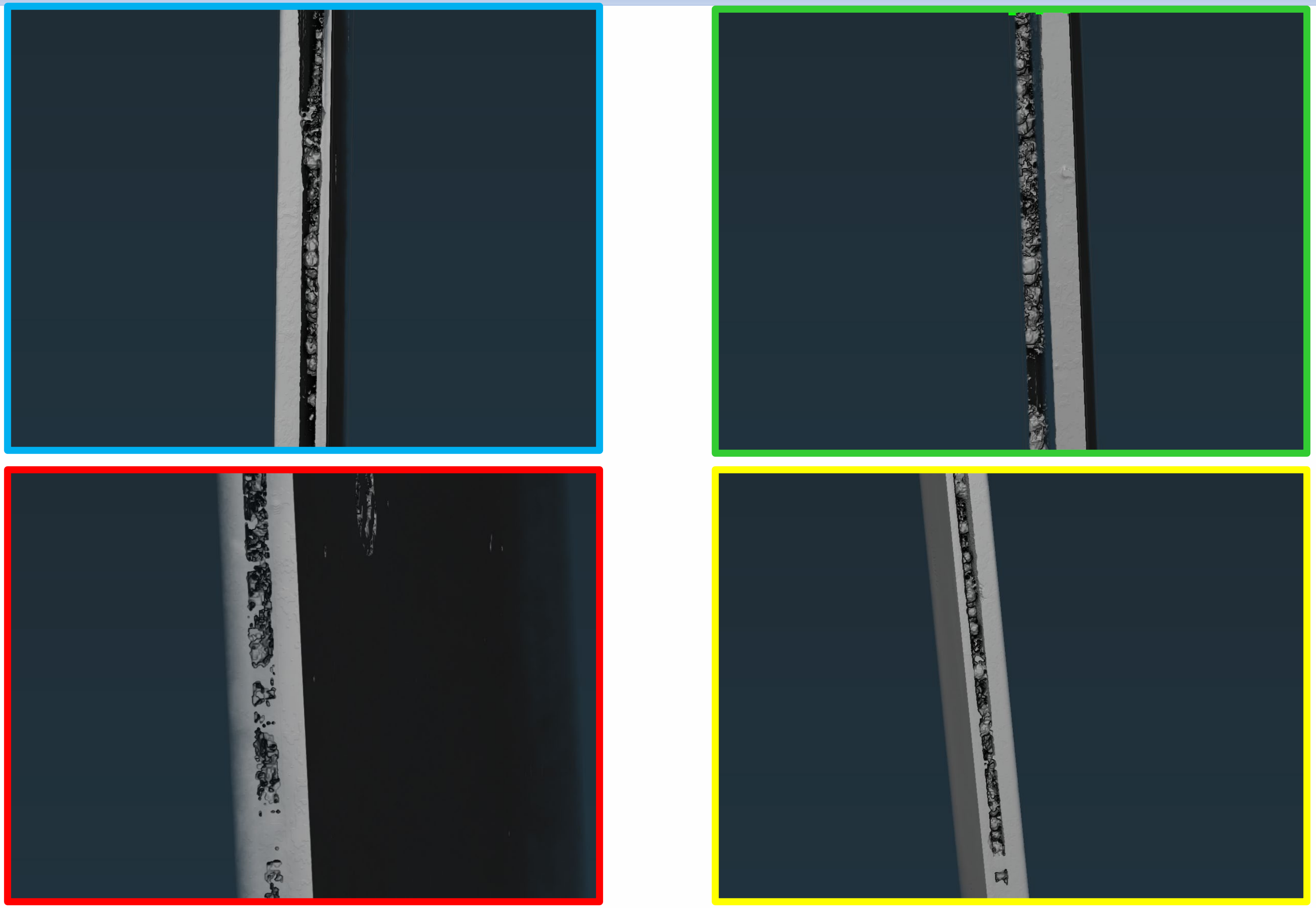

TENSILE TESTS

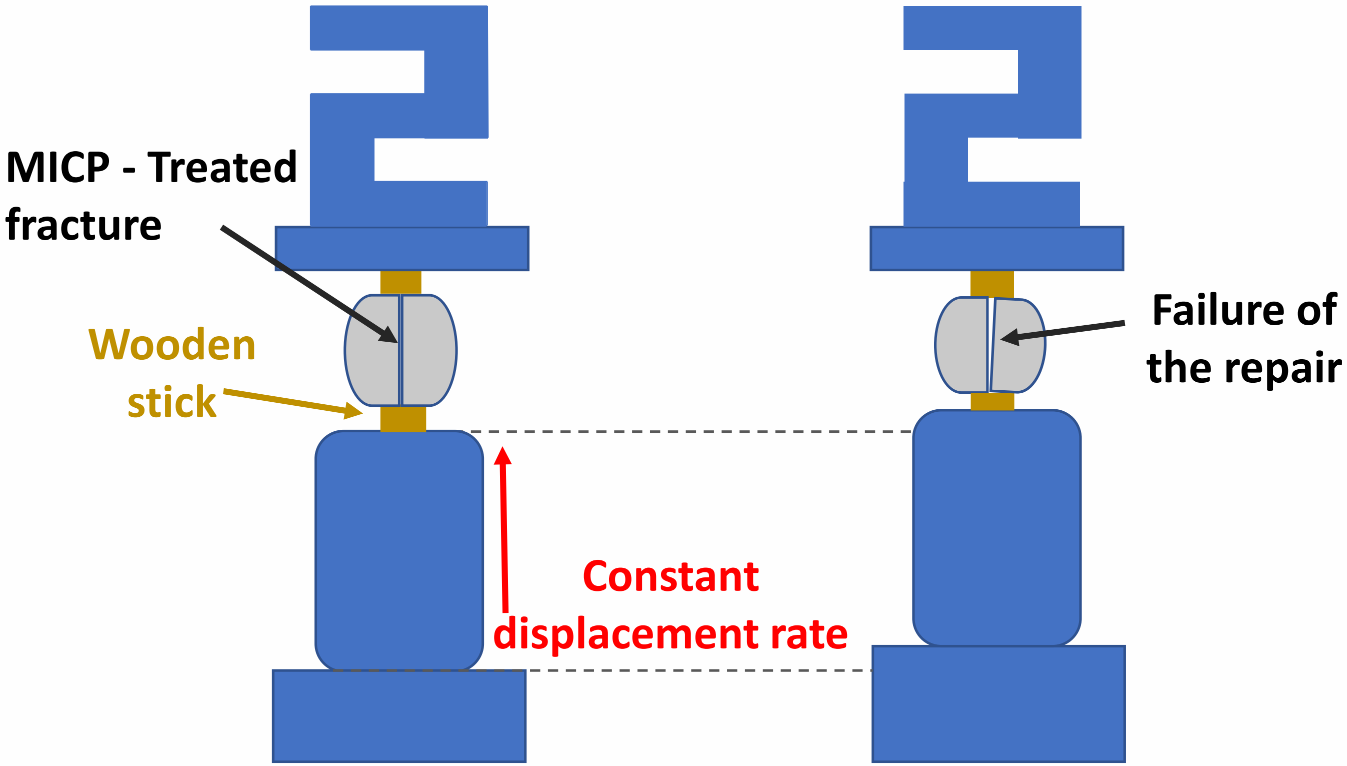

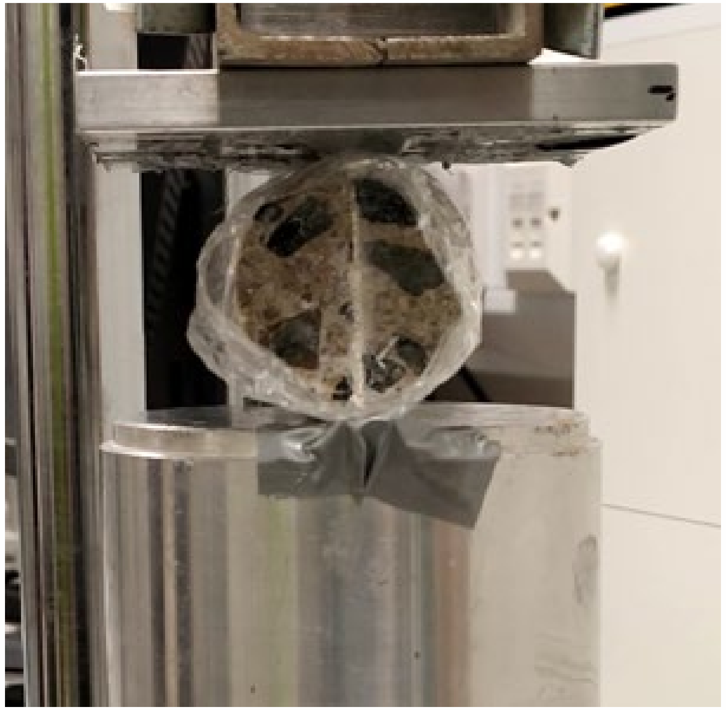

Concrete core subjected to tensile test

AFTER TENSILE TESTING

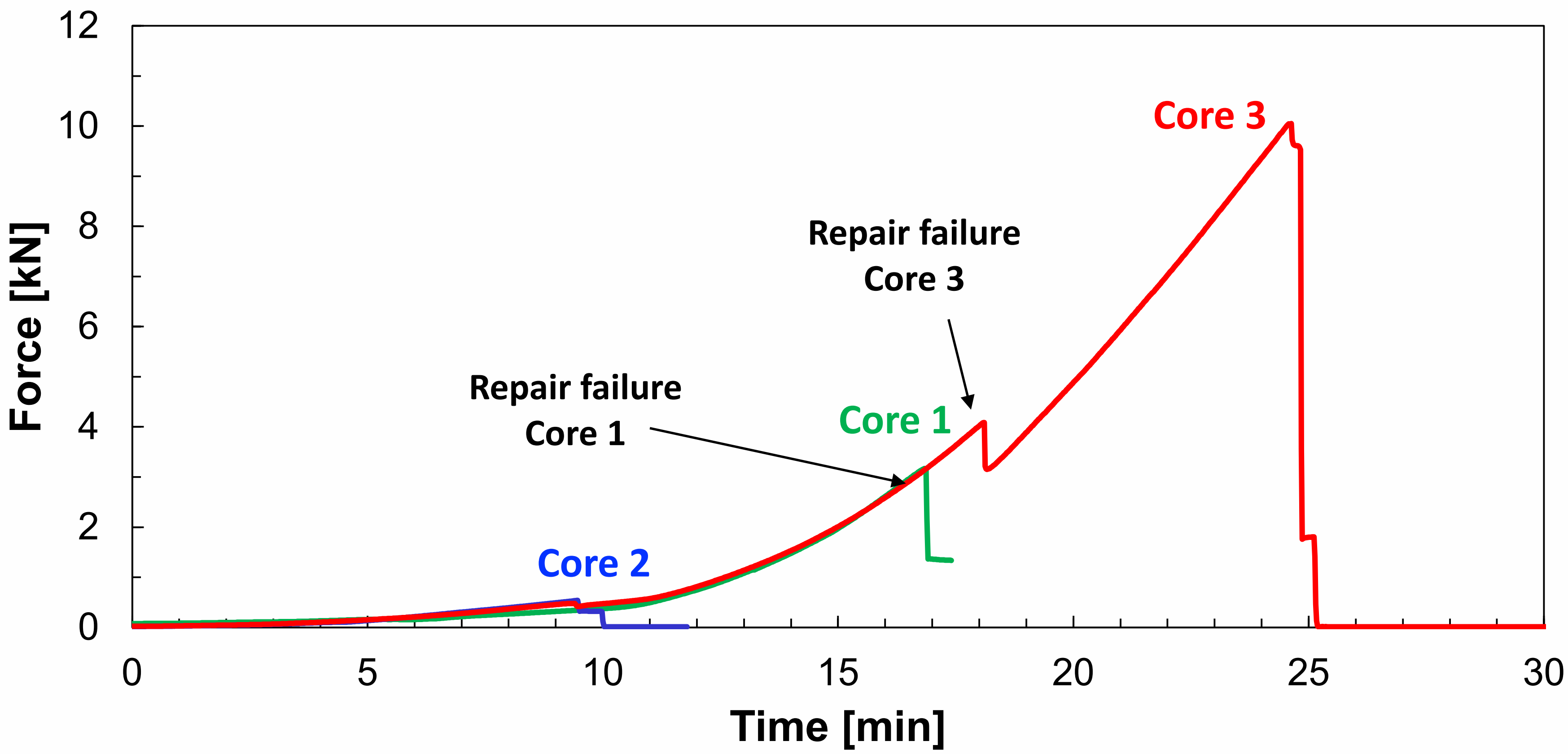

Core 2
irregularities

AFTER TENSILE TESTING

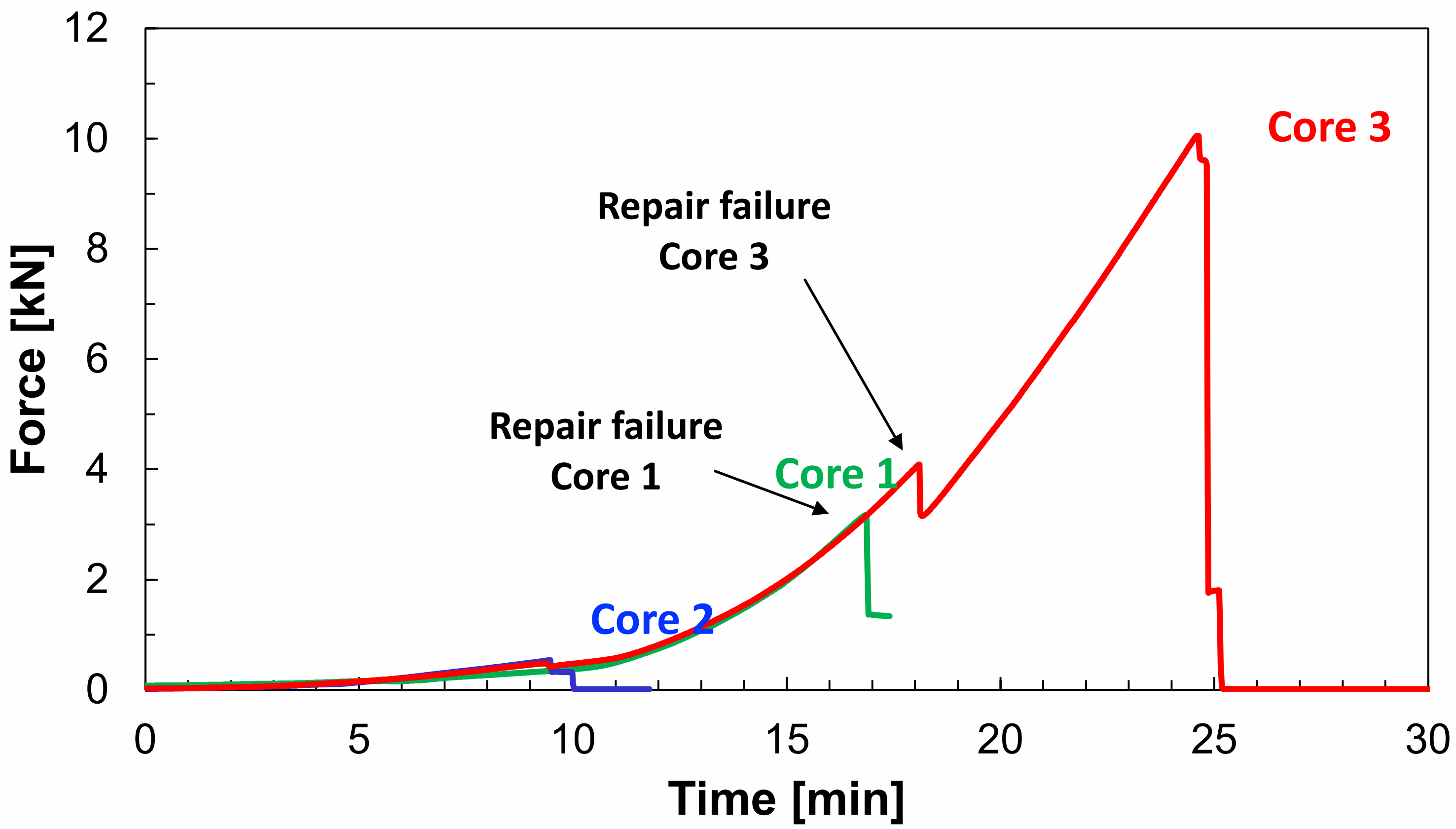

	% of contact points in the fracture	Tensile strength of the core [MPa]	Tensile strength of calcite [MPa]
Core 1	20.16	0.45	2.23
Core 2	22.98	-	-
Core 3	26.89	0.59	2.19
Core 4	To be analyzed	To be tested	To be tested
Core 5	To be analyzed	To be tested	To be tested

AFTER TENSILE TESTING

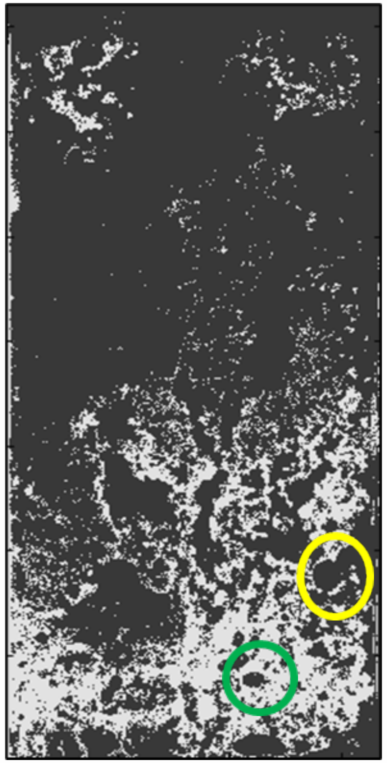

Image analysis of Core 1 before tensile testing

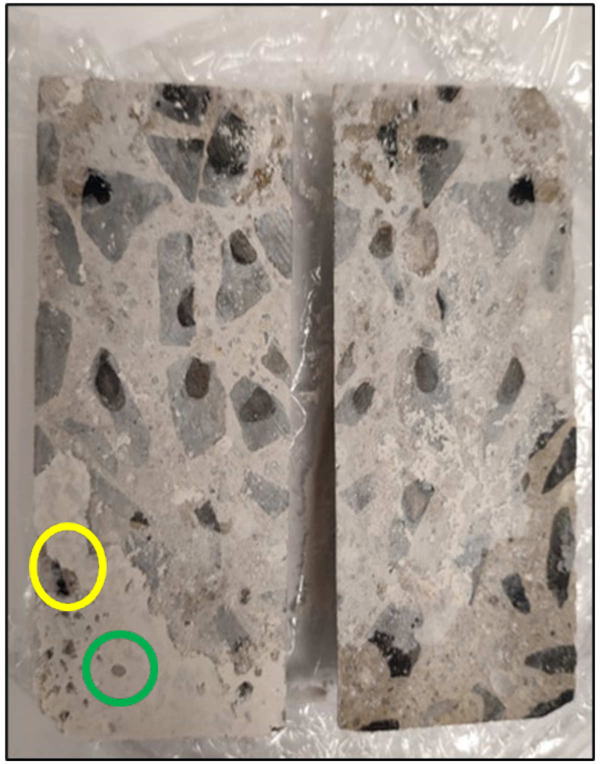

Figure of Core 1 after being subjected to tensile testing

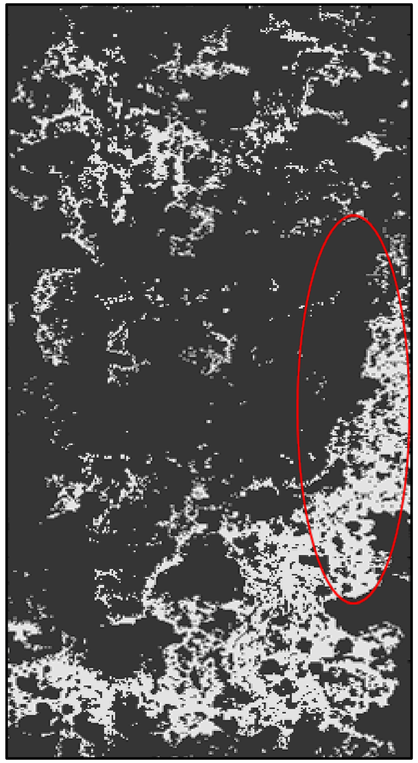

Image analysis of Core 2 before tensile testing

Figure of Core 2 after being subjected to tensile testing

CONCLUSIONS

- Microbially Induced Carbonate Precipitation treatments have been implemented to old artificially-cut concrete cores, exhibiting a substantial decrease in their initial Hydraulic Conductivity showcasing the presence of calcite crystals in the fractures.
- The XCT scans showed that a significant percentage of the fracture’s area has been bridged.
- Brazilian tests demonstrate the gain in tensile strength due to the precipitated calcite crystals in initially unbridged fractures.
- Preliminary results display a direct correlation between calcite contact area and recovered tensile strength.

FUTURE WORK

- Two additional cores will be treated with MICP to ensure statistical significance. The same methodology as the previous cores will be applied.
- Efforts will focus on the advance of a tensile-test Finite Elements Model that predicts MICP treated samples' mechanical behaviour.
- The tensile model will be upscale to predict MICP-gained strength in concrete blocks (30 cm side).

University of Strathclyde Glasgow

cavendish nuclear

Transformative Science and Engineering for Nuclear Decommissioning

Thank you

e-mail: athanasios.karampourniotis@strath.ac.uk

Interface Analysis Centre

Materials research for Energy Engineering and the Environment

IAC

Characterisation of Uranium Metal Encapsulated in Magnox Sludge

Philip Hutchinson

vr19802@bristol.ac.uk

Sellafield Ltd

[#]Interface Analysis Centre, University of Bristol,

Project Breakdown

Uranium Corrosion Behaviour

Sludge Properties & Behaviour

First Gen. Magnox Storage Pond (FGMSP)

- Large **open air** storage pond
- Commissioned in 1959: **60 years old**
- Intermediate holding area
- Decommissioning challenge: **Magnox Sludge**

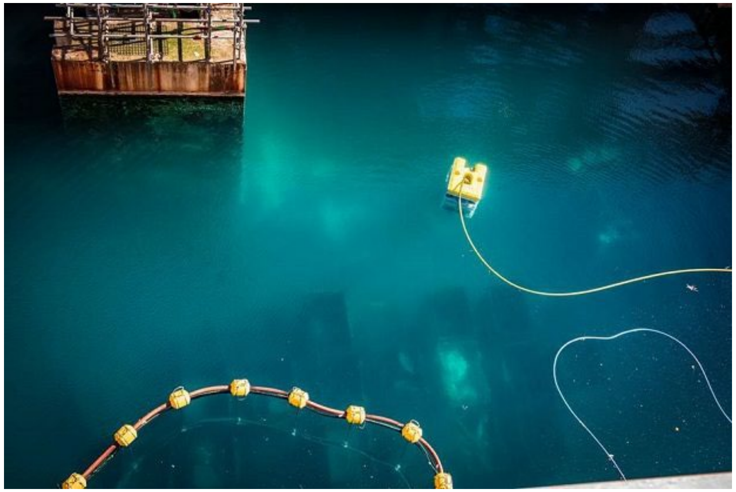

What is Magnox sludge?

- Magnox – **99%** magnesium, **0.8%** aluminium
- $Mg + 2H_2O \rightarrow Mg(OH)_2 + H_2$
- $Mg(OH)_2$ forms a fine **insoluble** particulate
- Uranium metal encapsulated in layers of sludge

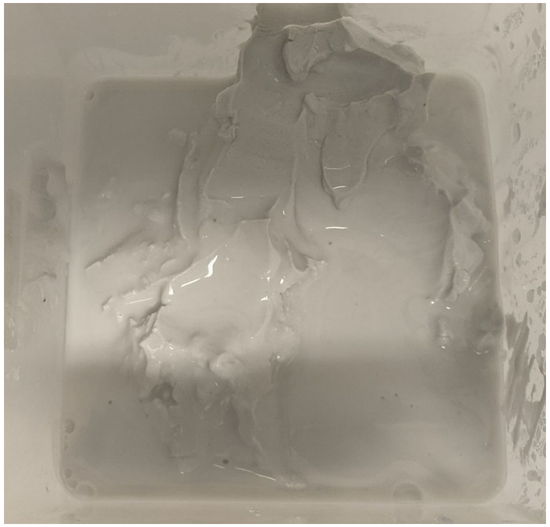

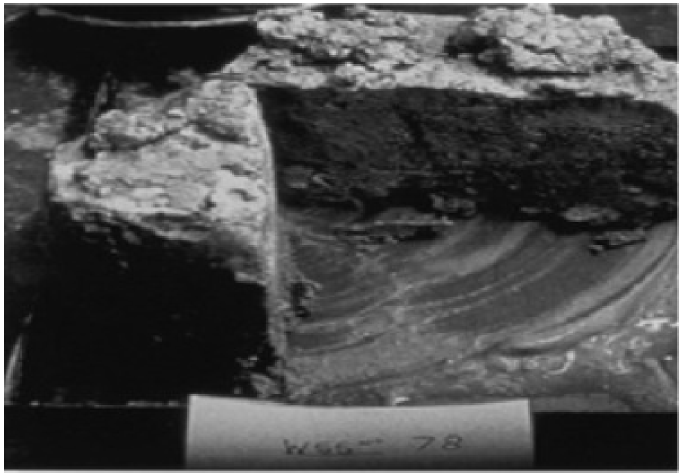

[#]Interface Analysis Centre, University of Bristol,

Project Breakdown

Uranium Corrosion Behaviour

Sludge Properties & Behaviour

Uranium metal corrosion – Water

- Main corrosive species: $\boldsymbol{OH^-, O^{2-}}$

- $U + 2H_2O \rightarrow UO_2 + 2H_2$
- $U + O_2 \rightarrow UO_2$

- Oxide forms a **protective barrier**

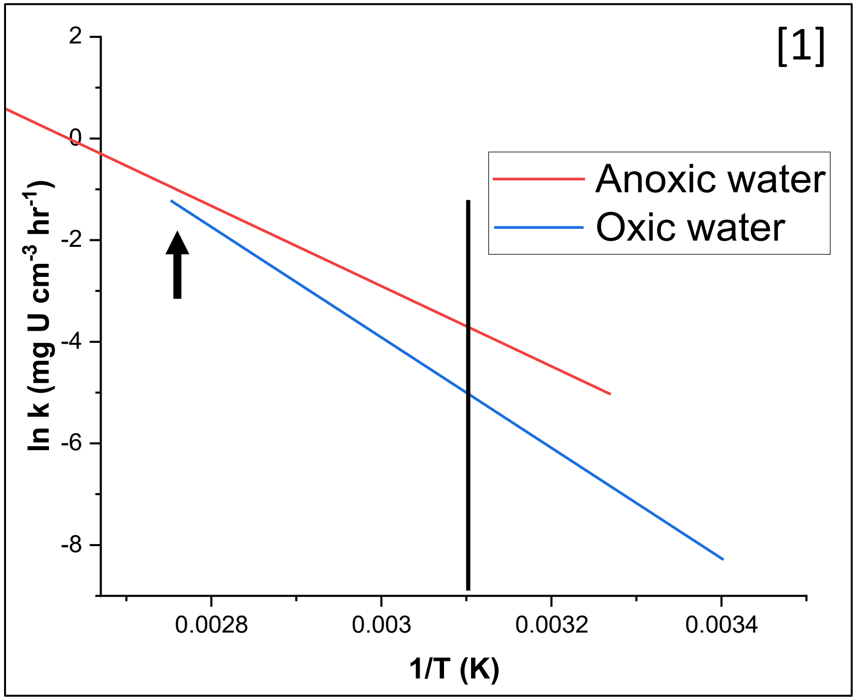

- Oxygen **poisoning** Uranium-water reaction:
  - O^{2-} occupies adsorption sites
  - O^{2-} in interstitial positions slows OH^- diffusion

#Interface Analysis Centre, University of Bristol,

Uranium metal corrosion – Encapsulated

- $U + 1.5H_2 \rightarrow UH_3$
- **Conversion** of UH_3 to UO_2:
  - $UH_3 + 2H_2O \rightarrow UO_2 + \frac{7}{2}H_2$
  - $UH_3 + \frac{7}{4}O_2 \rightarrow UO_2 + \frac{3}{2}H_2$
- Does UH_3 **persist**?
  - Limited access to water
  - H_2 **accumulation**

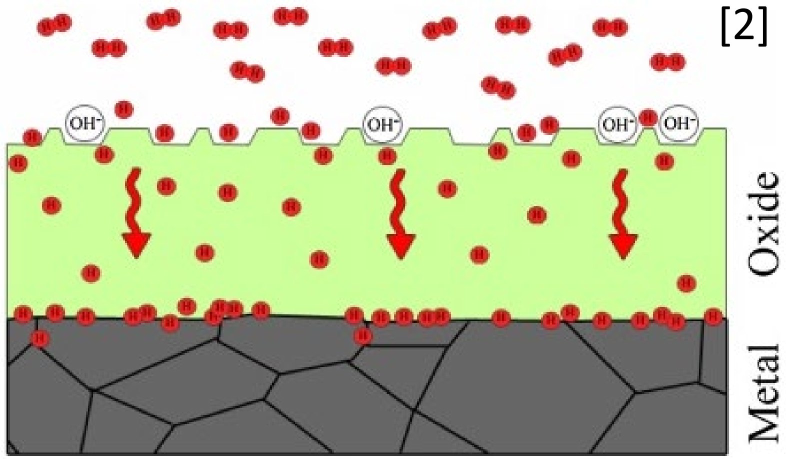

[2]

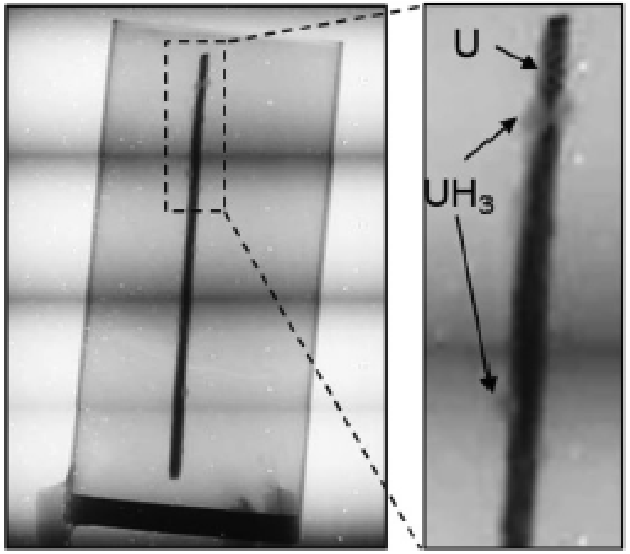

[3]

Sellafield Ltd

Project Breakdown

Uranium Corrosion Behaviour

Sludge Properties & Behaviour

Sludge Properties

- FGMSP sludge is **heterogenous**

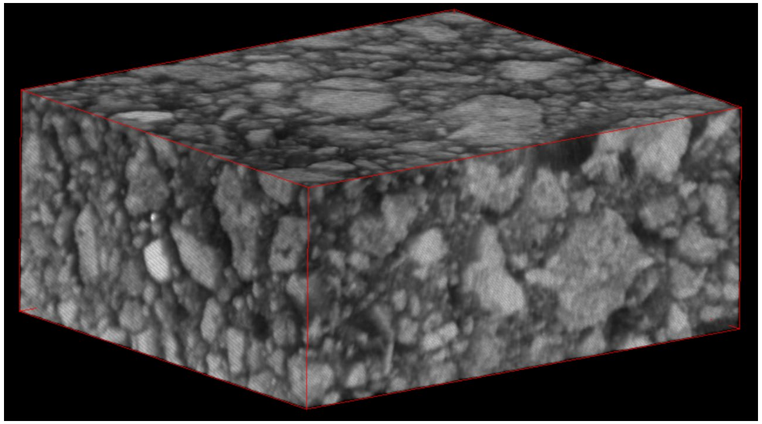

- Pond Sludge **dangerous** to handle:
  - Commercial $Mg(OH)_2$ **powder**
  - **DIY** Corroded Magnox
  - Corroded Magnox Simulant (**CMS**)

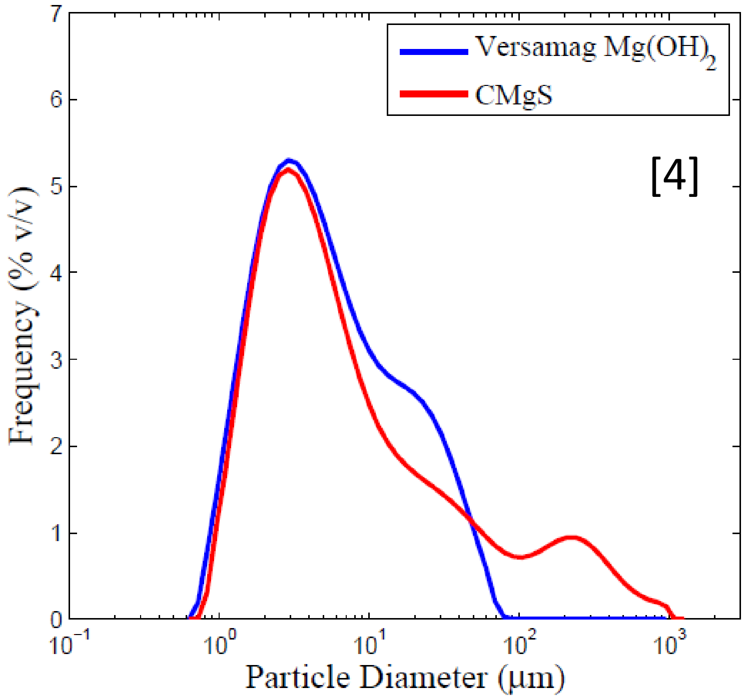

- Main **properties** of Sludge:
  - Particle size distribution
  - Solids concentration
  - Chemical interactions

#Interface Analysis Centre, University of Bristol,

Sellafield Ltd

Experimental method

- X-ray Tomography

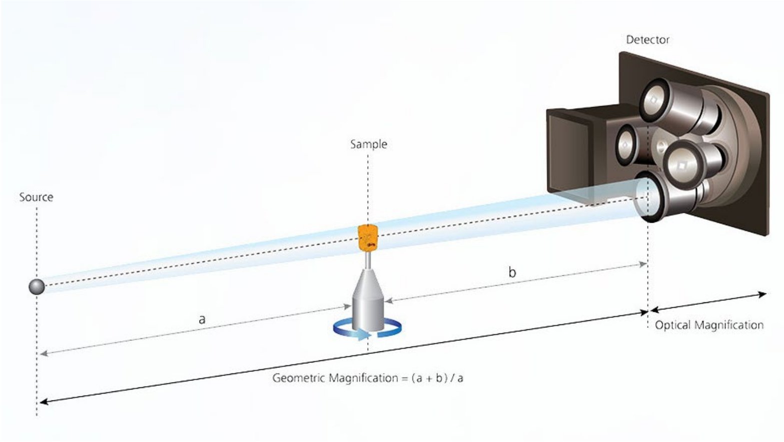

- Image Reconstruction algorithm:
  - 2D pixels → 3D voxels
  - Artifacts – **Beam hardening**

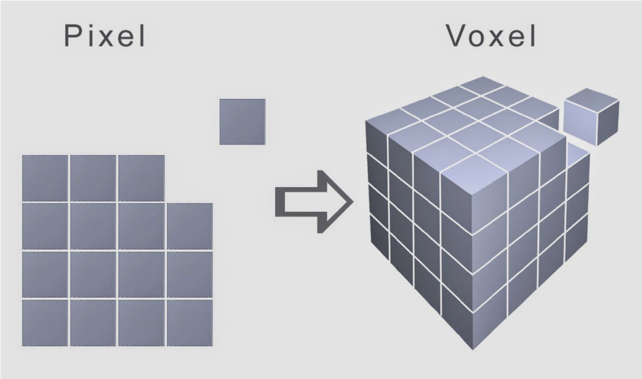

- Extracting quantitative data
  - Image **segmentation**
  - **Metal** vs corrosion product
  - Volume → **Mass**

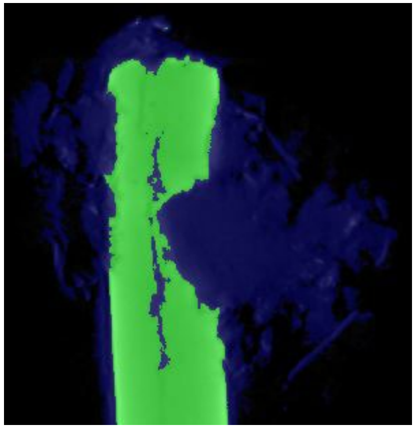

[#]Interface Analysis Centre, University of Bristol,

Sellafield Ltd

Uranium Corrosion Experiments

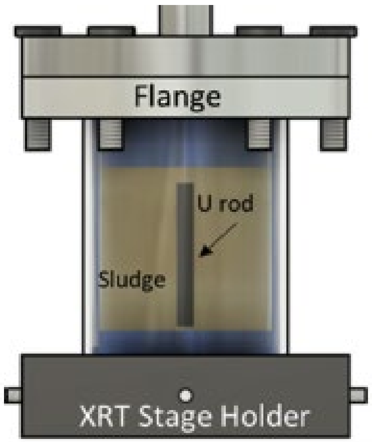

[5]

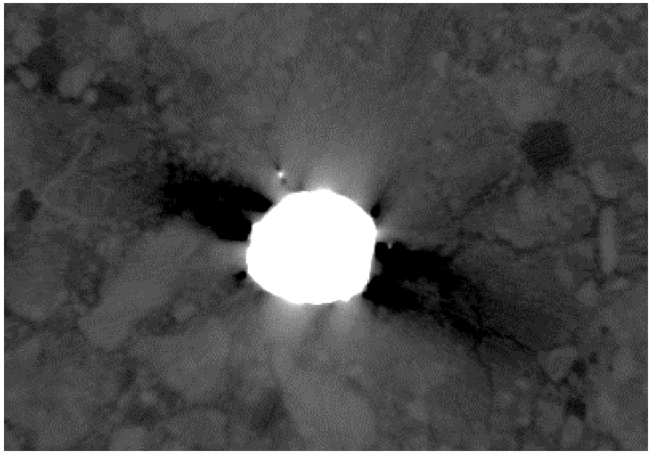

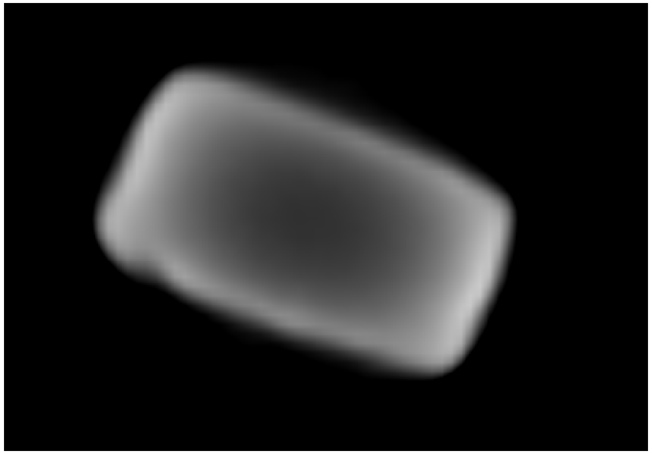

2 mm

1mm

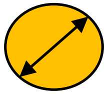

0.5mm

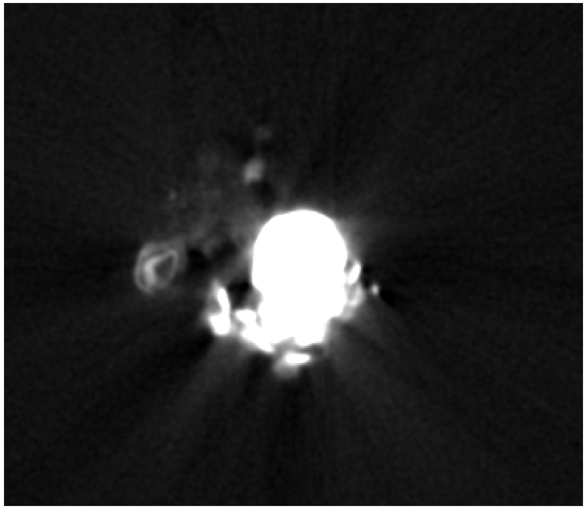

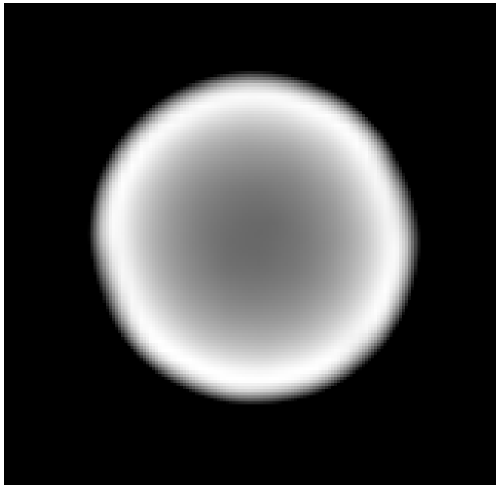

Uranium Corrosion Results

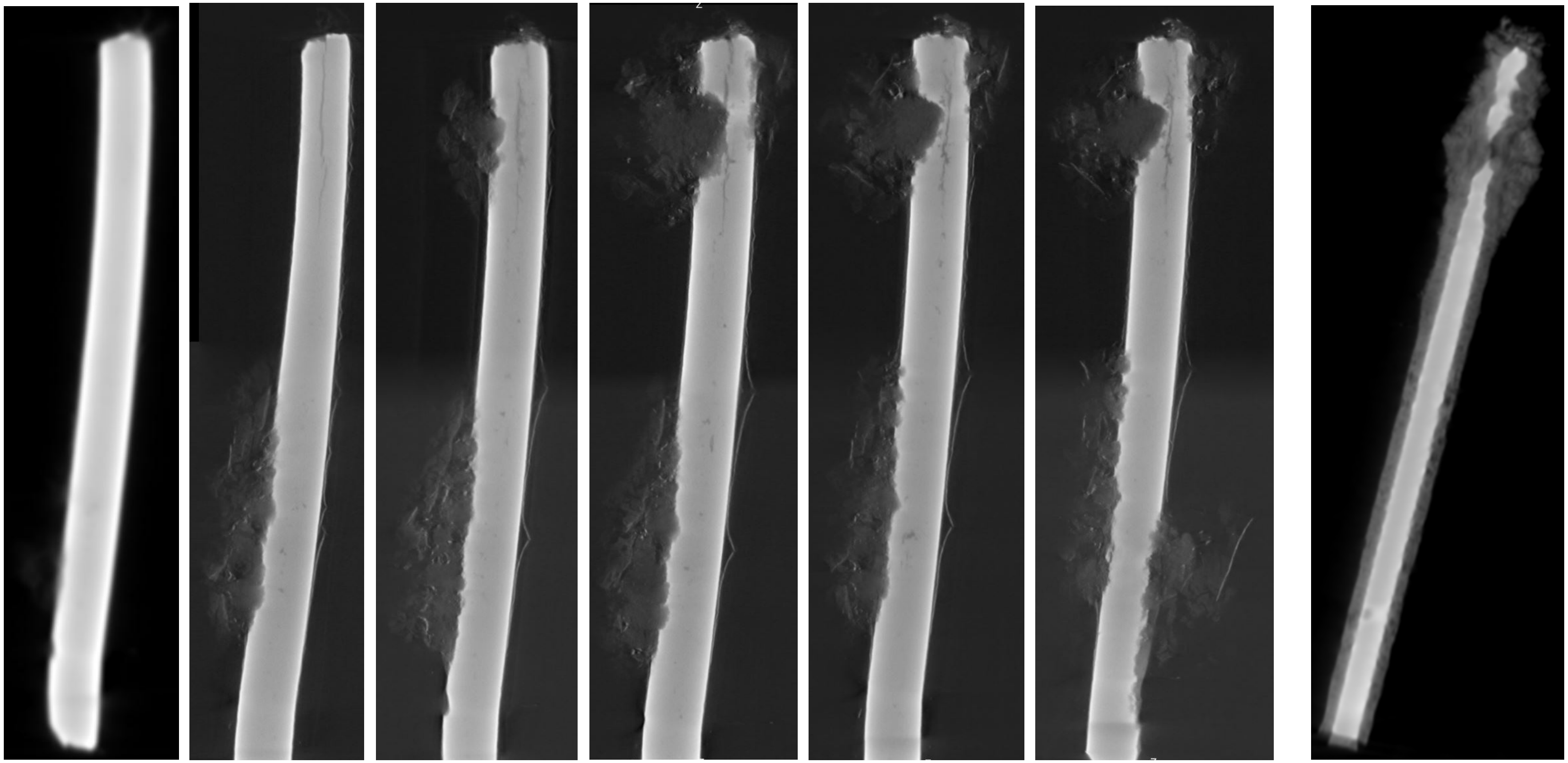

Day:	1	14	23	44	65	84	600

[5]

[#]Interface Analysis Centre, University of Bristol,

Uranium Corrosion Results

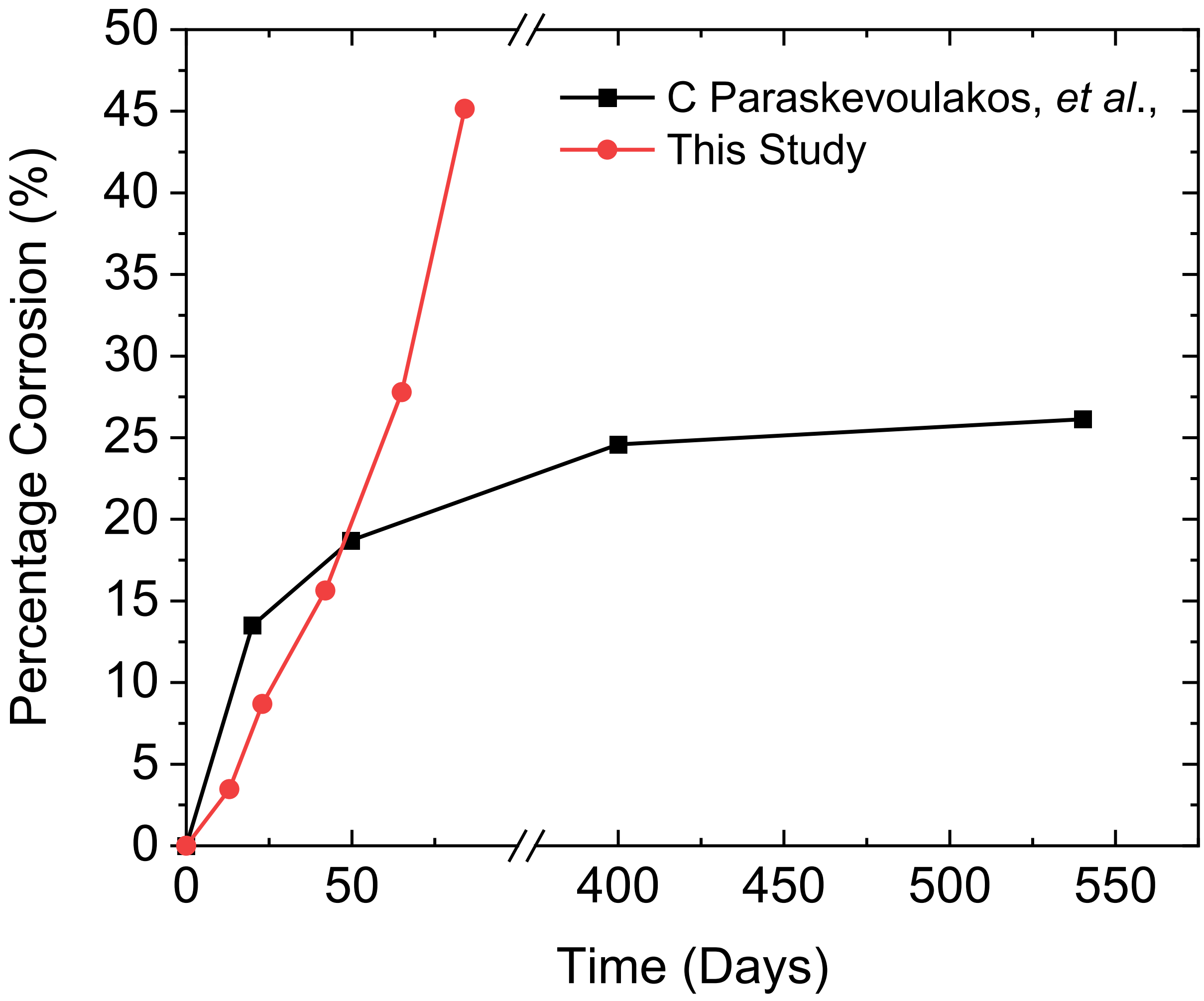

New Uranium Corrosion Samples

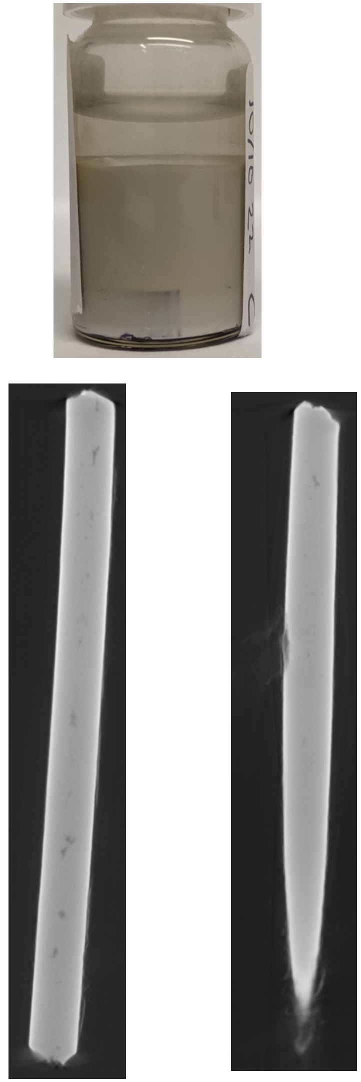

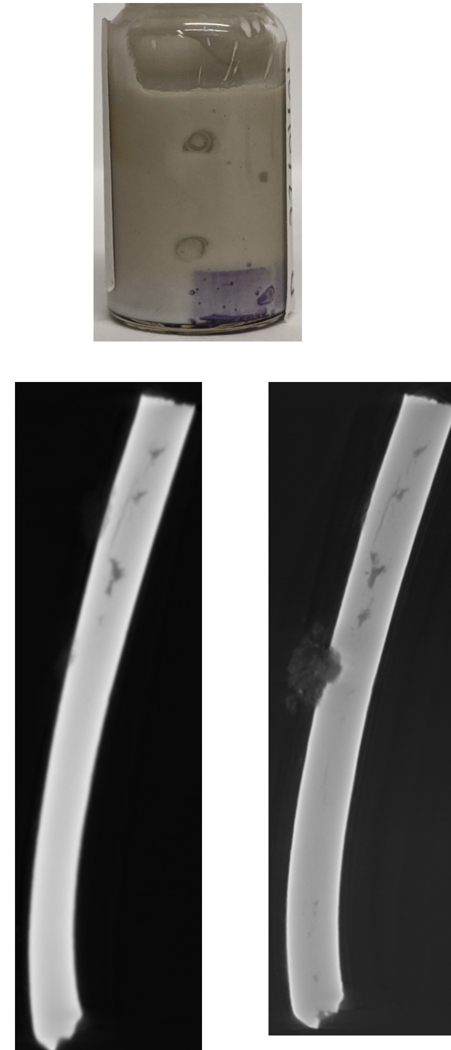

[#]Interface Analysis Centre, University of Bristol,

Sellafield Ltd

Future plans

- **Neutron** beam time
- More Samples
- Changes to **sludge structure**
  - Sludge drying
  - Pore Network Modelling

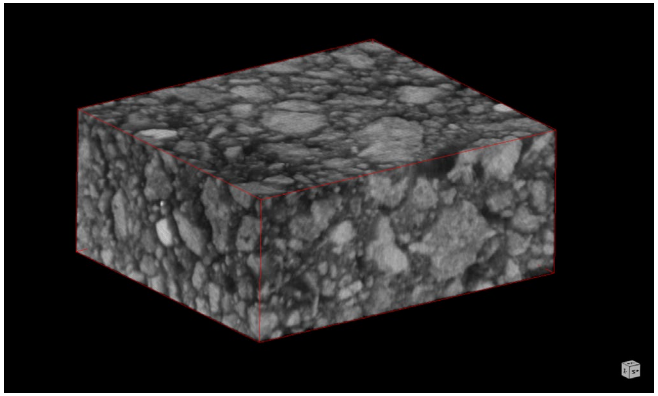

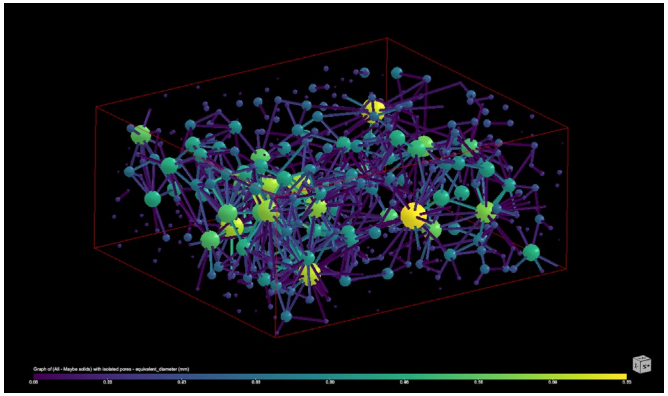

[#]Interface Analysis Centre, University of Bristol,

Acknowledgments:

Tom Scott
Ross Springell
Chris Jones
Haris Paraskevoulakos
Antonis Banos
Lottie Harding

Thank you for listening

vr19802@bristol.ac.uk

References:

[1] A Banos *et al.,* A review of the reaction rates of uranium corrosion in water, 2020
[2] A Banos *et al.,* A review of uranium corrosion by hydrogen and the formation of uranium hydride, 2018
[3] C Paraskevoulakos *et al.,* Monitoring the degradation of nuclear waste packages induced by interior metallic corrosion using synchrotron X-ray tomography, 2019
[4] M Johnson, Gas retention and release from nuclear legacy waste, 2018
[5] C Paraskevoulakos *et al.,* Monitoring uranium corrosion in Magnox sludge using X-ray computed tomography: A direct analogue to "legacy“ fuel storage ponds, 2020

Effect of shear rate and surface potential on particle interaction and aggregation in nanofluids

Dr. Lee Mortimer, University of Leeds

Prof. Mike Fairweather, University of Leeds

1st-2nd November 2022
TRANSCEND Annual Meeting
Glasgow, UK

BACKGROUND

- At **Sellafield Ltd**, waste suspension sludge flows transport solid-liquid mixtures of radioactive legacy material from ponds, silos and tanks to other interim locations where they can be safely stored.

- Such retrievals are currently underway during **POCO** operations in plants such as the First Generation Magnox Storage Pond and for a dewatering mechanism of dedicated sludge packaging plant 1 as well as a number of associated packaging, export and encapsulation plants, and settling, decant and storage tanks.

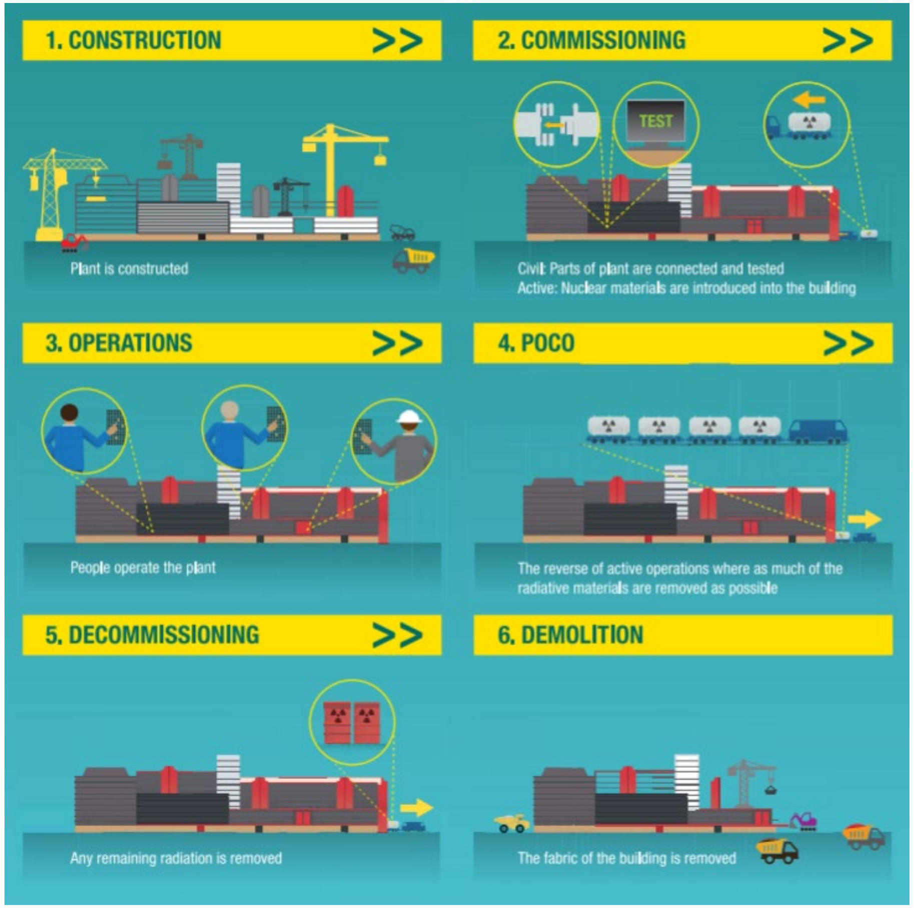

Sellafield magazine – Issue 02, 2015.

MOTIVATION & BEHAVIOURAL MODIFICATION

Pile fuel storage pool at Sellafield - IAEA Nuclear Energy Series No. NW-T-2.6 - Decommissioning of Pools in Nuclear Facilities, IAEA.

- That said, present transportation and settling processes containing sub-micron particles are often executed sub-optimally and carried out with caution due to the complex nature of the wastes and a lack of understanding of their flow or interaction behaviour.

- In practice, the behaviours associated with these activities are sensitive to the chemical and material properties as well as flow conditions and presence of other phases.

- This sensitivity is capable of being exploited and the modification of such quantities to obtain a desired outcome is referred to as **behavioural modification**.

MOTIVATION

- In developing such techniques, solutions can be generated to discourage or encourage particle agglomeration within transport flows and settling tanks, ultimately controlling the extent of long-term particle migration and flocculation.

MOTIVATION

- To develop beneficial behavioural modification techniques the system response to deviations in key parameters must be known.

- It is difficult to probe the effects of such variations experimentally for specific parameter sets.

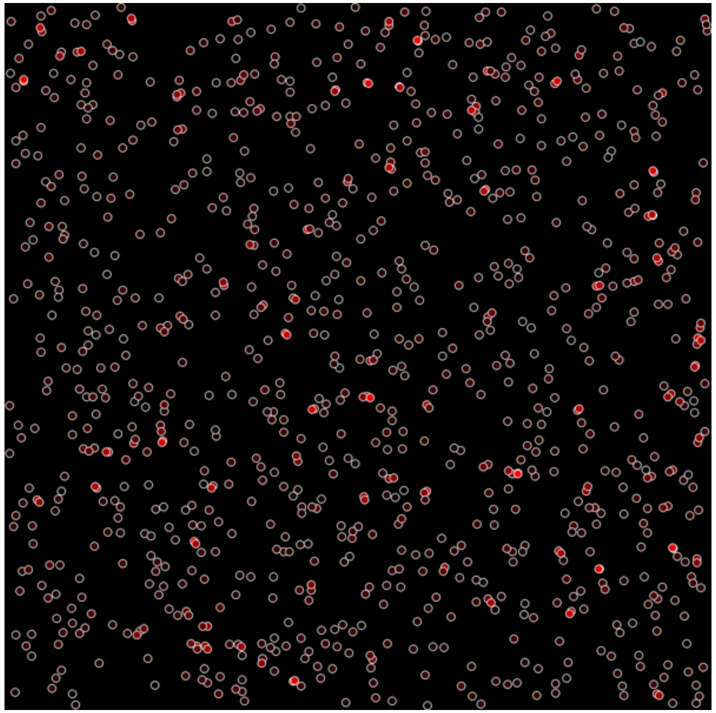

LOW HAMAKER CONSTANT

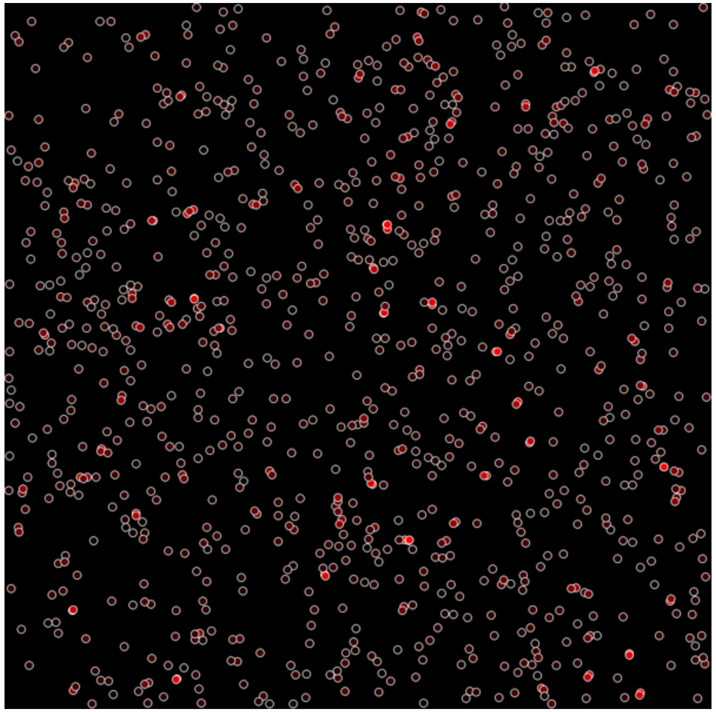

HIGH HAMAKER CONSTANT

- Computer simulations provide a means to overcome this difficulty by providing the capability to specify and explore the impact of changes to a set of precise system parameters.

DLVO THEORY

- Prediction of and control over the stability of nano- and micro-particulate suspensions remains an important issue of relevance to many industries including energy storage, medicine, and nuclear waste management.

- Calculation of intersurface forces is conventionally described by the well-known DLVO theory (Derjaguin and Landau 1941, Verwey and Overbeek 1948), which accounts for the van der Waals and electrostatic double layer forces.

- The former is a short-range attractive interaction, a consequence of quantum dynamics. The latter accounts for the electrostatic repulsion of the double layer, which aids to stabilize the suspension.

- At low ionic strengths, particles require a large amount of kinetic energy in order to overcome the energy barrier causes by the electrostatic interaction, whereas at high ionic strengths, the potential barrier collapses.

- Hence, particles are much more likely to reach small separation distances where van der Waals interaction dominates and the particles begin to aggregate, forming flocs.

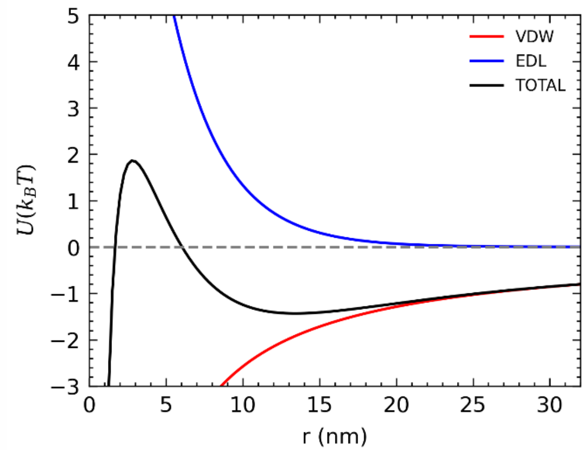

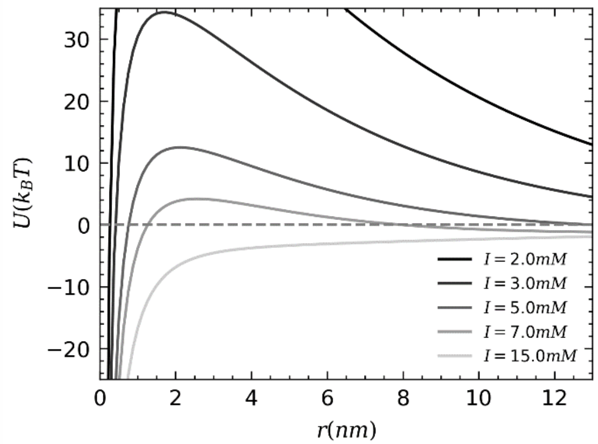

Parameter	Value
r_P	250nm
A	$5 \times 10^{-21} J$
σ	$0.002 C/m^2$
I	$0.008 M$

IONIZING RADIATION FOR BEHAVIOURAL MODIFICATION

- One technique capable of modifying these properties is to irradiate the particulate suspensions, which is in some cases unavoidable, such as in nuclear waste suspensions. Various experimental studies have been performed over the years to study these effects.

Holmboe et al. (2009):

- Effect of ionizing radiation (doses of 0–53.2 kGy) on colloidal Na^+-montmorillonite from bentonite barriers in spent nuclear fuel.
- They observed that irradiated colloidal particles displayed enhanced colloid stability compared to unirradiated colloidal particles and calculated an increase in the magnitude of the zeta potential of 0.67mV (sphere-sphere).
- The authors also suggest that this process could also be down to the generation of aqueous radiolysis products, but that the dominant mechanism was an increase in the surface potential.

(Jonsson, 2012):

- Review article on spent nuclear materials.
- Attributed the change in colloidal stability to the increase in particle surface potential.
- Showed that sedimentation effects are also altered by pre-irradiation wherein sedimentation is slower for irradiated suspensions when the ionic strength is increased.
- Confirms the surface potential theory by considering experiments where the liquid phase was removed and replaced after irradiation, with the observed effects persisting even after the liquid phase is replaced.

SIMULATION TECHNIQUES

- The accuracy and reliability of such calculations is based upon both the order of the discretisation techniques used for each phase, as well as the fidelity of the models used to predict the wide array of interactions between the phases.

CONTINUOUS PHASE

Direct numerical simulation (DNS)

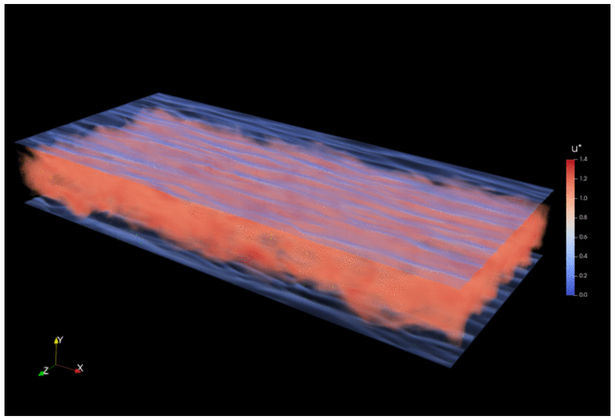

PARTICULATE PHASE

Lagrangian particle tracking (LPT)
Immersed boundaries method (IBM)

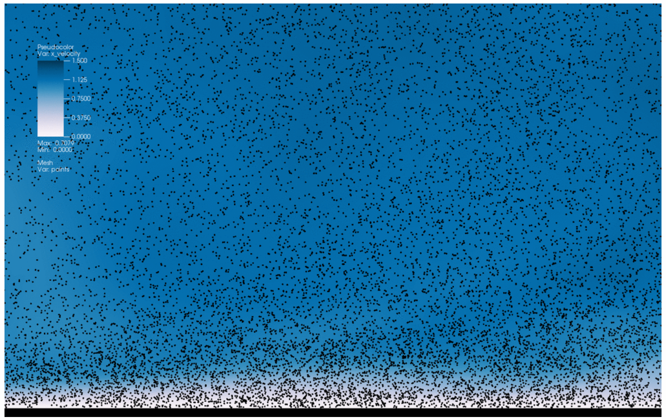

POLYMERIC PHASE

Finitely extensible nonlinear elastic model (FENE)

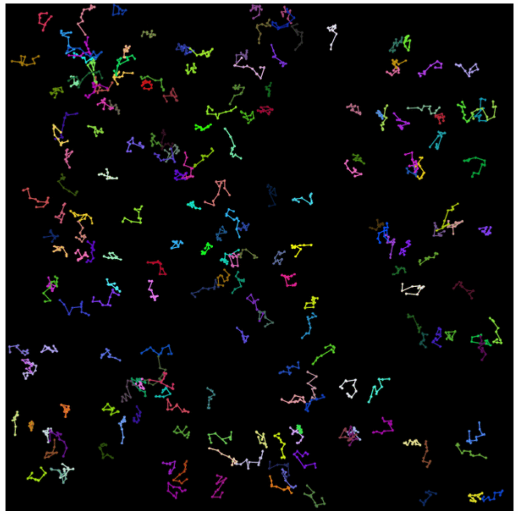

- Focus on coupling methods together to obtain a solver capable of predicting particle-fluid, particle-particle and particle-polymer interaction.

SIMULATION TECHNIQUE - PARTICLE TRACKING

$$\frac{d\boldsymbol{v_p}}{dt} = -\nabla U_T - \zeta \boldsymbol{v_p} + \boldsymbol{\eta}(t)\sqrt{\frac{6\zeta T k_B}{dt}} + \boldsymbol{F}_{SS}$$

$$U_T = U_W(r') + U_{VDW}(r) + U_{EDL}(r)$$

$$\boldsymbol{F}_{SS}(r') = \frac{4}{3}\sqrt{r_{eff}}E_{eff}r'\boldsymbol{\hat{n}}$$

$$U_{VDW}(r) = -\frac{Ar_P}{12r}$$

$$U_{EDL}(r) = \frac{2\pi r_P \sigma^2}{\epsilon_0 \epsilon_r \kappa^2} e^{-\kappa r}$$

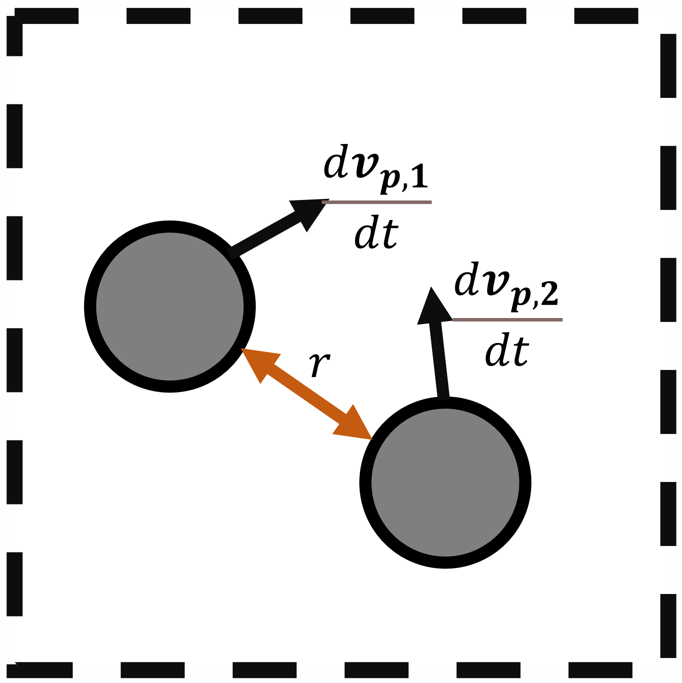

Parameter	SIM1	SIM2	SIM3	SIM4	SIM5	SIM6
$r_P (nm)$	25	25	25	25	25	25
$A\ (10^{-21} J)$	22.3	22.3	22.3	22.3	22.3	22.3
$\psi\ (mV)$	5	10	20	30	40	50
$I\ (M)$	0.01	0.01	0.01	0.01	0.01	0.01
$E\ (10^9 Pa)$	72.35	72.35	72.35	72.35	72.35	72.35
$\nu_P\ (-)$	0.31	0.31	0.31	0.31	0.31	0.31

DLVO THEORY – SIMULATION POTENTIALS

$$U_{VDW}(r) = -\frac{Ar_P}{12r}$$

$$U_{EDL}(r) = \frac{2\pi r_P \sigma^2}{\epsilon_0 \epsilon_r \kappa^2} e^{-\kappa r}$$

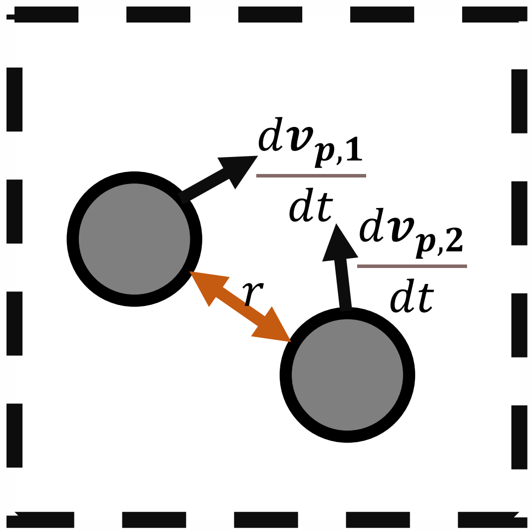

r : Separation distance
A : Hamaker constant
r_P : Particle radius
σ : Surface charge density of the particles
ϵ_0 : Permittivity of vacuum
ϵ_r : Relative permittivity (or dielectric constant)
κ : Inverse Debye length (related to ionic strength by $\kappa^{-1} = 0.3\ nm/\sqrt{I}$ in water).

- Clearly the main parameters are A, r_P, σ and I, with the ionic strength relating through to κ^{-1}.

- The surface charge density is related to the surface potential, ψ, by $\sigma = \epsilon_0 \epsilon_r \kappa \psi$.

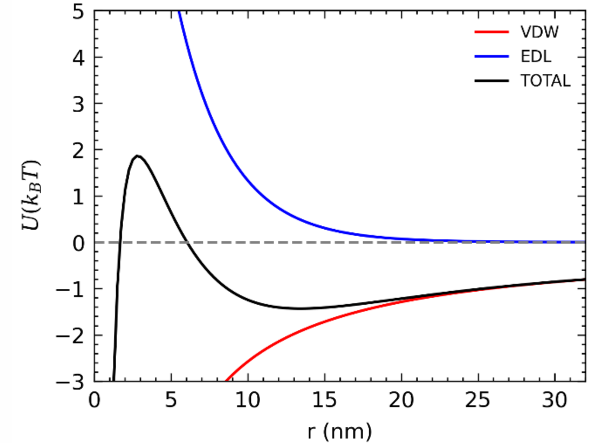

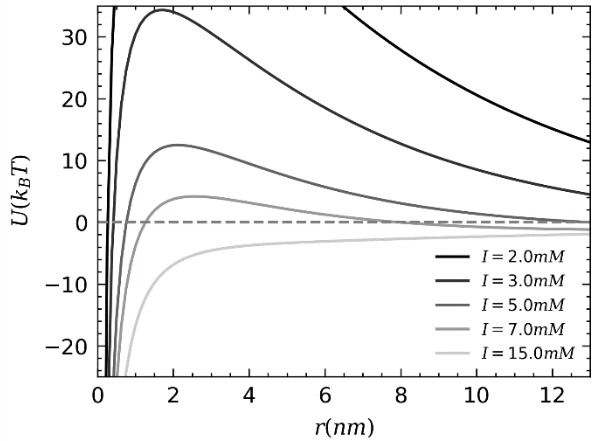

Parameter	Value
r_P	250nm
A	$5 \times 10^{-21} J$
σ	$0.002 C/m^2$
I	$0.008 M$

DLVO THEORY – SIMULATION POTENTIALS

$$U_{VDW}(r) = -\frac{Ar_P}{12r}$$

$$U_{EDL}(r) = \frac{2\pi r_P \sigma^2}{\epsilon_0 \epsilon_r \kappa^2} e^{-\kappa r}$$

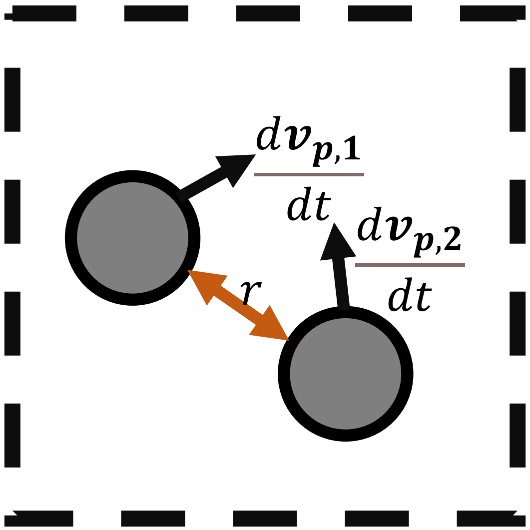

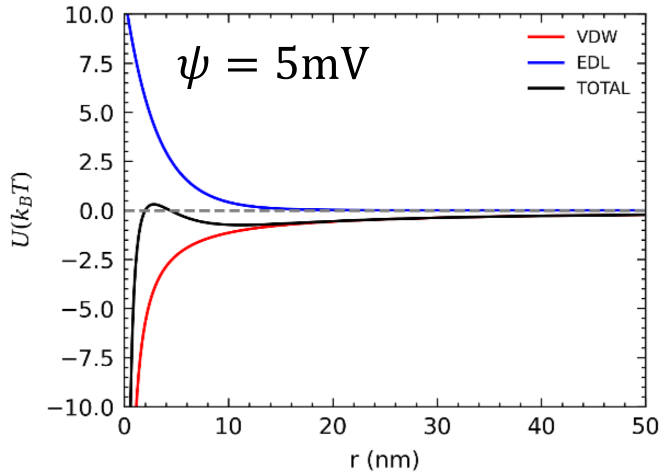

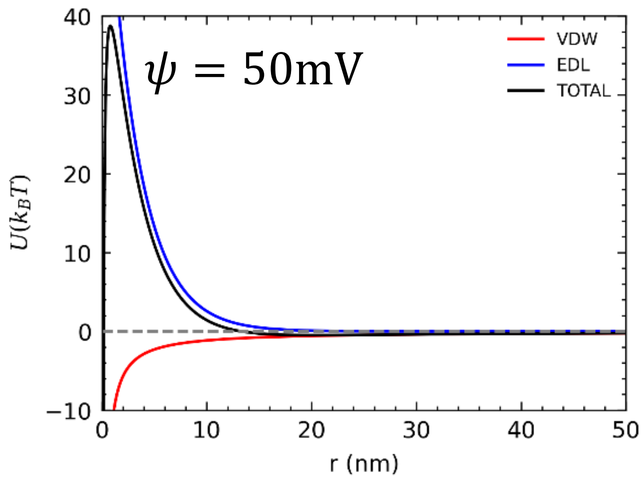

Parameter	A	B
$r_P (nm)$	25	25
$A\ (10^{-21} J)$	22.3	22.3
$\psi\ (mV)$	5	50
$I\ (M)$	0.01	0.01
$E\ (10^9 Pa)$	72.35	72.35
$\nu_P\ (-)$	0.31	0.31

RESULTS – 2D SIMULATIONS (25nm radius)

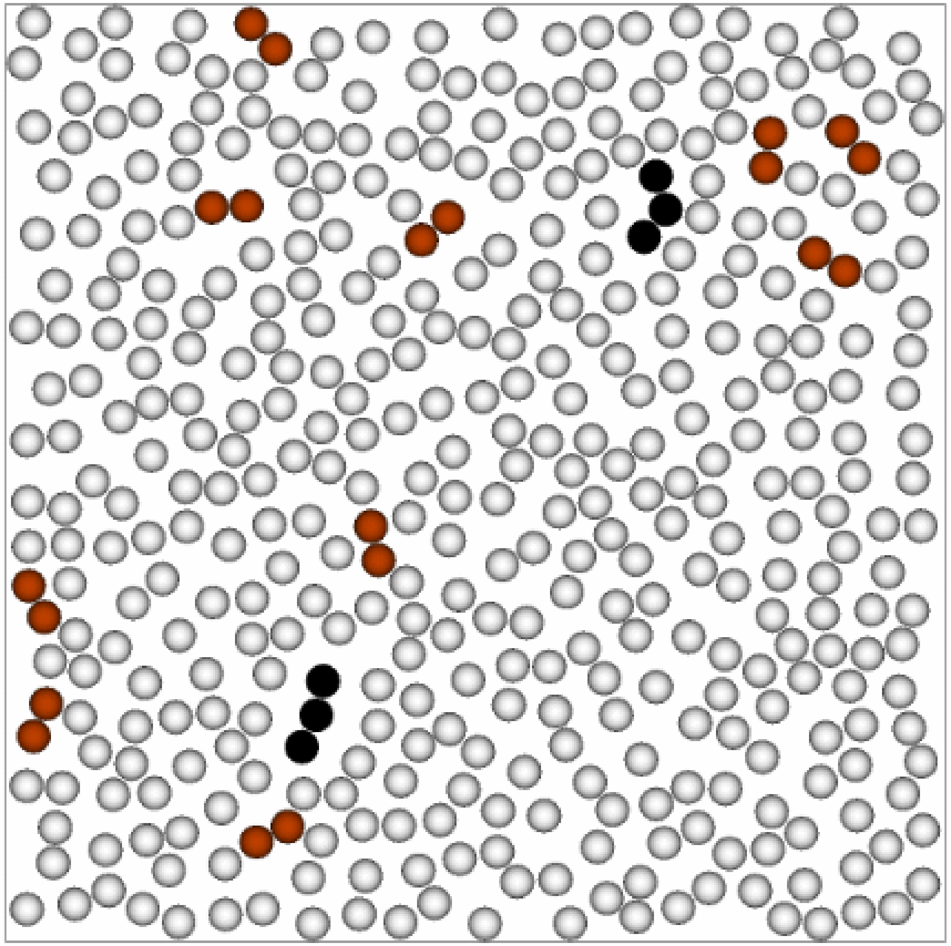

Parameter	SIM1
$r_P (nm)$	25
$A\ (10^{-21} J)$	22.3
$\psi\ (mV)$	5
$I\ (M)$	0.01
$E\ (10^9 Pa)$	72.35
$\nu_P\ (-)$	0.31

RESULTS – 2D SIMULATIONS (25nm radius)

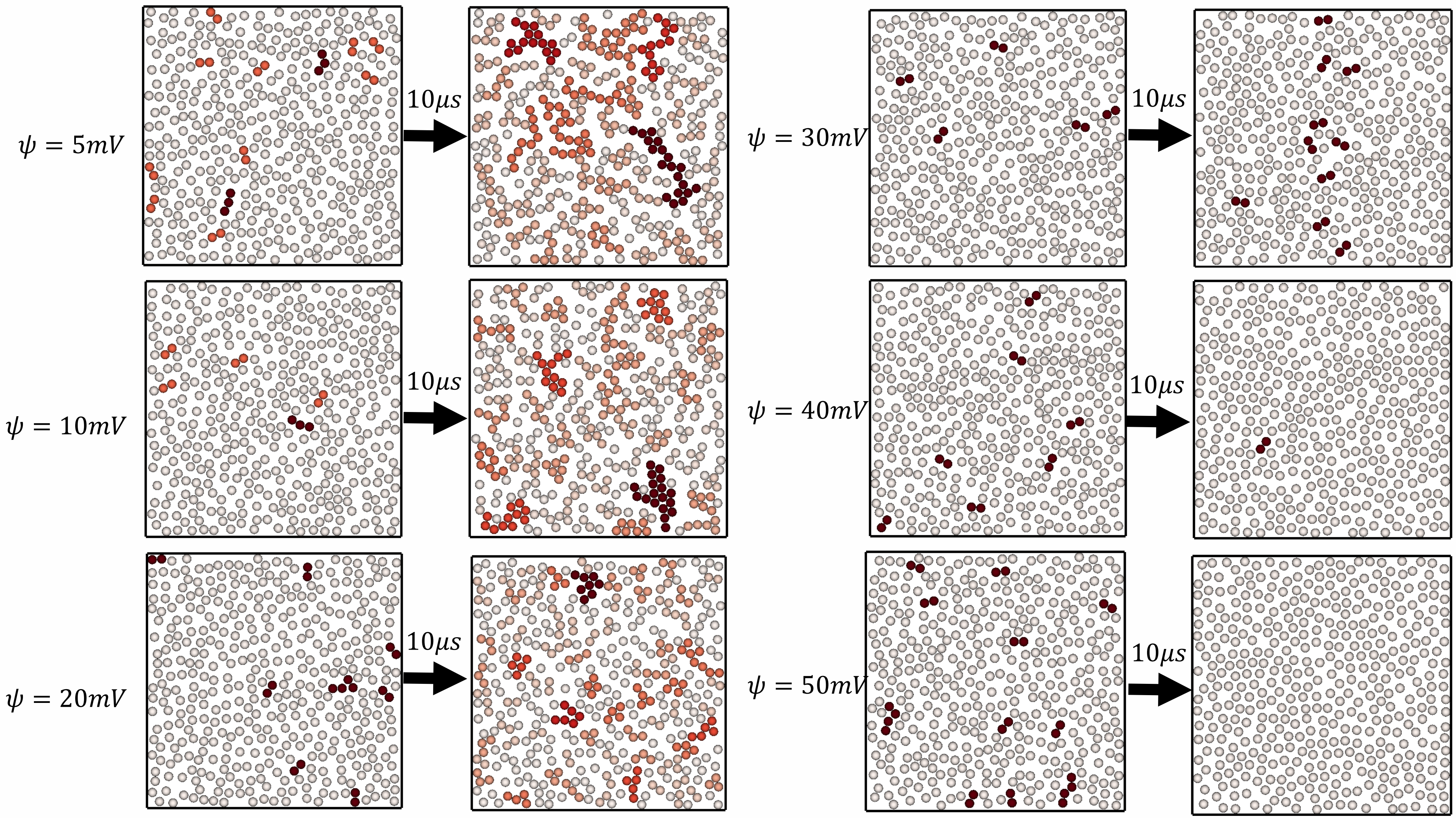

RESULTS – 2D SIMULATIONS (25nm radius)

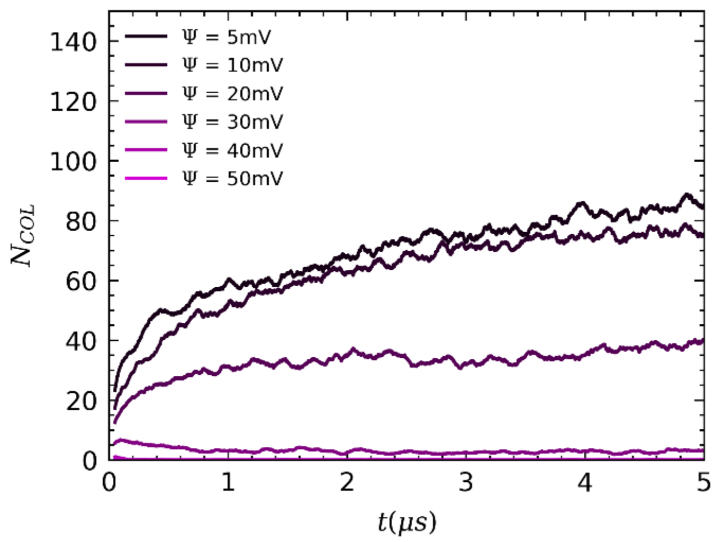

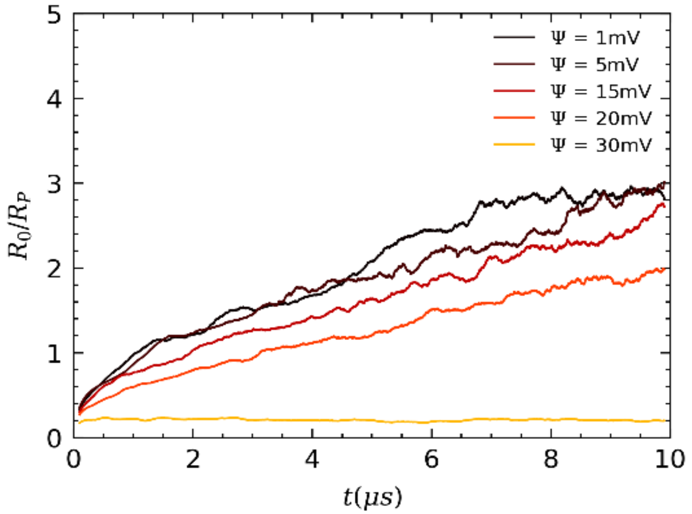

Collision rate

- Increase in surface potential due to ionizing radiation leads to fewer collisions between particles, reducing to zero collisions beyond 30mV.
- 5mV and 10mV dynamics comparable, with 20mV leading to drastic decrease in small surface-surface distance interactions

Radius of gyration of aggregate structures

- As surface potential is increased, mean radius of gyration of structures is also reduced, leading to more stable suspension.
- Size of clusters is proportional to collision rate, and similar magnitude observations are demonstrated as above.

RESULTS – 2D SIMULATIONS (25nm radius)

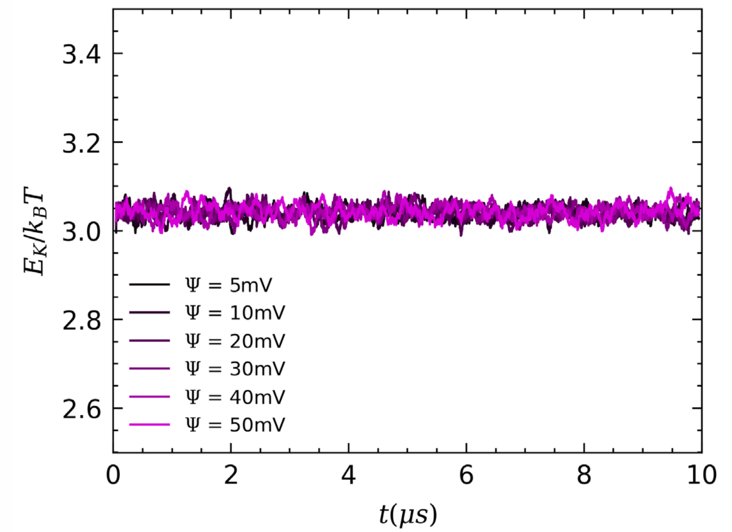

Mean kinetic energy per particle

- Mean kinetic energy per particle remains approximately constant throughout the simulation.

- Comparing to interaction potentials, we observe that the average $E_K/k_BT = 3.05mV$ is sufficient to overcome the primary maximum for $\psi = 5mV$, whereas by $\psi = 50mV$, the potential barrier is too large.

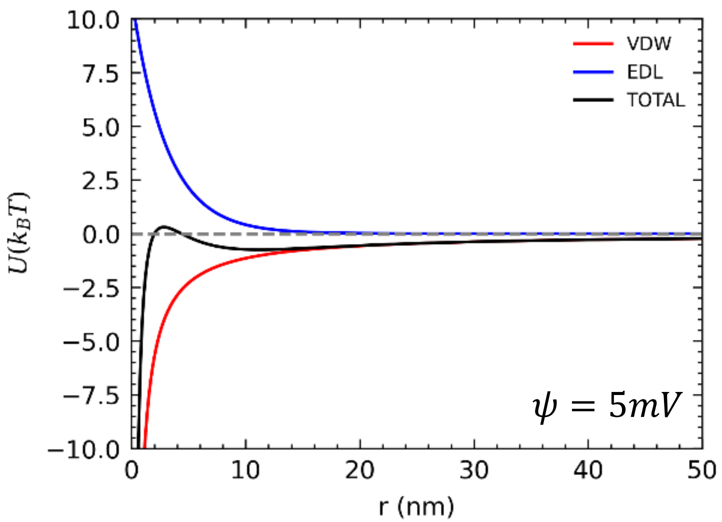

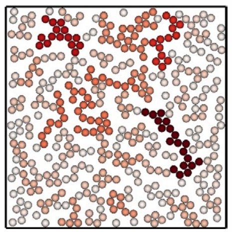

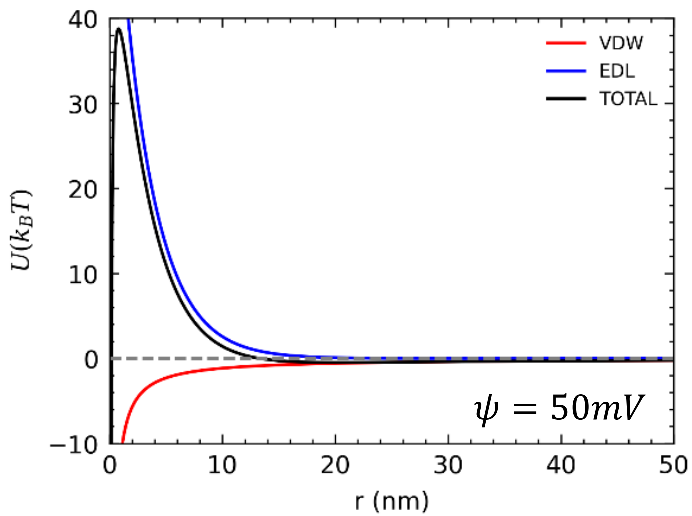

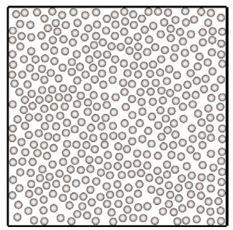

Transformative Science and Engineering for Nuclear Decommissioning

RESULTS – SHEAR FLOW

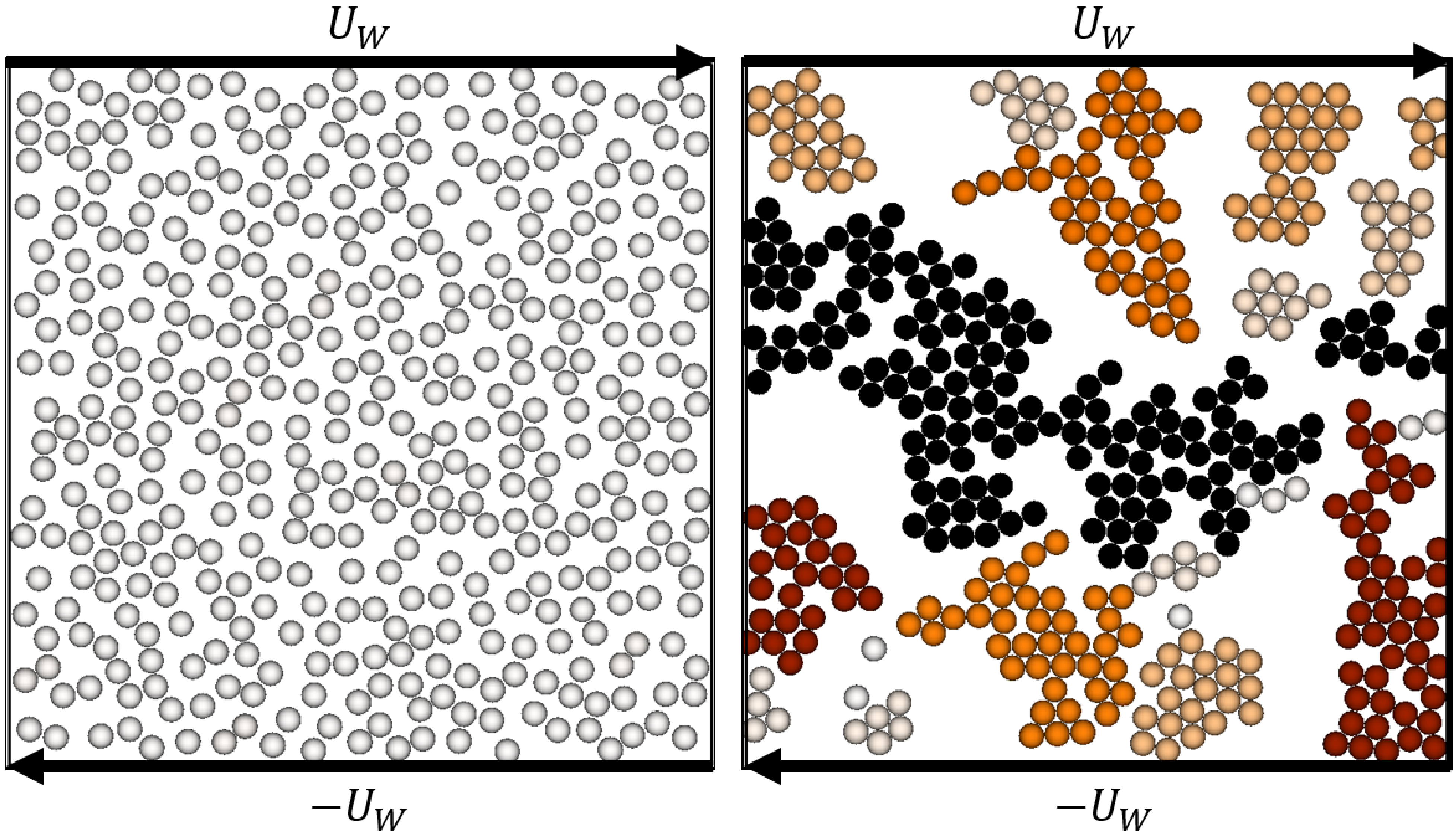

RESULTS – SHEAR FLOW

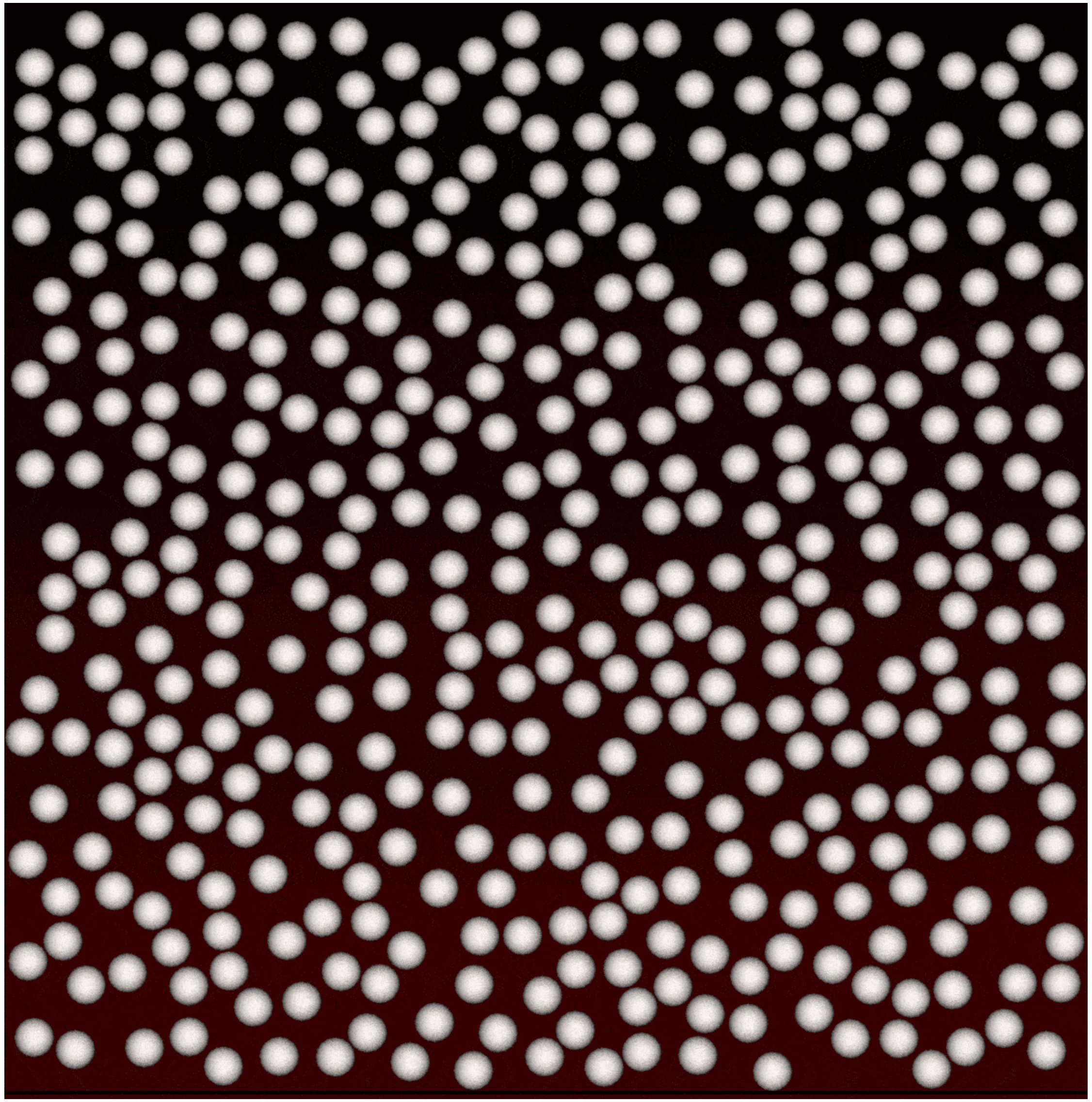

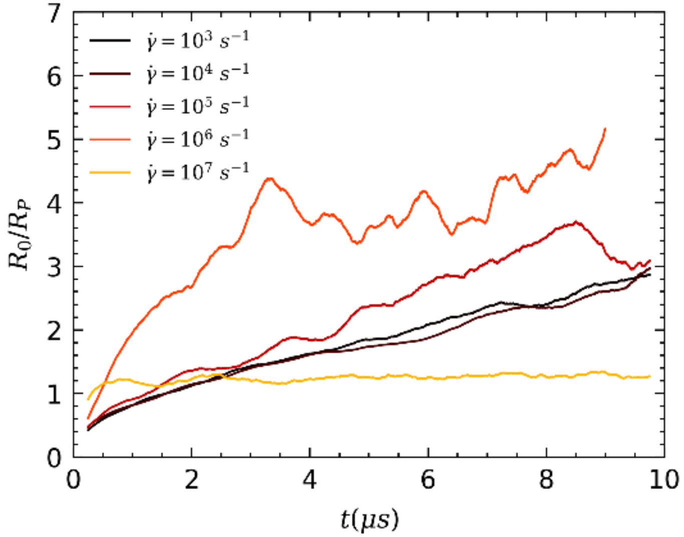

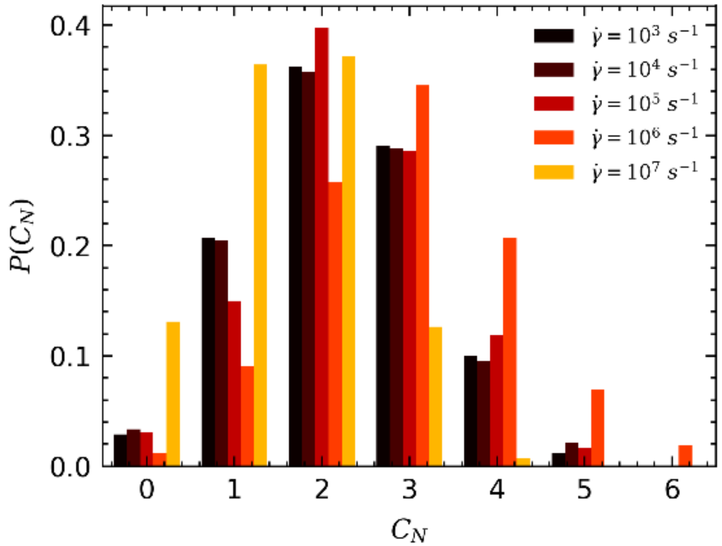

COORDINATION NUMBER

Conclusions & Further studies

Conclusions

- Calcite-water nanoparticulate suspensions have been simulated using Langevin dynamics and DLVO interaction in order to study the effect of surface potential and shear rate on aggregation dynamics.

- It has been demonstrated that reducing the surface potential instigates increased aggregation in stagnant flows. Under shear conditions, particles undergo aggregation up to $\dot{\gamma} = 10^6\ s^{-1}$, beyond which the clustering processes are hindered.

3D simulations, specific validations, sensitivity studies

- Additional dimension just requires more compute time and resources, but would provide more accurate data surrounding important properties such as radius of gyration and fractal dimension / porosity of clusters. Also validation against experimental data of aggregating systems.

Experimental work on surface potential increase (zeta potential measurements)

- Knowledge surrounding zeta potential increase due to exposure to radiation would be useful in order to use the model to predict stability timescales, since the effects seem temporary once removed from radiation source.

More complex interaction dynamics

- Various other extensions to DLVO theory, as well as other interaction forces (lubrication etc.) which should be explored.

PUBLISHED WORK ON BEHAVIOURAL MODIFICATION

Mortimer LF, Fairweather M., 2022. Langevin dynamics prediction of the effect of shear rate on polymer-induced flocculation. Tech. Mech. (Under review)

Mortimer LF, Fairweather M., 2022. Prediction of polymer extension, drag reduction and vortex interaction in direct numerical simulation of turbulent channel flows. Physics of Fluids. 33 (7), 073318 doi: 10.1063/5.0094978

Mortimer, L. F. and Fairweather, M., 2021. Assessment of behavioral modification techniques through immersed boundary method simulation of binary particle interactions in isotropic turbulence. *Physics of Fluids.* 33 (3), 073307 doi: 10.1063/5.0049779

Mortimer, L. F. and Fairweather, M., 2020. Density ratio effects on the topology of coherent turbulent structures in two-way coupled particle-laden channel flows. *Physics of Fluids. 32* (10), 103302. doi: 10.1063/5.0017458

Mortimer L. F., Njobuenwu D. O. , Fairweather M., 2020. Agglomeration dynamics in liquid–solid particle-laden turbulent channel flows using an energy-based deterministic approach. *Physics of Fluids.* 32 (4) doi: 10.1063/5.0001596

Mortimer L. F., Njobuenwu D. O. , Fairweather M., 2019. Near-wall dynamics of inertial particles in dilute turbulent channel flows. *Physics of Fluids. 31 (6)* 063302 doi:10.1063/1.5093391

ACKNOWLEDGEMENTS

This work is supported by a UK Engineering and Physical Sciences Research Council grant at the University of Leeds from the TRANSCEND (Transformative Science and Engineering for Nuclear Decommissioning) project.

Thank you for your attention, happy to take any questions!

Dr. Lee Mortimer
PhD, MPhys (Hons)
Research Fellow
Office 2.22 Chemical and Process Engineering Building
School of Chemical and Process Engineering
University of Leeds
l.f.mortimer@leeds.ac.uk

Transformative Science and Engineering for Nuclear Decommissioning

Application of Electrokinetics for Remediation of Difficult-to-Measure Radionuclides from Cementitious Materials

Shaun Hemming

University of Southampton

TRANSCEND Annual Meeting
2/11/22

For a Low Carbon Future

Difficult-to-Measure Radionuclides

- Low-energy or no γ emissions
- Abundant at nuclear sites but can be overlooked due difficulty detecting them

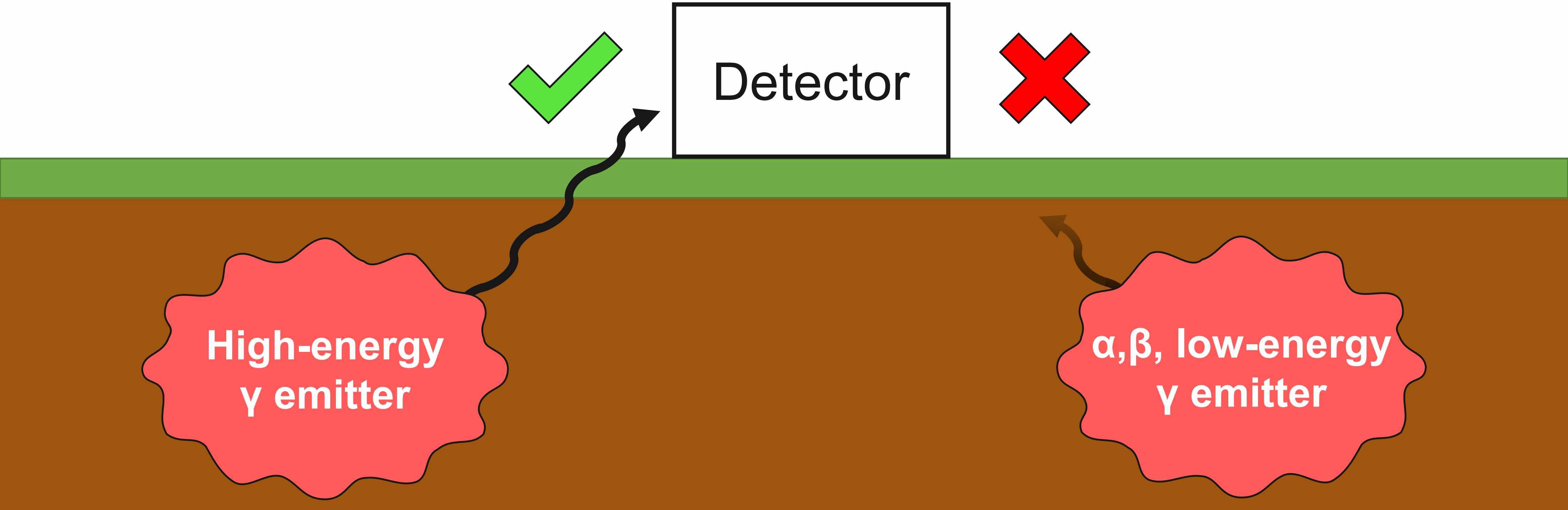

Time to reDirect Current thinking - Electrokinetic Remediation (EKR)

a) Electromigration
– Movement of ions

b) Electrophoresis
– Movement of colloids

c) Electro-osmosis
– Movement of water

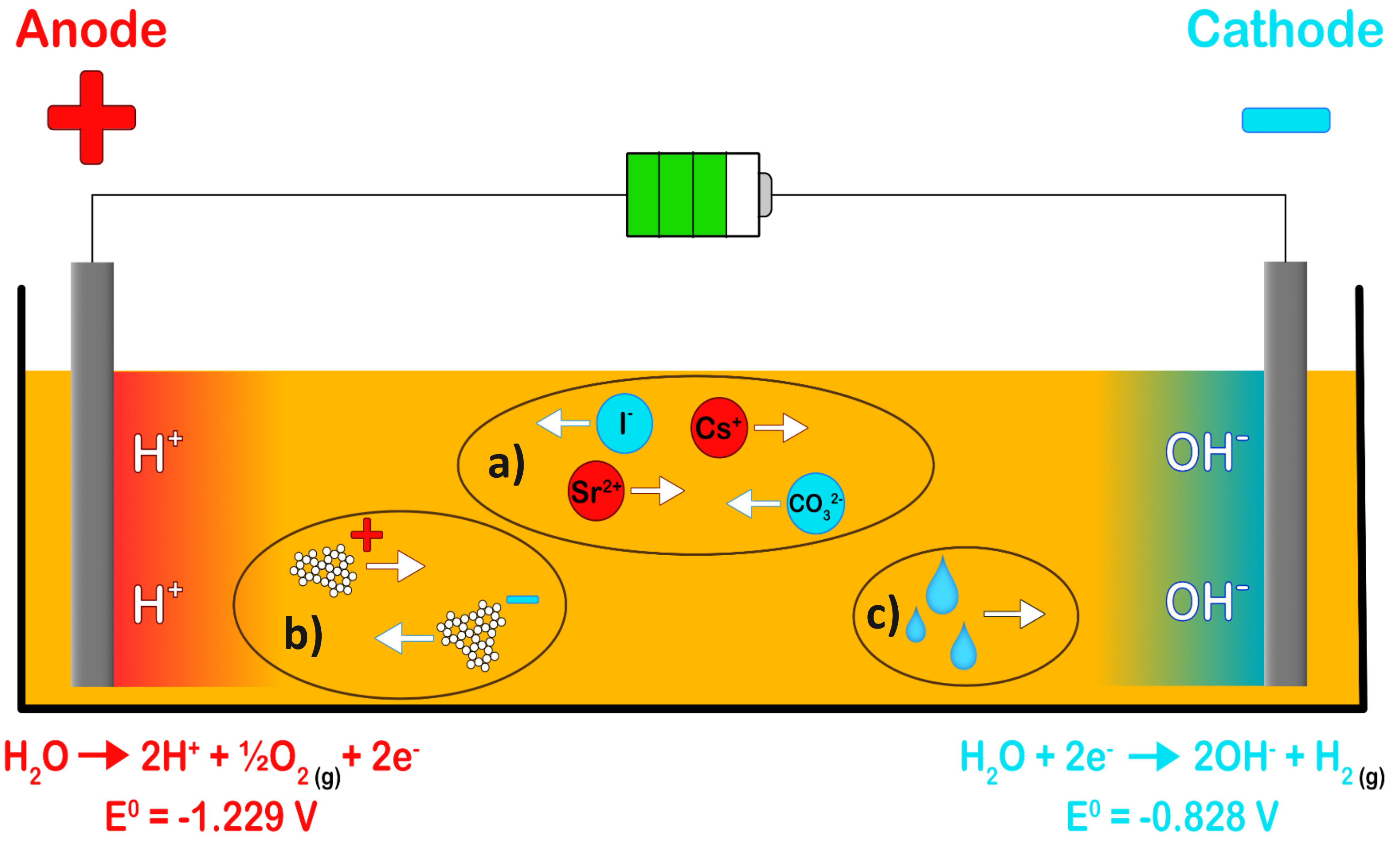

My Work – Watt am I up to?

Application of EKR for:

- **Groundwater**
  (already reported)

- **Cements**

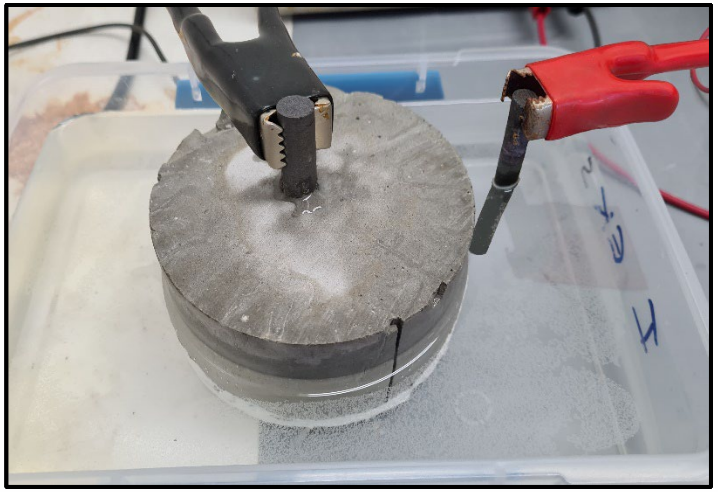

- **Sediments**
  (to come in 2023)

It-cement to be – Cement Experiments

- Targeting (per core): ^{236}**U** (9 Bq), ^{137}**Cs** (570 Bq), ^{129}**I** (1.4 KBq), ^{90}**Sr** (580 Bq) and ^{3}**H** (5.6 KBq)

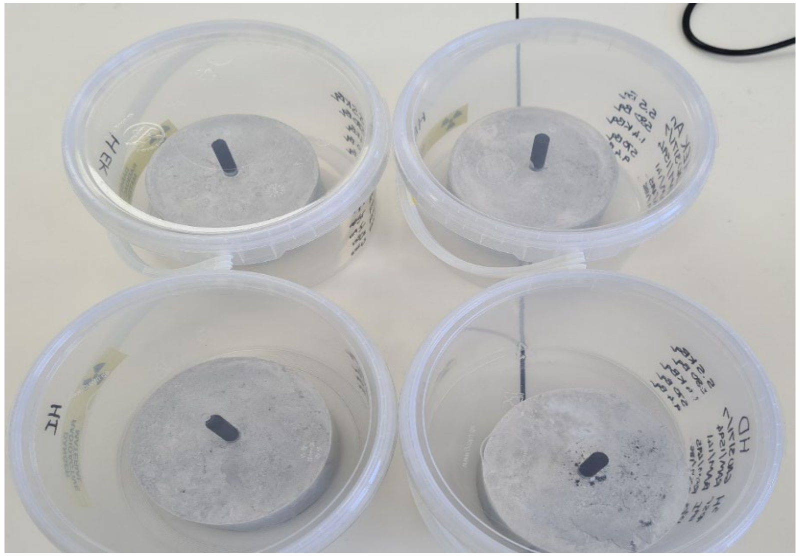

- 2 sets of cement cores:
  - Soaking Set (**S-Set**) – cores are left to harden for 28 days and then left in a radionuclide bath for 43 days
  - Homogeneous Set (**H-Set**) – radionuclides are added to the cement and water before they are mixed and left to harden for 28 days

Shocking Design – Electrokinetic Setup

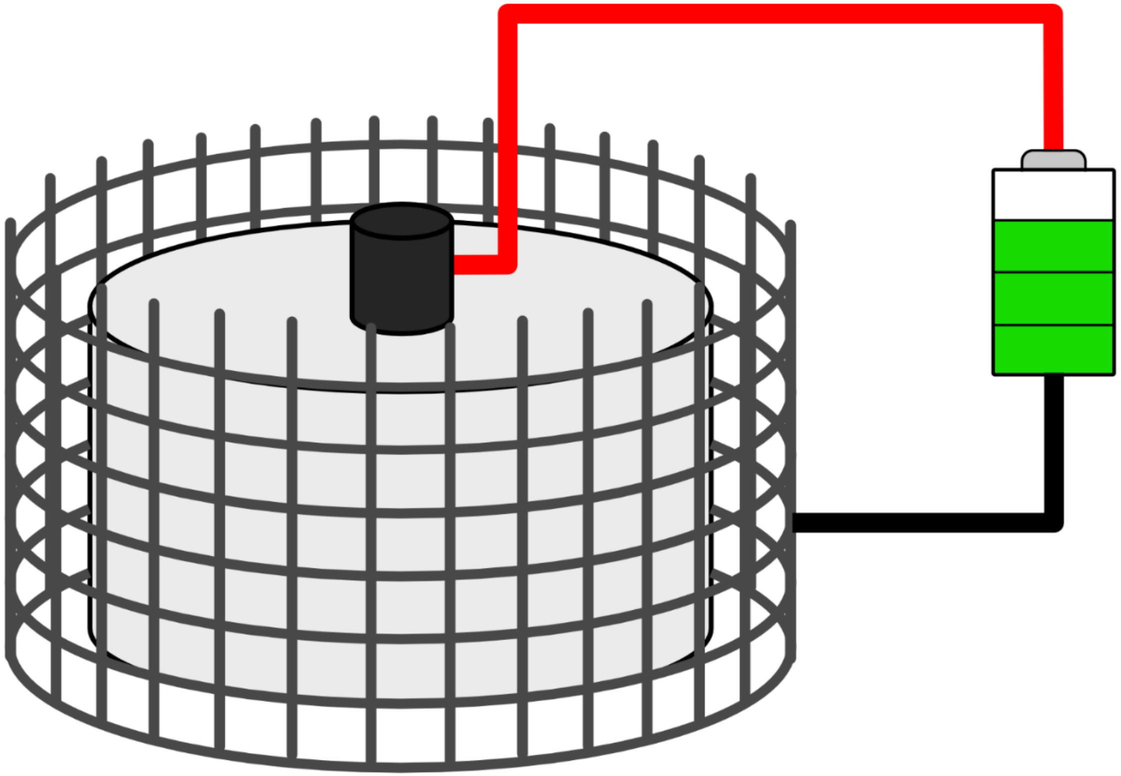

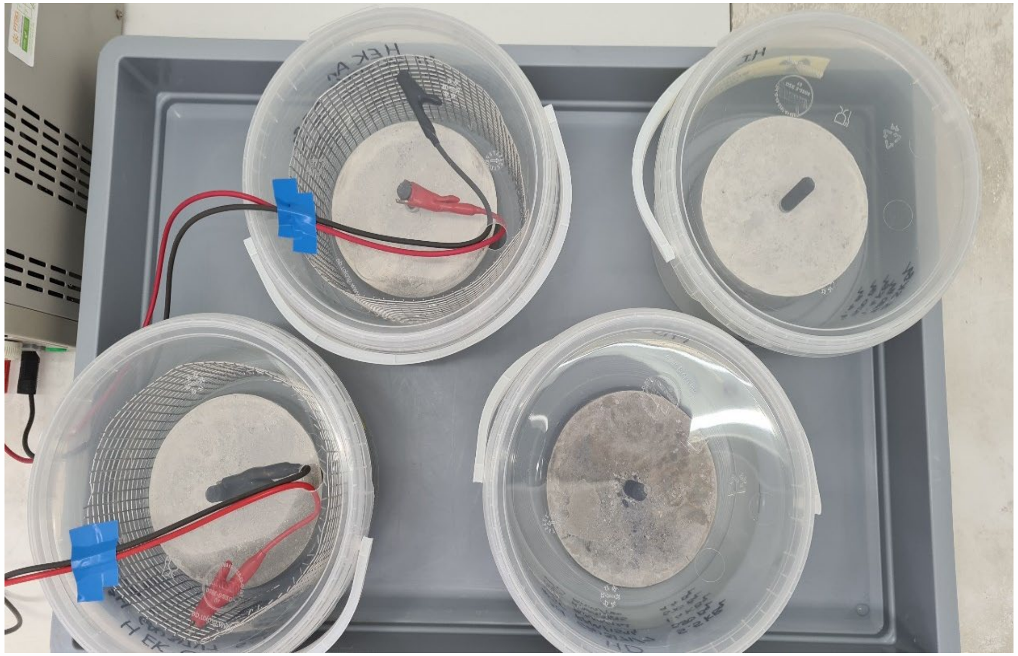

Post-EKR Observations

Wow, You've Aged – H-Set, Post-EKR

H Control

(contaminated, then left alone)

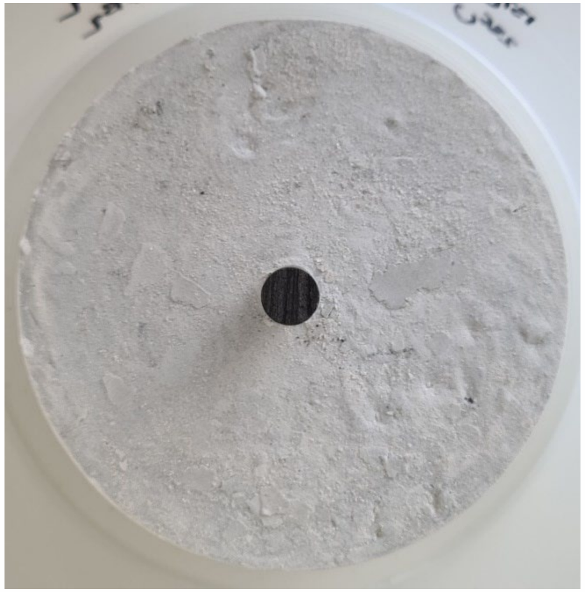

H EK Cathode

(when graphite is cathode)

H Diffusion

(contaminated, sat in electrolyte with no current)

H EK Anode

(when graphite is anode)

Transformative Science and Engineering for Nuclear Decommissioning

Déjà Vu - S-Set, Post-EKR

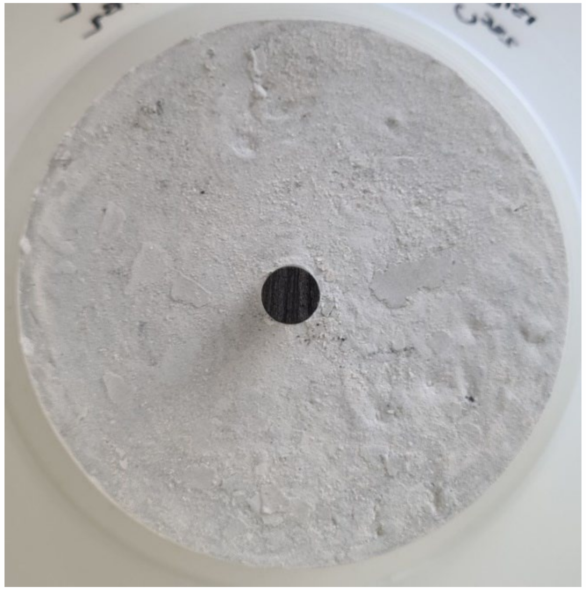

S Control

(contaminated, then left alone)

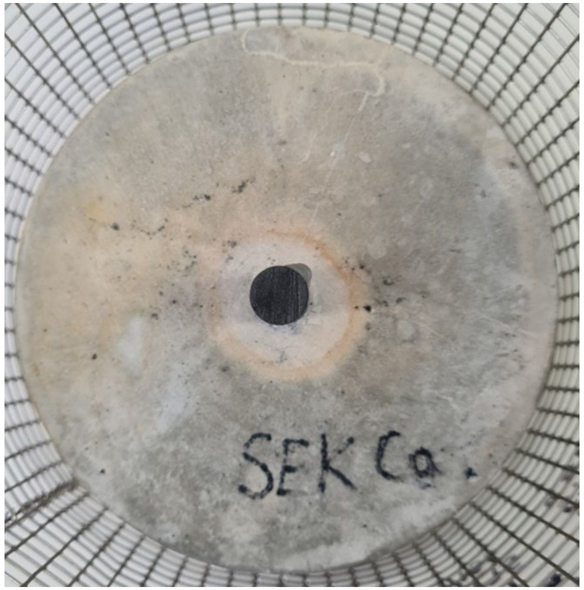

S EK Cathode

(when graphite is cathode)

S Diffusion

(contaminated, sat in electrolyte with no current)

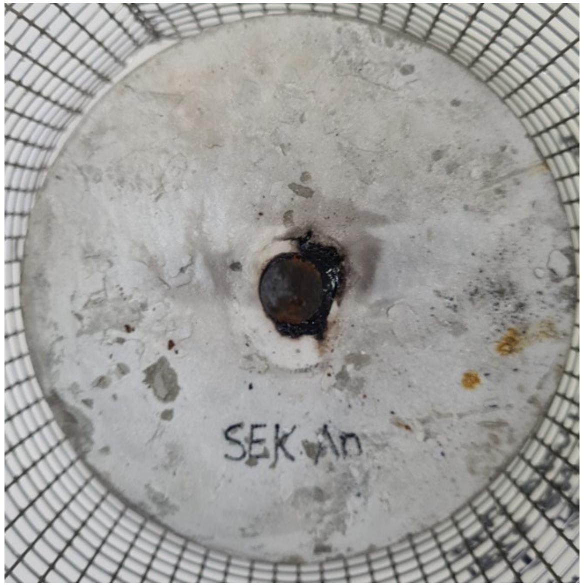

S EK Anode

(when graphite is anode)

We Came, We Sawed, We Conquered

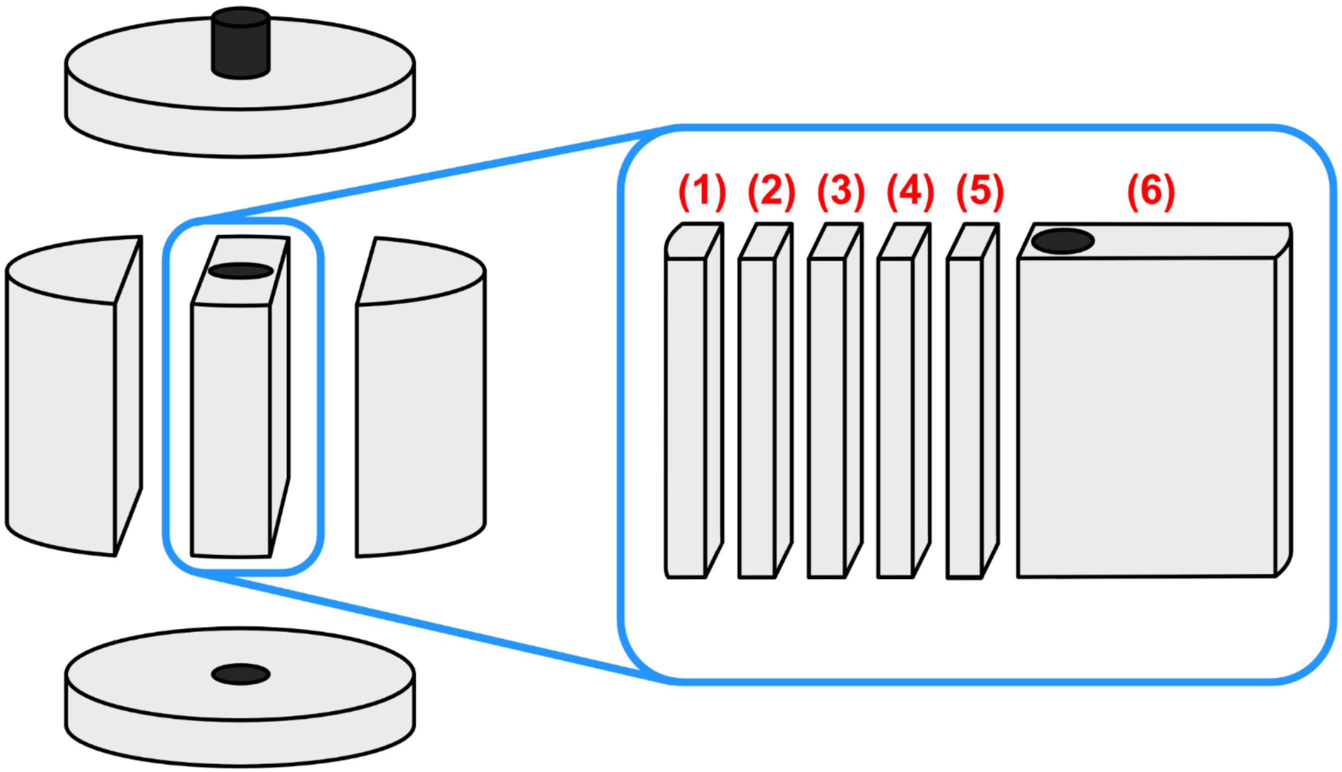

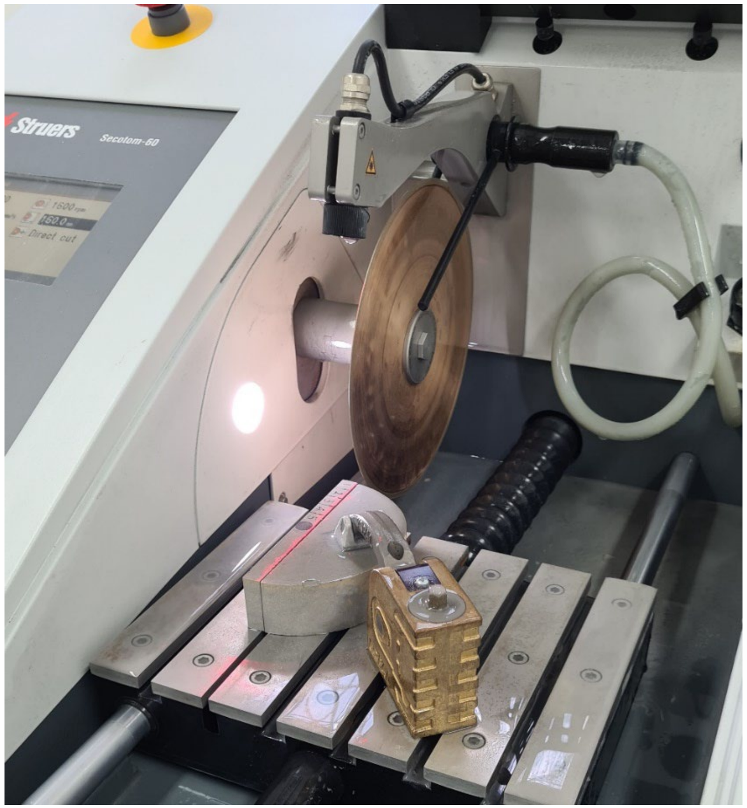

Analysis

Radionuclides Entering S-Set Cores from Soak Solution

	^{3}H	^{90}Sr	^{129}I	^{137}Cs	^{236}U
S Control	30%	26%	63%	5%	99.6%
S Diff	30%	30%	63%	4%	99.9%
S EK Cathode	26%	32%	60%	3%	99.6%
S EK Anode	26%	24%	67%	8%	99.9%
Average	**28%**	**28%**	**63%**	**5%**	**99.7%**

Transformative Science and Engineering for Nuclear Decommissioning

Where the Heck-trokinetics are They Going?!

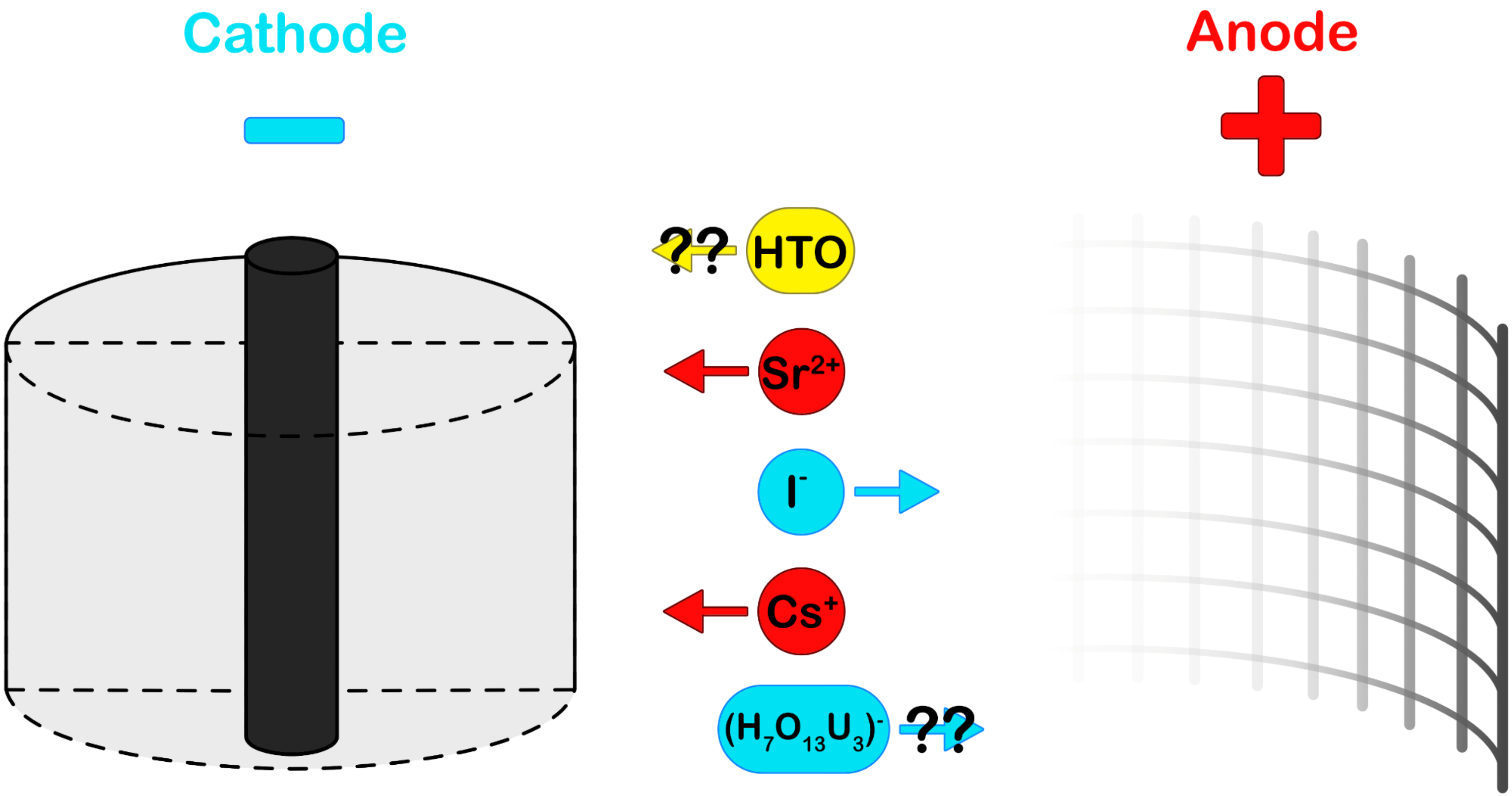

TRANSCEND

Transformative Science and Engineering for Nuclear Decommissioning

Hot off the Plate… H-Set

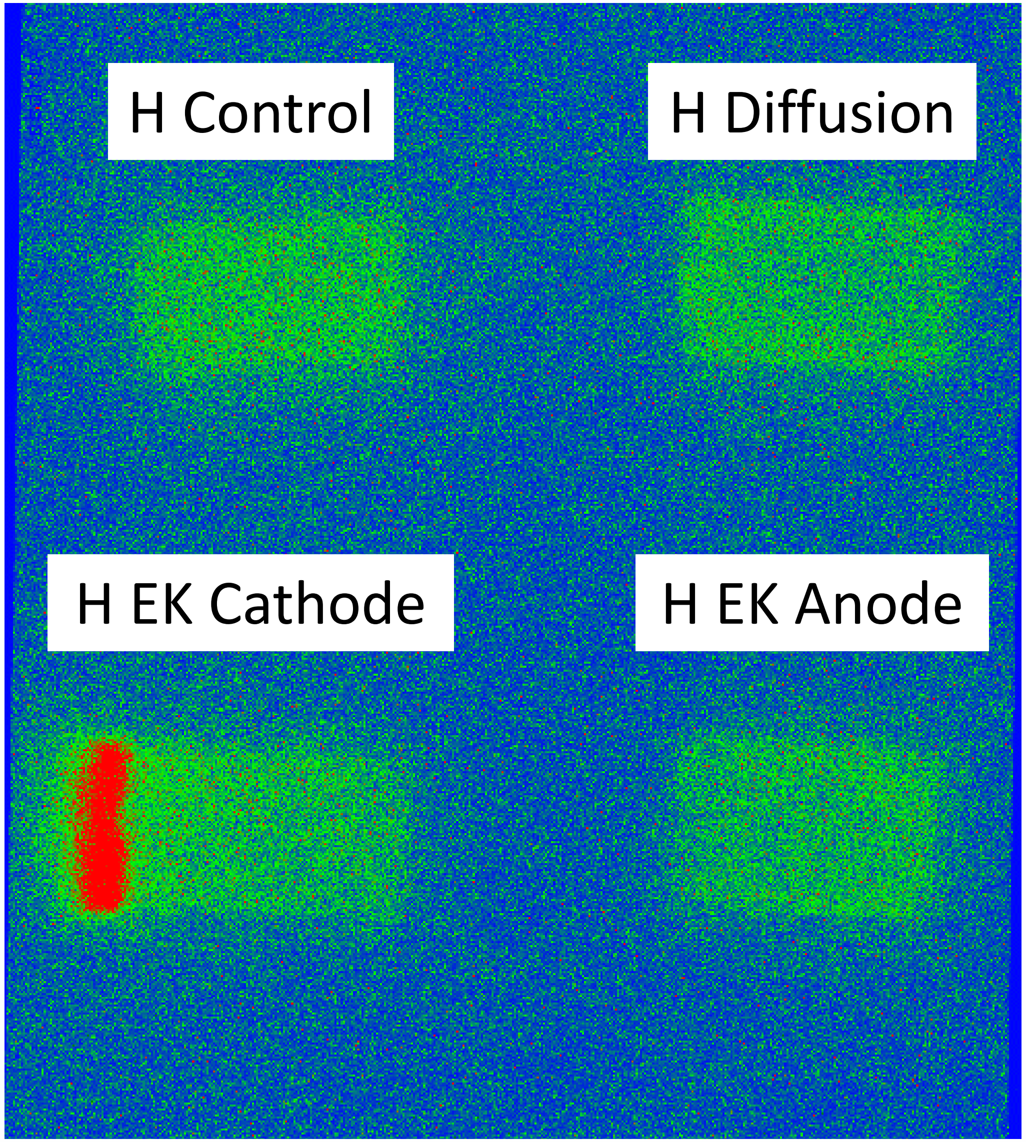

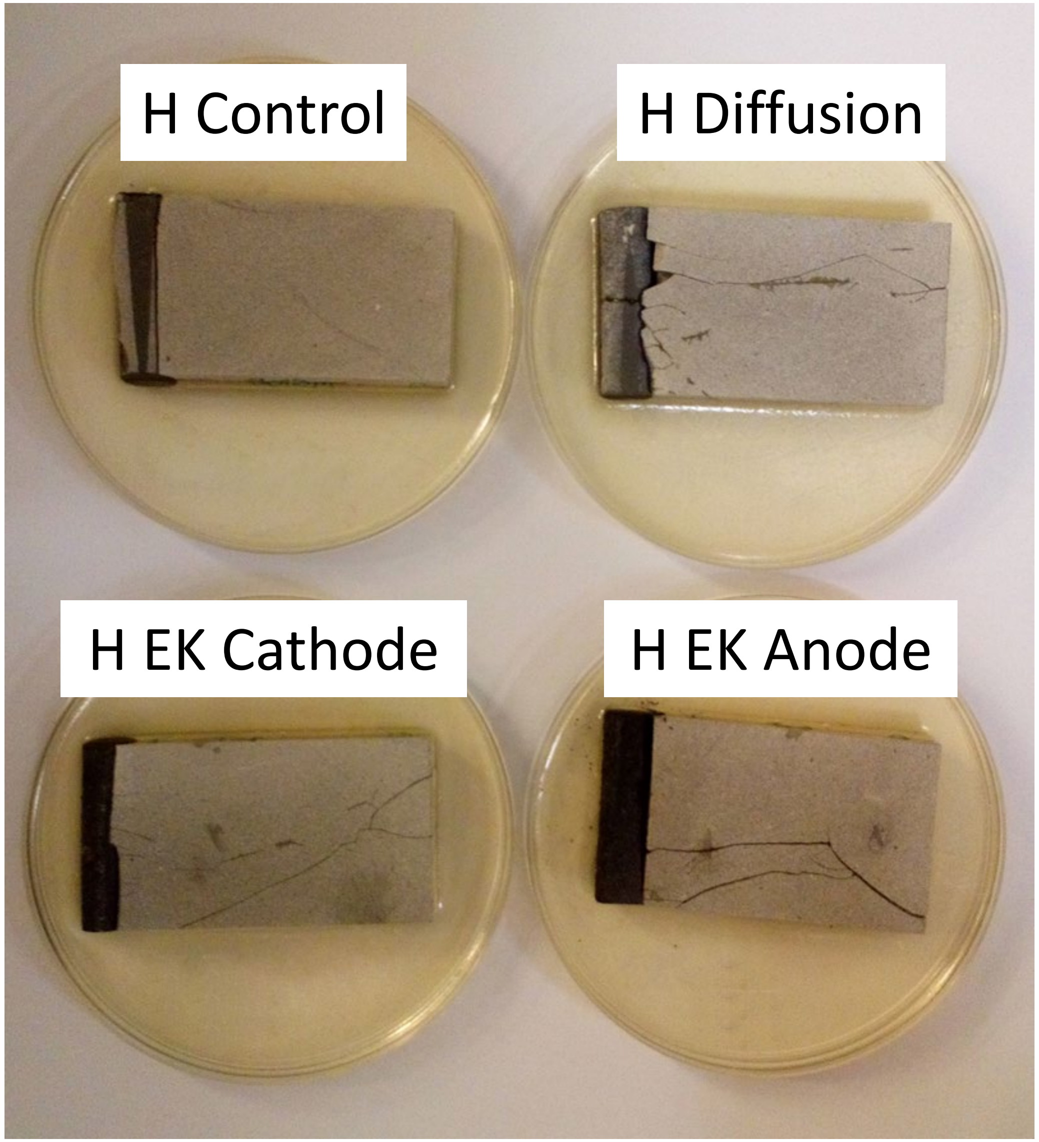

Autoradiography performed by British Geological Survey

Hot off the Plate – S-Set

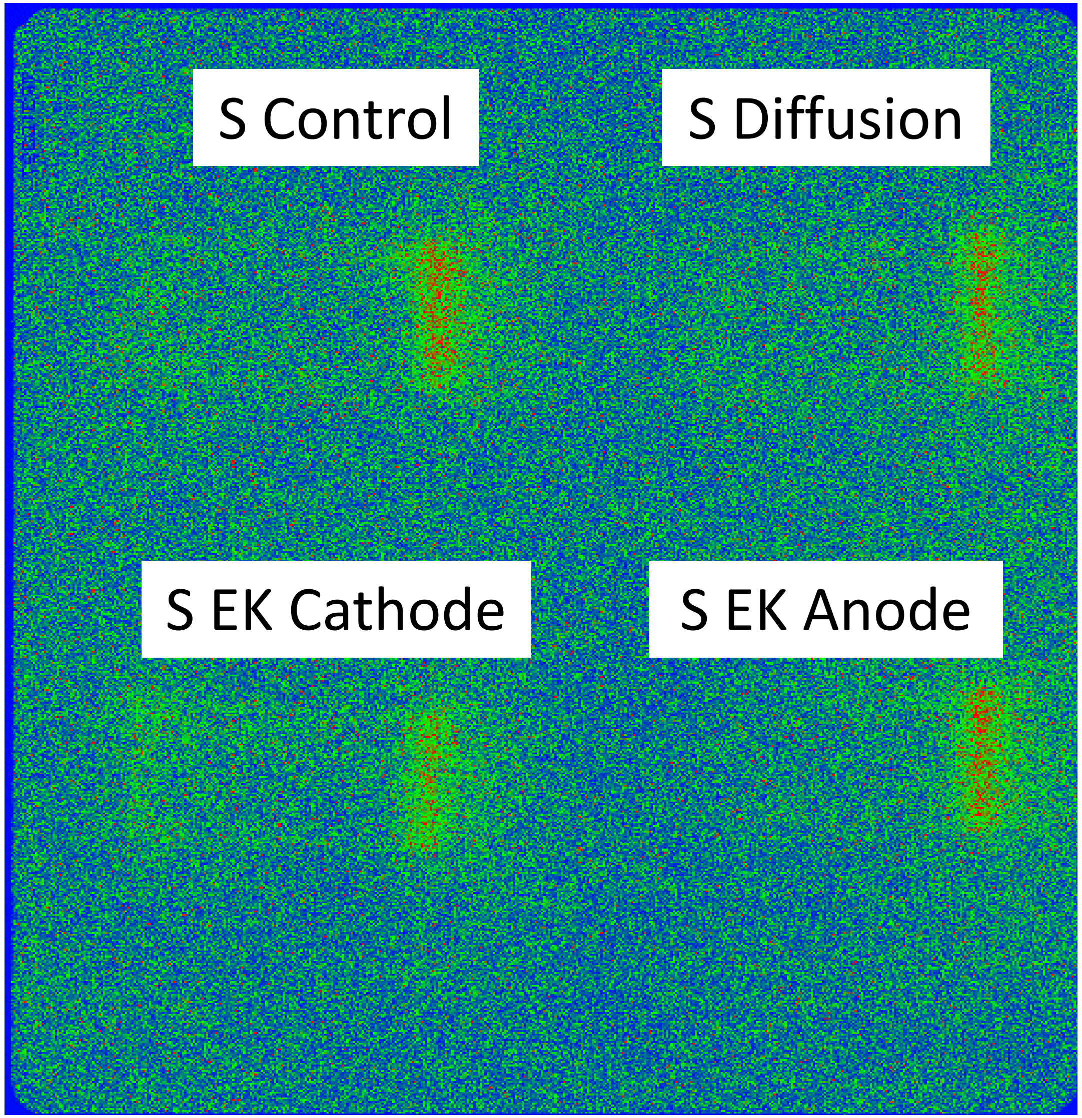

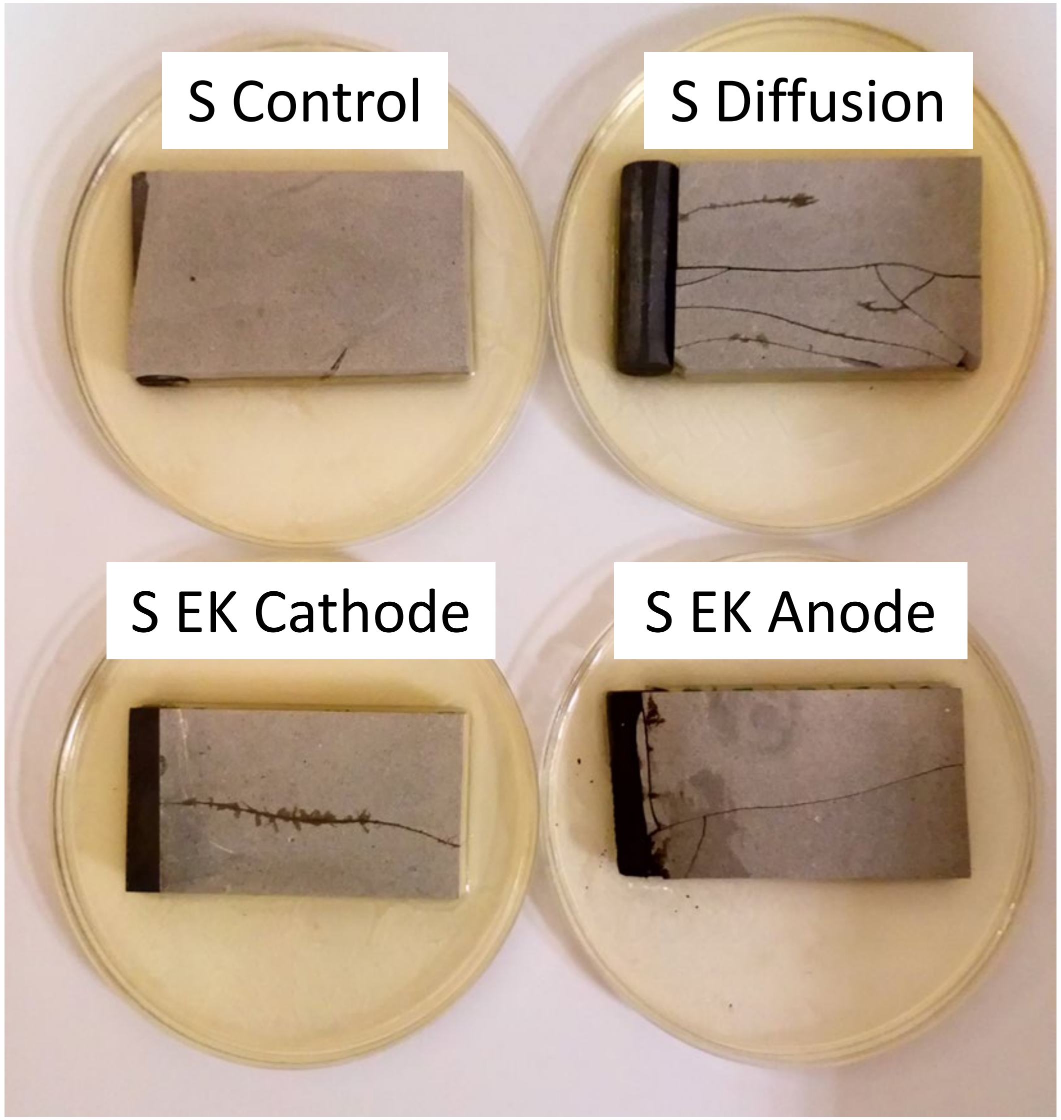

Autoradiography performed by British Geological Survey

Take Ohm Messages and Next Steps

- Cores have been treated and cut into sections
- Analysis of soak solutions show different radionuclides have different mobilities within the core
- Autoradiography strongly indicates movement of something with a positive charge – its identity is currently unknown…
- Full-core analysis will provide further information and identification

Acknowledgements

Andy Cundy
Frances Burrell
Richard Marsh
Phil Warwick
Ian Burke
James Graham
Jamie Purkis
GAU Radioanalytical Staff
British Geological Survey
INSPIRE DTP

s.d.hemming@soton.ac.uk

NNUF National Nuclear User Facility

NNUF EXACT

GAU Radioanalytical Laboratories

BGS British Geological Survey

University of Southampton

UNIVERSITY OF LEEDS

INSPIRE

TRANSCEND

Transformative Science and Engineering for Nuclear Decommissioning

Simulated Advanced Gas-Cooled Reactor Spent Nuclear Fuels – An XRD, XPS and Raman Study

TRANSCEND Meeting 2nd of November 2022

Presenter: Richard Wilbraham

Authors: Richard Wilbraham, Colin Boxall, David Hambley, Elizabeth Howett, Jessica Higgins

Contents

1. Why make an AGR SIMFuel?
2. Composition and Manufacture
3. Physical Properties
4. XRD of AGR SIMFuel
5. Raman of AGR SIMFuel
6. XPS of AGR SIMFuel
7. OM Ratio Calculations
8. Conclusions

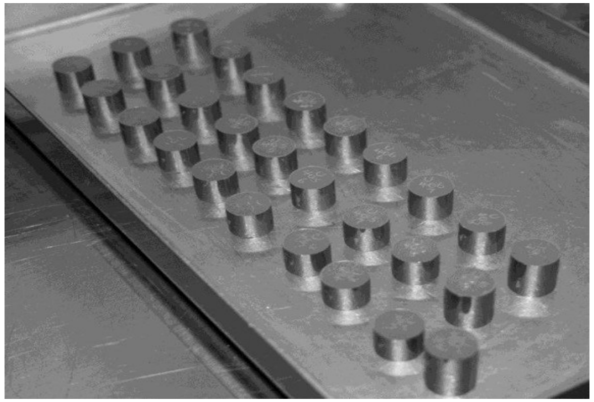

The Advanced Gas Reactor

- Since 1971 the UK has operated a fleet of commercial reactors based on a rather different design to the light water reactor, the Advanced Gas Reactor (AGR).
- AGR reactors have several unique features:

1. Fuel pellets are annular in shape
2. Cladding is composed of high temperature stainless steel (20/25/Nb) rather than zircaloy.
3. Fuel assemblies are moderated by a graphite core

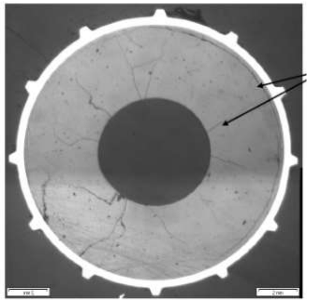

Geological Disposal

- Since 2014 the UK has seen a shift in disposal strategy from reprocessing to geological disposal.
- Requirement to understand the durability of AGR fuels under disposal conditions relevant to UK geology.
- The SNF consortium set up, comprising the NDA, NNL, Imperial College London, Cambridge University and Lancaster University to provide scientific underpinning for a UK disposal strategy.
- HOWEVER, the handling of highly radioactive AGR spent nuclear fuel is difficult outside of an industrial environment.

Can a suitable spent AGR fuel simulant be produced?

Calculation of Fission Product Concentrations

FISPIN Output Element Groupings	25 GWd/t U Simulated Burnup (Mol per ton of heavy metal)	43 GWd/t U Simulated Burnup (Mol per ton of heavy metal)
Gaseous (Kr, Xe, He)	32.22	55.35
U + Pu + Np +Am + Cm	4093.94	4016.63
Nd + Sm + Eu + Gd + Pr + Tb	32.53	55.601
Zr	33.93	55.26
Mo	26.26	44.49
Ru + Tc	21.89	38.65
Ba	14.01	24.95
Ce	12.72	21.61
Pd	8.33	18.42
Rh	3.44	4.96
La	6.67	11.10
Sr	3.46	5.47
Y	4.08	6.44
Rb + Cs	13.30	21.45
I + Br	1.46	2.55
Te + Se	3.12	5.65
Sn + Sb	0.152	0.44
Cd + Ag	0.727	1.96
Pb + Nb	0.00	0.00
Other minor elements	1.16	1.05

SIMFuel Compounds (at%)	25 GWd/t U Burnup	43 GWd/t U Burnup
UO_2	95.705	92.748
Nd_2O_3	0.761	1.284
ZrO_2	0.793	1.276
MoO_3	0.614	1.027
RuO_2	0.512	0.892
$BaCO_3$	0.328	0.576
CeO_2	0.297	0.499
PdO	0.195	0.425
Rh_2O_3	0.080	0.115
La_2O_3	0.156	0.256
SrO	0.081	0.126
Y_2O_3	0.095	0.149
Cs_2CO_3	0.311	0.495
TeO_2	0.073	0.130

- FISPIN results shown on the left assuming 100 years cooling time.
- SIMFuel compound mix shown on the right
- Calculated and produced two different burnups – 25 GWd/tU and 43 GWd/tU

Manufacture

1. 60 g blend created based on FISPIN simulation.
2. Ball milled and sieved.
3. Powders pre-compacted into granulates at a pressure of 75 MPa.
4. 0.2 wt. % zinc stearate added as a lubricant and slowly mixed in using a rotary mixer.
5. Granulates pressed into green pellets in a uniaxial press by applying a pressure of 400 Mpa.
6. Sintered in a refractory metal furnace at a heating rate of 5 °C/min to 300 °C, and then 15 °C/min to 1730 °C.
7. Finished pellets cut into slices using a precision cut-off machine with diamond cut-off wheel.

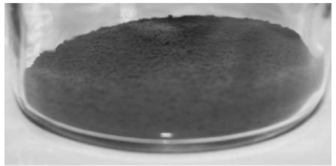

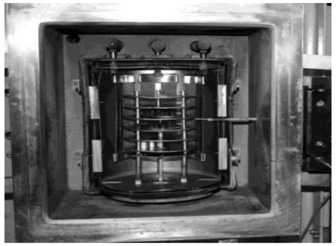

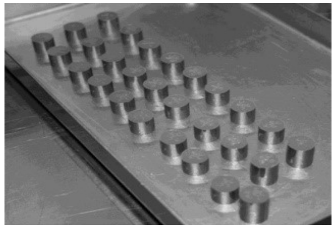

Z. Hiezl, D.I. Hambley, C. Padovani, W.E. Lee, *J. Nucl. Mat.* **456** (2015) 74-84.

Physical Properties

	Undoped UO_2	25 GWd/tU	43 GWd/tU
SEM Image (50x mag, SEI)	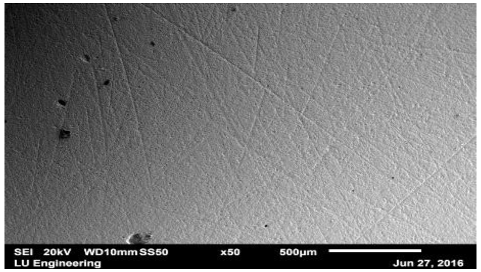	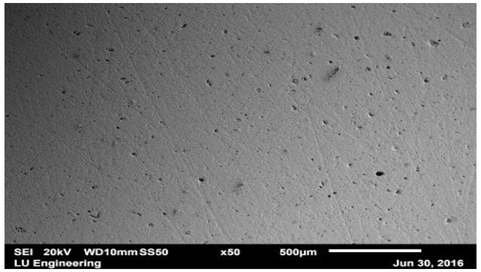	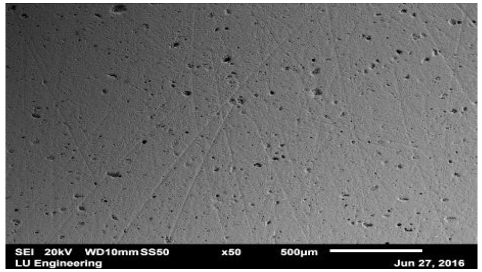
Grain Size	9.70±2.3 μm	4.21±0.59 μm	2.95±1.3 μm
Density	10.62 g/cm^3	9.76 g/cm^3	9.67 g/cm^3
R_u (current interrupt @ -1.2V)	3318 Ω/cm	232.3 Ω/cm	182.9 Ω/cm
Phases identified with EDX	Bulk: U	Bulk: Nd, La, Ce, U, Y, Te, Cs Perovskite: Ba, Zr, Sr, Ce Noble Metal: Pd, Ru, Rh, Mo	Bulk: Nd, La, Ce, U, Y, Te, Cs Perovskite: Ba, Zr, Sr, Ce Noble Metal: Pd, Ru, Rh, Mo

Z. Hiezl, D.I. Hambley, C. Padovani, W.E. Lee, *J. Nucl. Mat.* **456** (2015) 74-84.

XRD of AGR SIMFuel Samples

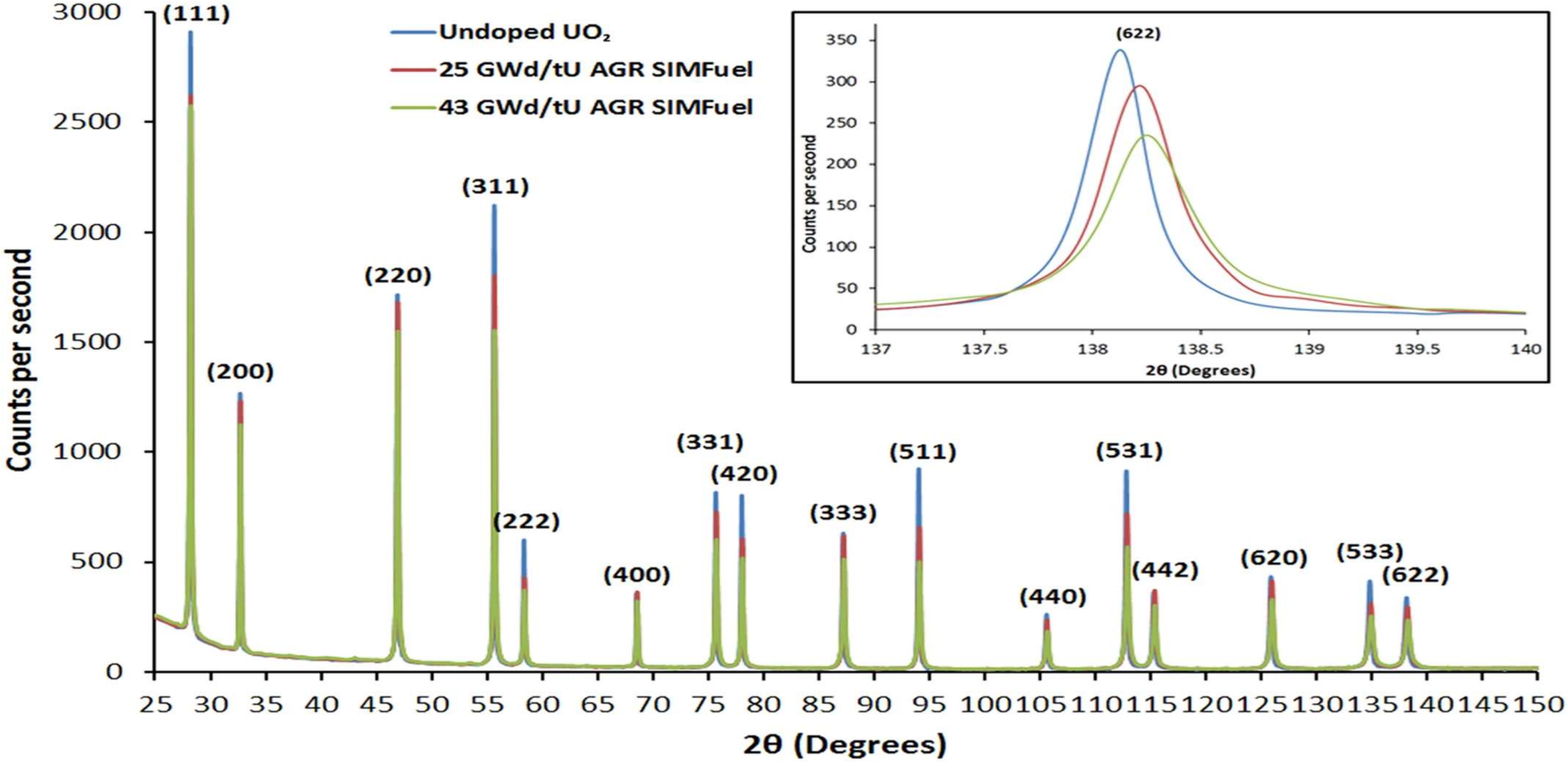

Lattice Parameter from Rietveld Refinement

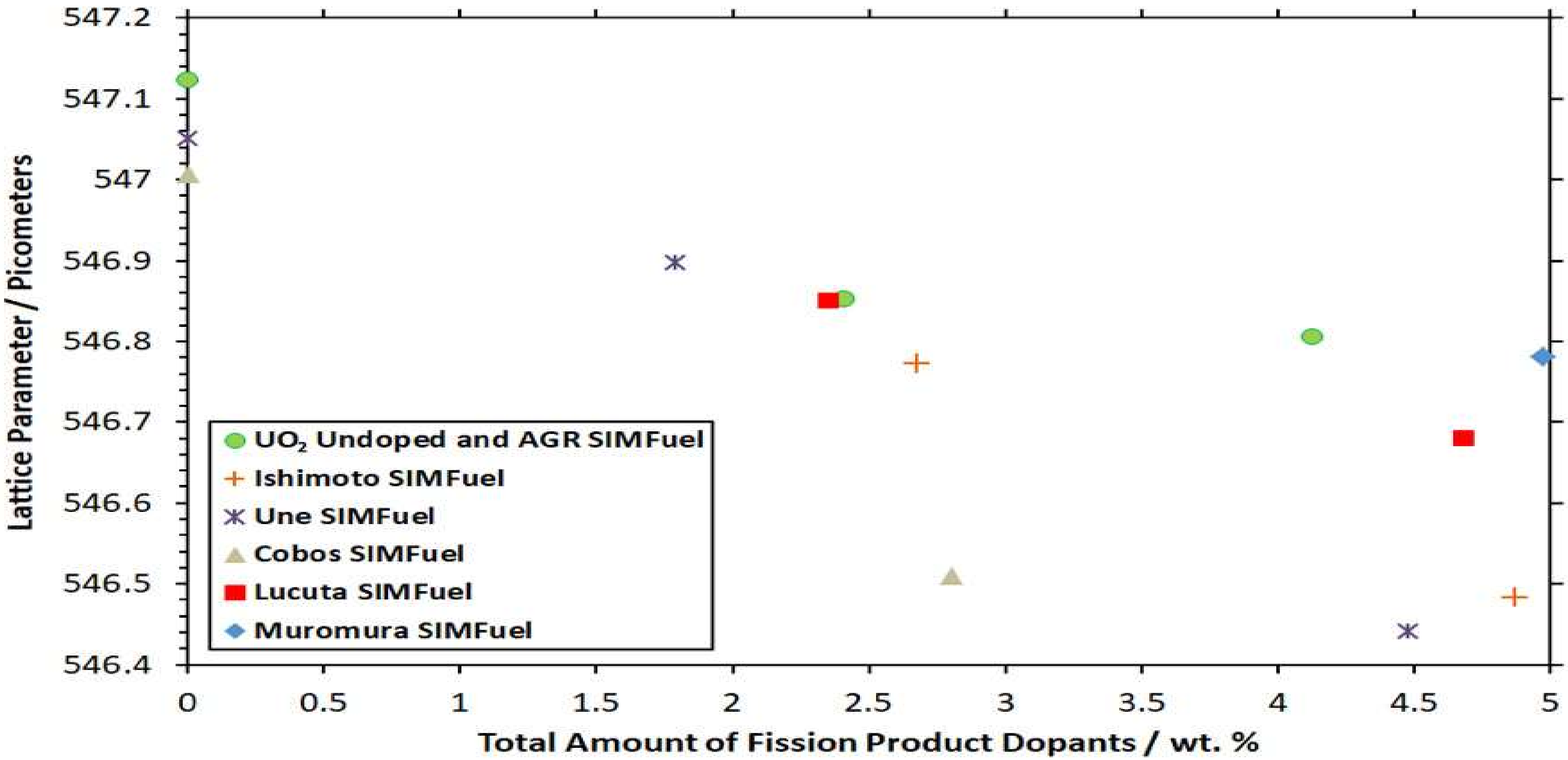

J. Spino and D. Papaioannou, *J. Nucl. Mater.* **281** (2000) 146-162.

Previous Analysis of CANDU SIMFuel

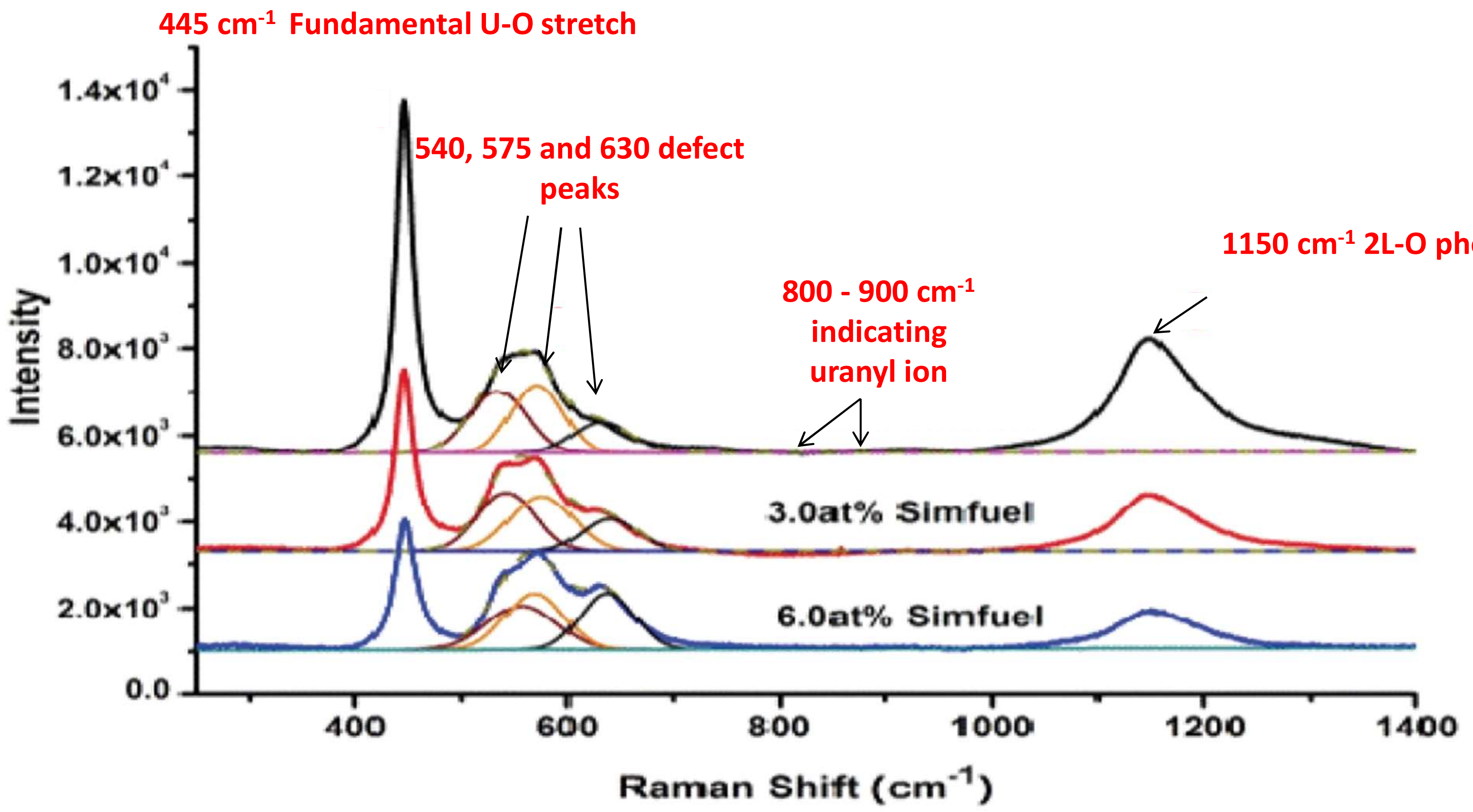

H. He, P.G. Keech, M.E. Broczkowski, J.J. Noël, D.W. Shoesmith, *Can. J. Chem.* **85** (2007) 702-713.
Corrosion of Nuclear Fuel (UO_2) Inside a Failed Nuclear Waste Container, **D. Shoesmith,** NWMO TR-2012-09, Nuclear Waste Management Organization, 2012

Comparison of Undoped UO_2 and Two Different Burnup SIMFuels

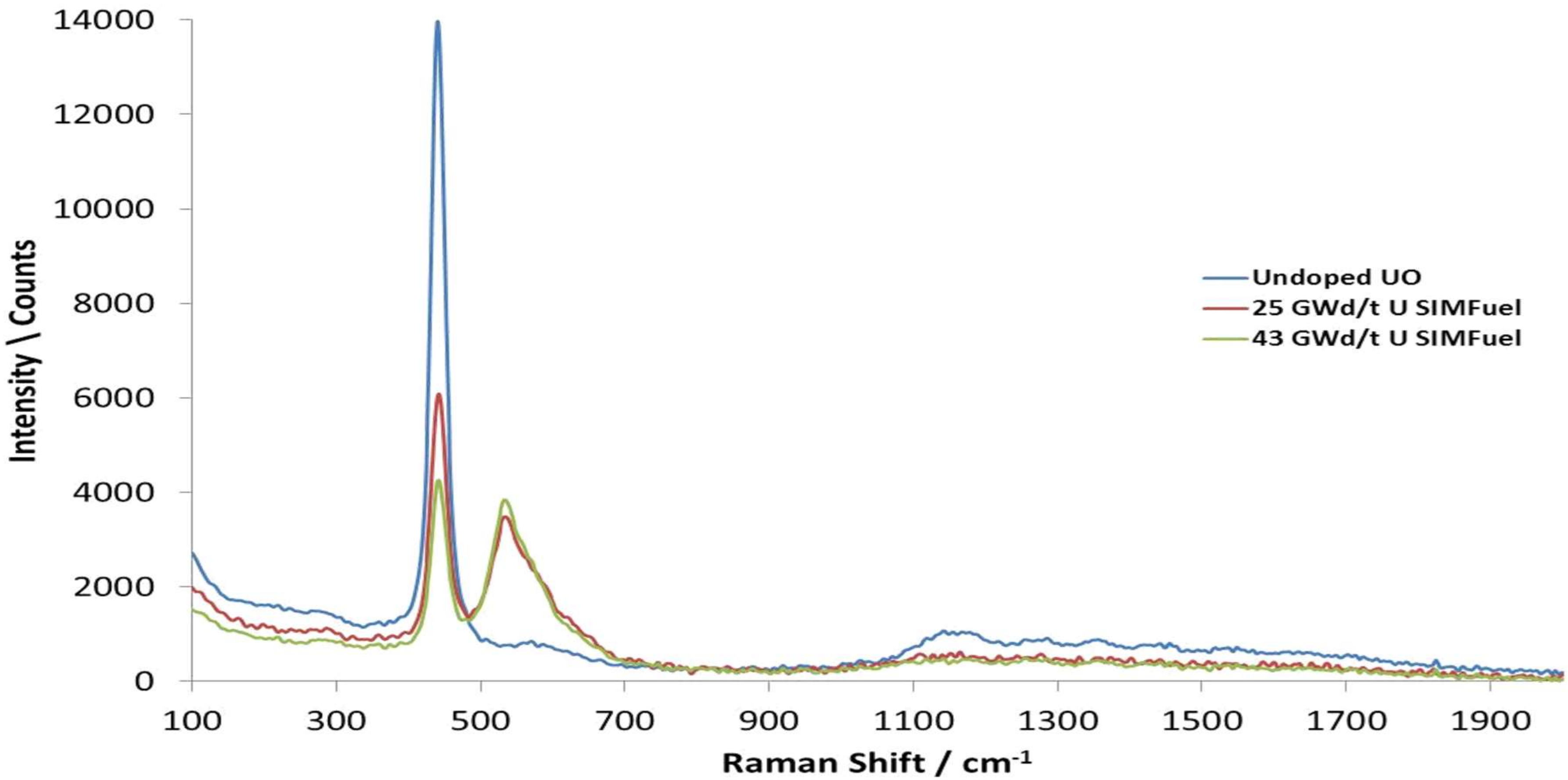

Example Lorentzian Peak Fit of AGR SIMFuel Samples

<u>25 GWd/t U SIMFuel</u>

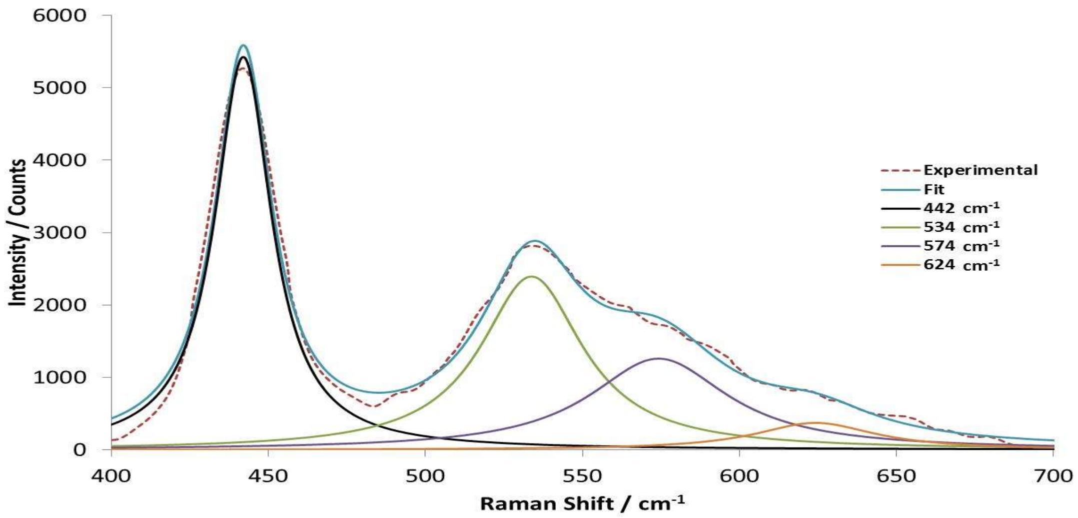

<u>43 GWd/t U SIMFuel</u>

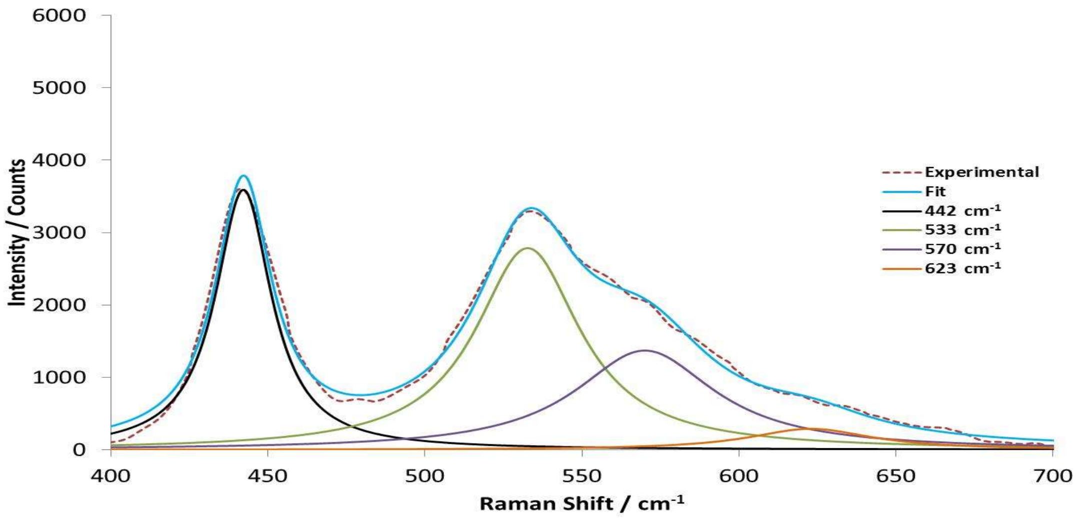

- Both SIMFuel samples fit very similar peaks to LWR SIMFuel.
- 1) 540 cm^{-1} = Oxygen vacancy phonon related to solid solution dopant
- 2) 575 cm^{-1} = Lattice phonon due to movement away from perfect fluorite
- 3) 620 cm^{-1} = U_4O_9 type behaviour, indicative of interstitial oxygen

XPS Analysis – Survey Scan

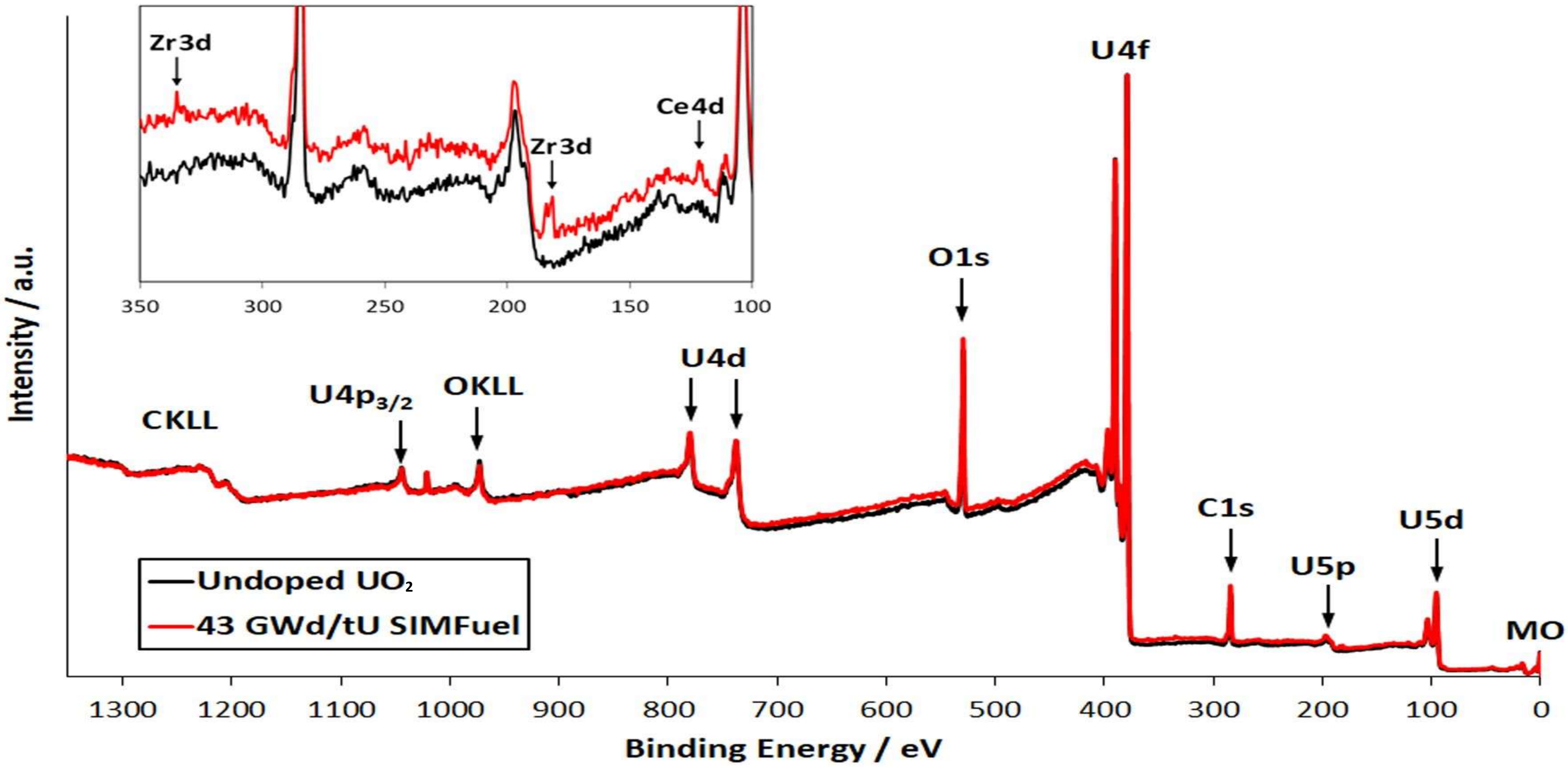

XPS Analysis – High Resolution Scans

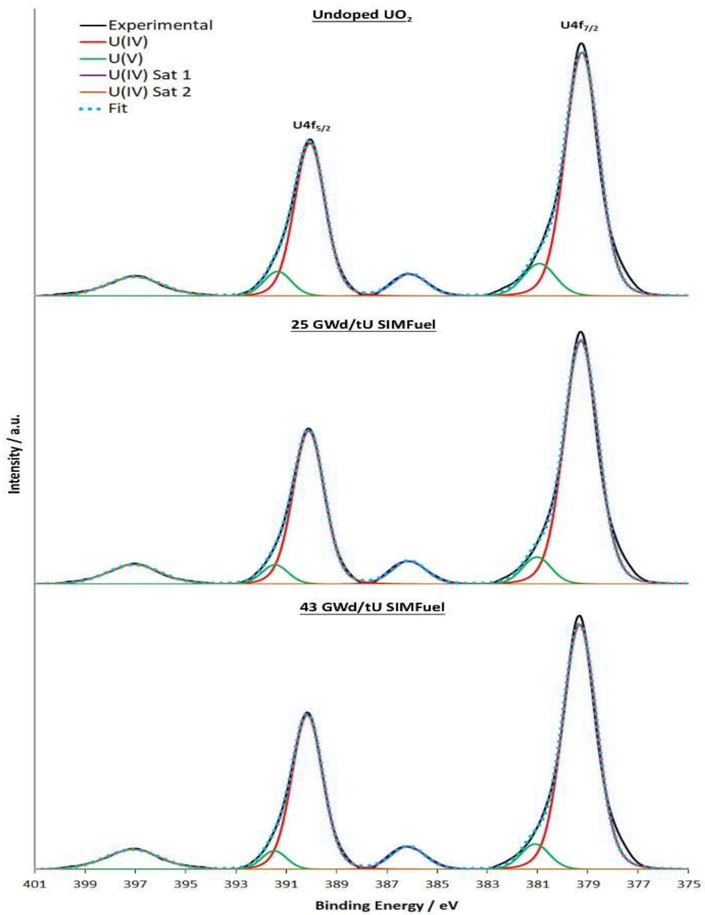

- There are no significant differences in the binding energy positions of each identified peak across the tested materials.
- However, a U(V) rather than U(VI) component is apparent in all samples.
- Cannot rule out some mild surface oxidation.
- U_4O_9 has been reported to be a mix of U(IV) and U(V) phases with little U(VI) component.

OM Ratio Calculations

- Using the generated XRD, XPS and Raman data the OM ratio of the AGR SIMFuels and undoped UO_2 sample have been calculated:

- XRD attempted using the lattice parameter deduction method of Benedict *et al*. Quickly found to be too inaccurate due a lack of understanding of partitioning of fission products between the bulk lattice and grey phase.

- Raman calculations were based on a method from Ellorieta *et al.*, that compares the ratio of the 440 peak to the 630 peak:
- v630 (cm^{-1}) = 645 ± 4 – (610 ± 60)x

- XPS analysis was carried out using a recent method by Teterin *et al*., whereby the ratio of the area of the U5f peak, *I1*, to that of the $U4f_{7/2}$ peak, *I2,* is calculated and related to the oxygen coefficient, k_0:

$$k_0 = \frac{3 - (10000 * I_1 / I_2)}{383}$$

U. Benedict, M. Coquerelle, J. De Bueger, and C. Dufour, *J. Nucl. Mater.,* **45** (1972) 217-229.
J.M. Elorrieta, L.J. Bonales, N. Rodriguez-Villagra, V.G. Baonza, and J. Cobos, *Phys. Chem. Chem. Phys.,* **18** (2016) 28209-28216.
Y.A. Teterin, A.J. Popel, K.I. Maslakov, A.Y. Teterin, K.E. Ivanov, S.N. Kalmykov, R. Springell, T.B. Scott, and I. Farnan, *Inorg. Chem.,* **55** (2016) 8059-8070.

Results of OM Ratio Analysis

Sample	XRD	XPS (U5f)	Raman	Technique Averaged
Undoped UO_2	$UO_{2.00}$ (±0.00)	$UO_{2.05}$ (±0.05)	$UO_{2.03}$ (±0.01)	$UO_{2.03}$ (±0.05)
25 GWd/t U SIMFuel	N/A	$UO_{2.04}$ (±0.05)	$UO_{2.04}$ (±0.01)	$UO_{2.04}$ (±0.05)
43 GWd/t U SIMFuel	N/A	$UO_{2.07}$ (±0.02)	$UO_{2.04}$ (±0.01)	$UO_{2.06}$ (±0.02)

- General agreement between XPS and Raman spectroscopy with regards to OM ratio.
- OM ratio of SIMFuel is stoichiometric/slightly hyperstochiometric in agreement with real and simulated LWR.
- Promising for use as Raman as a quick OM ratio technique.

Conclusions

- Simulated AGR fuel has been created based on FISPIN code calculations.
- XRD results reveal a UO_2 lattice contraction with increasing simulated burnup, with the trend in lattice contraction similar to that previously reported for LWR SIMFuels.
- XPS results show clear peaks in the binding energy regions for uranium, oxygen and adventitious carbon. Few additional peaks are present that could be associated with solid solution or precipitated fission product simulant dopants.
- Raman reveals that the cubic fluorite lattice of UO_2 becomes more defective with simulated burnup as 3+ lanthanides and associated oxygen vacancies are incorporated.
- OM Ratio has been calculated using all three methods, with XPS and Raman results in good agreement.

TRANSCEND

UTGARD LABORATORY

Lancaster University

Thank You and Questions

ELSEVIER

Journal of Nuclear Materials

Volume 568, September 2022, 153867

Simulated advanced gas-cooled reactor spent nuclear fuels: Determination of the O/U ratio - an XRD, XPS and Raman study

Richard J. Wilbraham [a], Elizabeth A. Howett [a], Colin Boxall [a], David I. Hambley [b], Jessica K. Higgins [c]

EPSRC
Engineering and Physical Sciences Research Council

NDA
Nuclear Decommissioning Authority

National Nuclear Laboratory

UNIVERSITY OF CAMBRIDGE

Imperial College London

NNUF
National Nuclear User Facility

TRANSCEND

Transformative Science and Engineering for Nuclear Decommissioning

Off-Gas Emission Control From Vitrification of Radioactive Waste

Alex Stone, Sheffield Hallam University

TRANSCEND Annual Meeting 2022

A. Scrimshire, F. Burrell, R. Marsh, A. Cundy, A. Holloway, S. Morgan, D. McKendrick, P. Bingham

- Introduction
- Low Temperature Glasses
- High Temperature Glasses
- The Future

TRANSCEND

Transformative Science and Engineering for Nuclear Decommissioning

The Problem

- The UK has 133,000 m^3 of radioactive waste in storage and an estimated 4,420,000 m^3 arising in the future[1]
- Intermediate level radioactive waste is high volume in the UK and more will arise from decommissioning
- High volume wastes of ILW classification:
  - SIXEP Sand/Clinoptilolite ion exchange material
  - Pond and Process Sludges (e.g. Magnox, THORP)
  - Plutonium Contaminated Material (PCM)
- Contaminated with Cs-137, I-129, Cl-37 from various decay processes

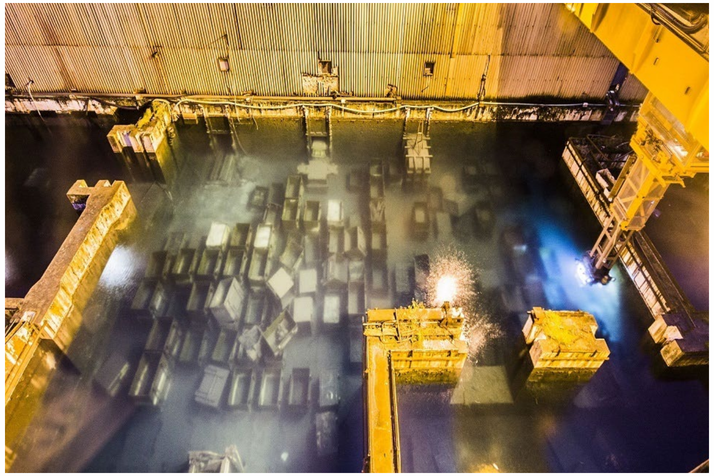

Figure 1. Magnox Storage Pond

1. NDA. (2020). *The 2019 Inventory*. NDA Department for Business, Energy and Industrial Strategy. https://ukinventory.nda.gov.uk/the-2019-inventory/2019-uk-data/

Thermal Treatment

- Vitrification as a waste treatment technique is already in use for HLW and has potential for ILW. This involves forming a glass or glass/ceramic product[2]
- Cold crucible ceramic, Joule Heated Ceramic and plasma melters are all being considered for treatment
- All require temperatures from 950-1500 °C which could volatilise some of the waste components
- A full inventory of radioactive material must be kept and reducing volatility reduces the error and risk associated with thermal treatment techniques

Figure 2. GeoMelt® Vitrification System

2. Caurant, D. (2009). *Glasses, glass-ceramics and ceramics for immobilization of highly radioactive nuclear wastes*. Nova Science Publishers, Inc.

Pyrolysis

Pyrolysis

- Active and inactive facilities available
- Designed for gaseous radionuclide analysis
- Maximum temperature 1000°C

Current Progress

- Base Glass modified Ca/Zn
- Iodine-127 and Iodine-129
- Caesium-137

Future Progress

- Chlorine-35.5
- Nitrogen Atmosphere

	Dopant			
	^{127}I	^{129}I	^{137}Cs	$^{35.5}Cl$
Base Glass (With Dopants)	1	1	2	5
Clinoptilolite 10-50wt%	1	1	2	5
Corroded Magnox Sludge 10-50wt%	1	1	2	5
Xanthan Gum Additive	2	2	4	5
Graphite Additive	2	2	4	5
Reduced Boron Frit	3	3	4	5

Table 1. Table of experimental plan with priority order (1 high - 5 low)

Figure 3. Raddec-6 Pyrolyser unit

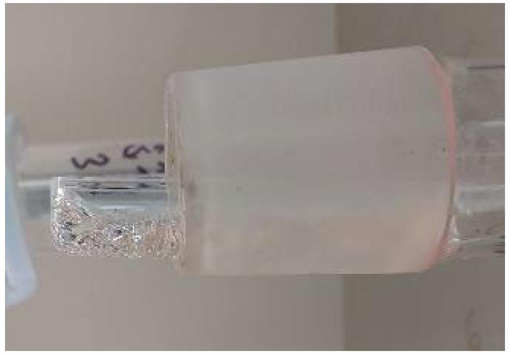

Figure 4. Example of final sample product

- Introduction
- High Temperature Glasses
- Low Temperature Glasses
- The Future

TG-MS

- Caesium mass loss is **greater** in MW glass than CaZn
- The bulk of the mass loss relates to caesium release as a **high temperature** gaseous species
- CaZn is better at incorporating caesium into its structure
- Little difference in thermal events other than decomposition of the Cs_2CO_3 reagent

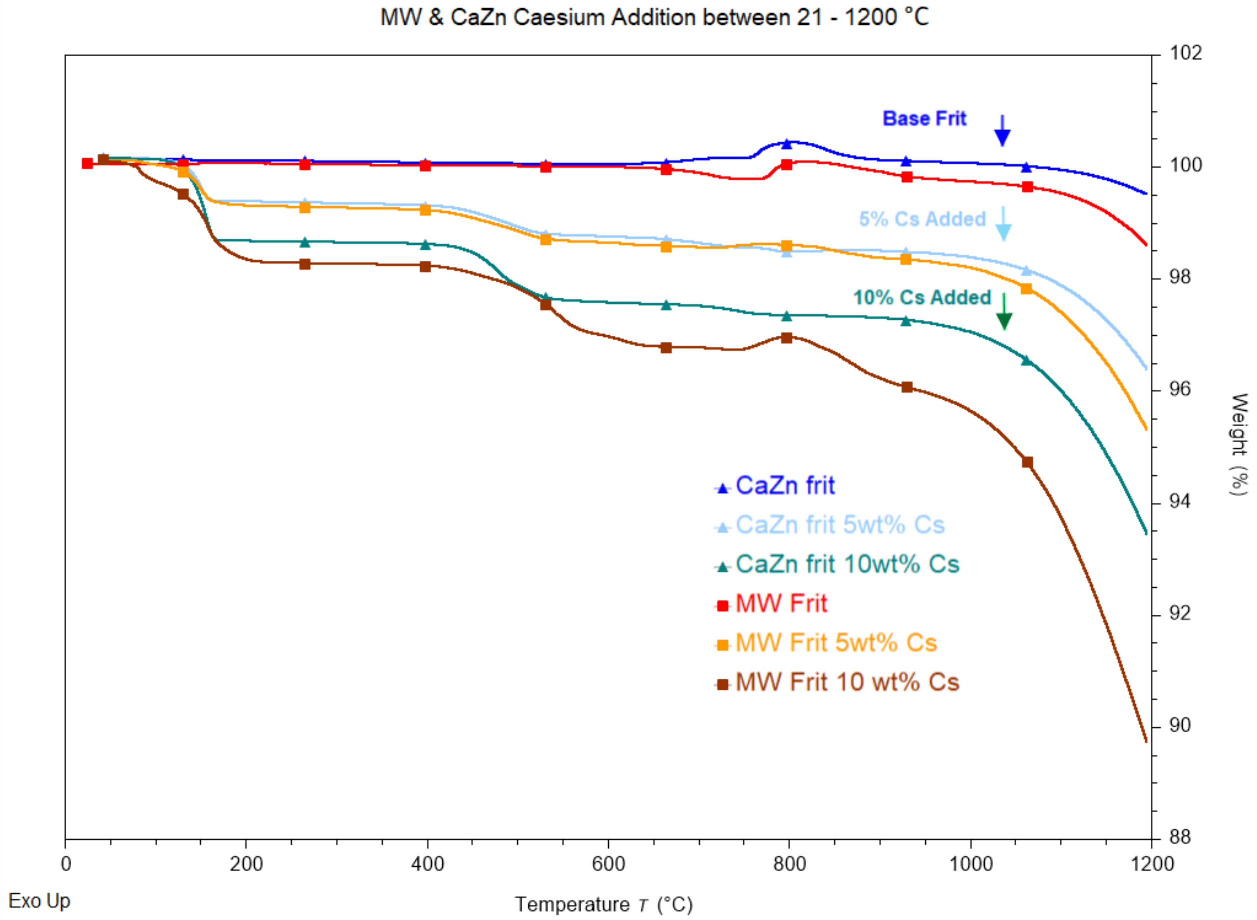

Transformative Science and Engineering for Nuclear Decommissioning

TG-MS

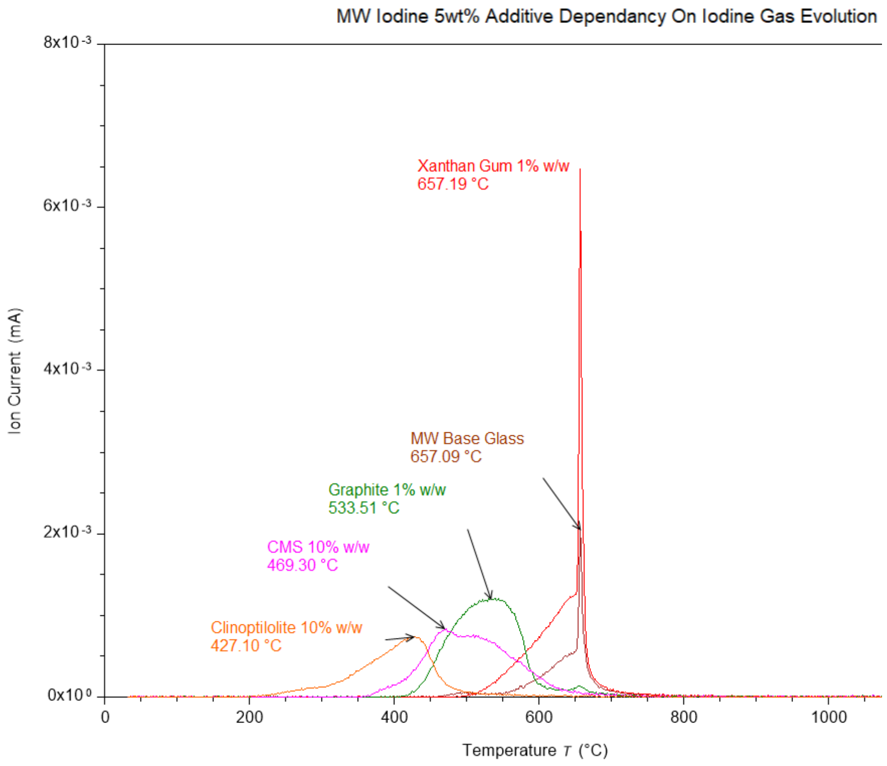

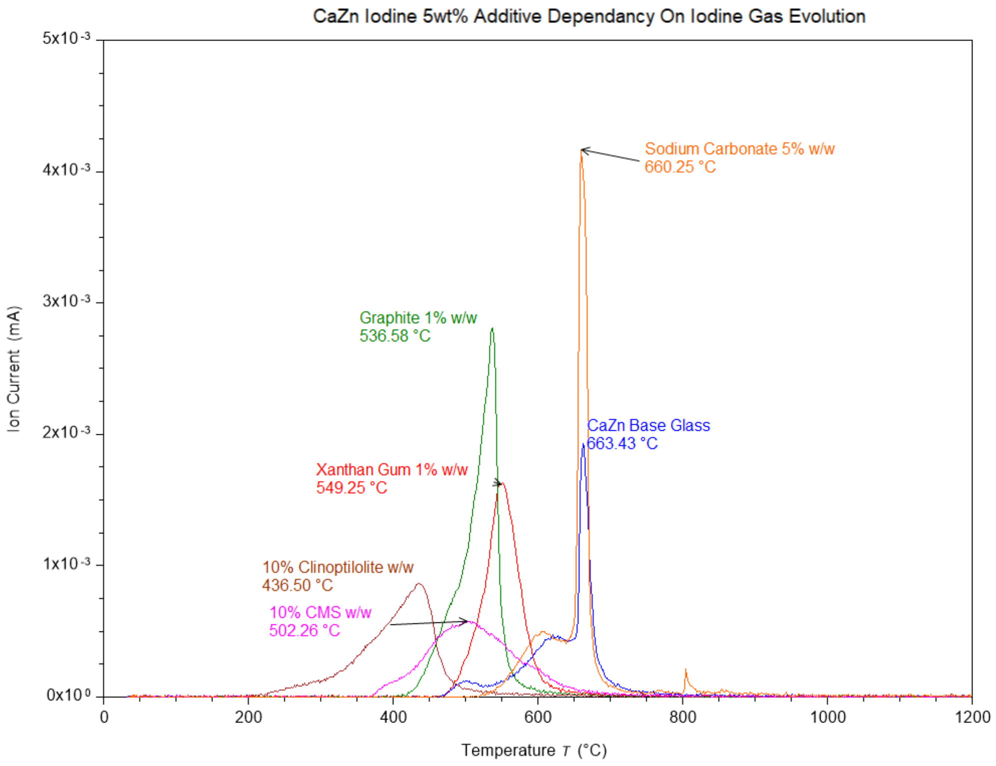

- Intensity of I_2 gas versus temperature from frit glasses
- Temperature of I_2 loss between base glasses is **unchanged**
- Most additives **reduce** the temperature at which I_2 volatilises
- CaZn base glass frit marginally **increases** temperature at which I_2 volatilises compared to MW

- Introduction
- High Temperature Glasses
- Low Temperature Glasses
- The Future

Glass Modifications

The comparatively low temperatures for pyrolysis require us to develop glasses that melt at 900 – 1000 °C

Sodium lithium borate and borosilicate glasses based on MW and Ca/Zn were trialled at **950 °C**

Frit particle size and melting temperature were investigated to optimise frit production and waste loading

MW Low Temperature Glass Nominal Compositions (wt%)							
Oxide Glass	0% SiO_2	10% SiO_2	20% SiO_2	30% SiO_2	40% SiO_2	50% SiO_2	Full SiO_2
SiO_2	0.00	10.00	20.00	30.00	40.00	50.00	61.74
Na_2O	28.88	25.99	23.11	20.22	17.33	14.44	11.05
B_2O_3	57.19	51.47	45.75	40.03	34.31	28.59	21.88
Li_2O	13.93	12.54	11.14	9.75	8.36	6.97	5.33

CaZn Low Temperature Glass Nominal Compositions (wt%)							
Oxide Glass	0% SiO_2	10% SiO_2	20% SiO_2	30% SiO_2	40% SiO_2	50% SiO_2	Full SiO_2
SiO_2	0.00	10.00	20.00	30.00	40.00	50.00	47.60
Na_2O	16.41	14.77	13.13	11.49	9.85	8.21	8.60
B_2O_3	44.66	40.19	35.73	31.26	26.79	22.33	23.40
Li_2O	8.02	7.21	6.41	5.61	4.81	4.01	4.20
Al_2O_3	8.02	7.21	6.41	5.61	4.81	4.01	4.20
ZnO	11.45	10.31	9.16	8.02	6.87	5.73	6.00
CaO	11.45	10.31	9.16	8.02	6.87	5.73	6.00

Glass Modifications for Frit (XRD)

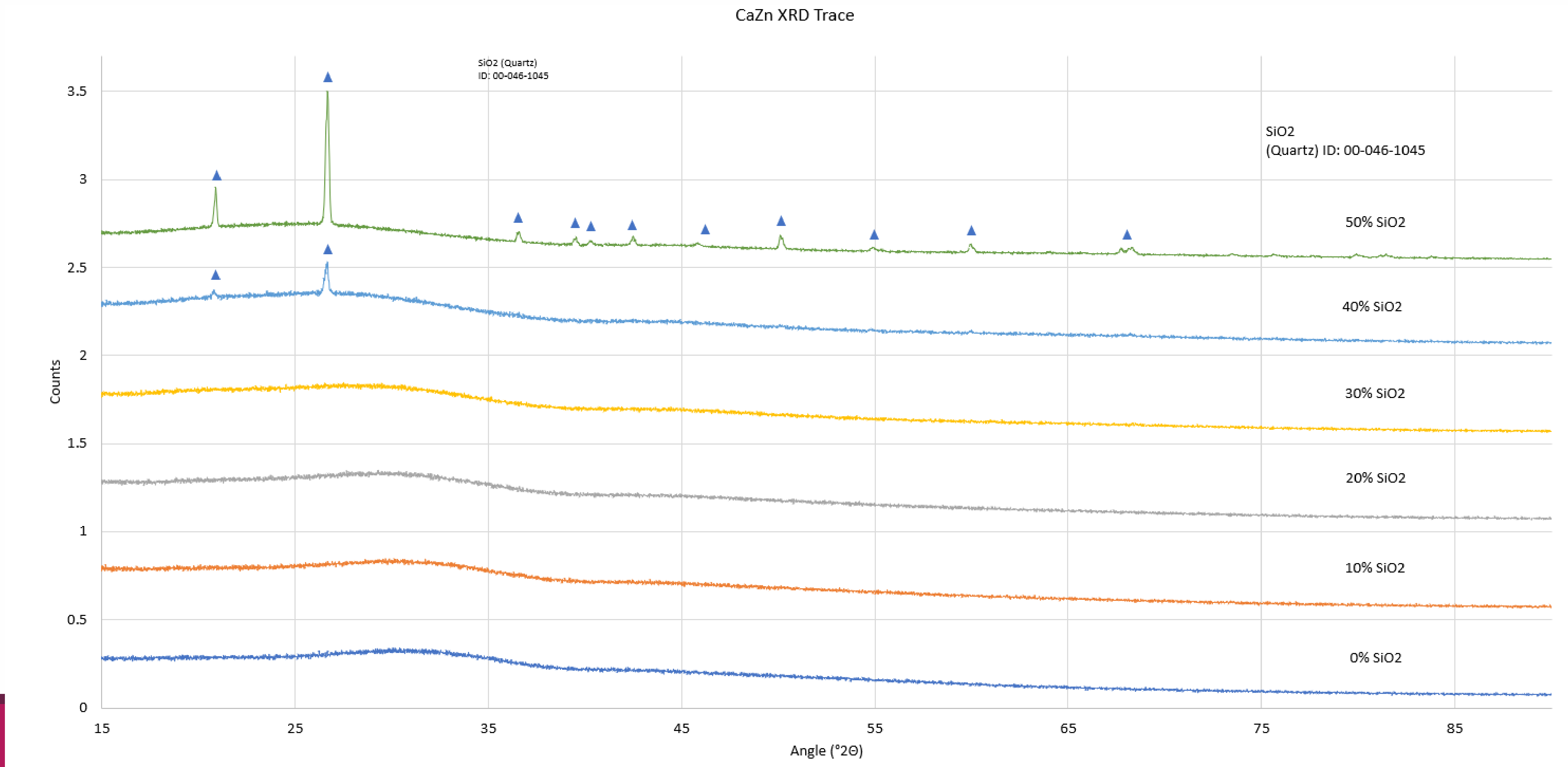

Waste Loading 0% SiO2 CaZn (XRD)

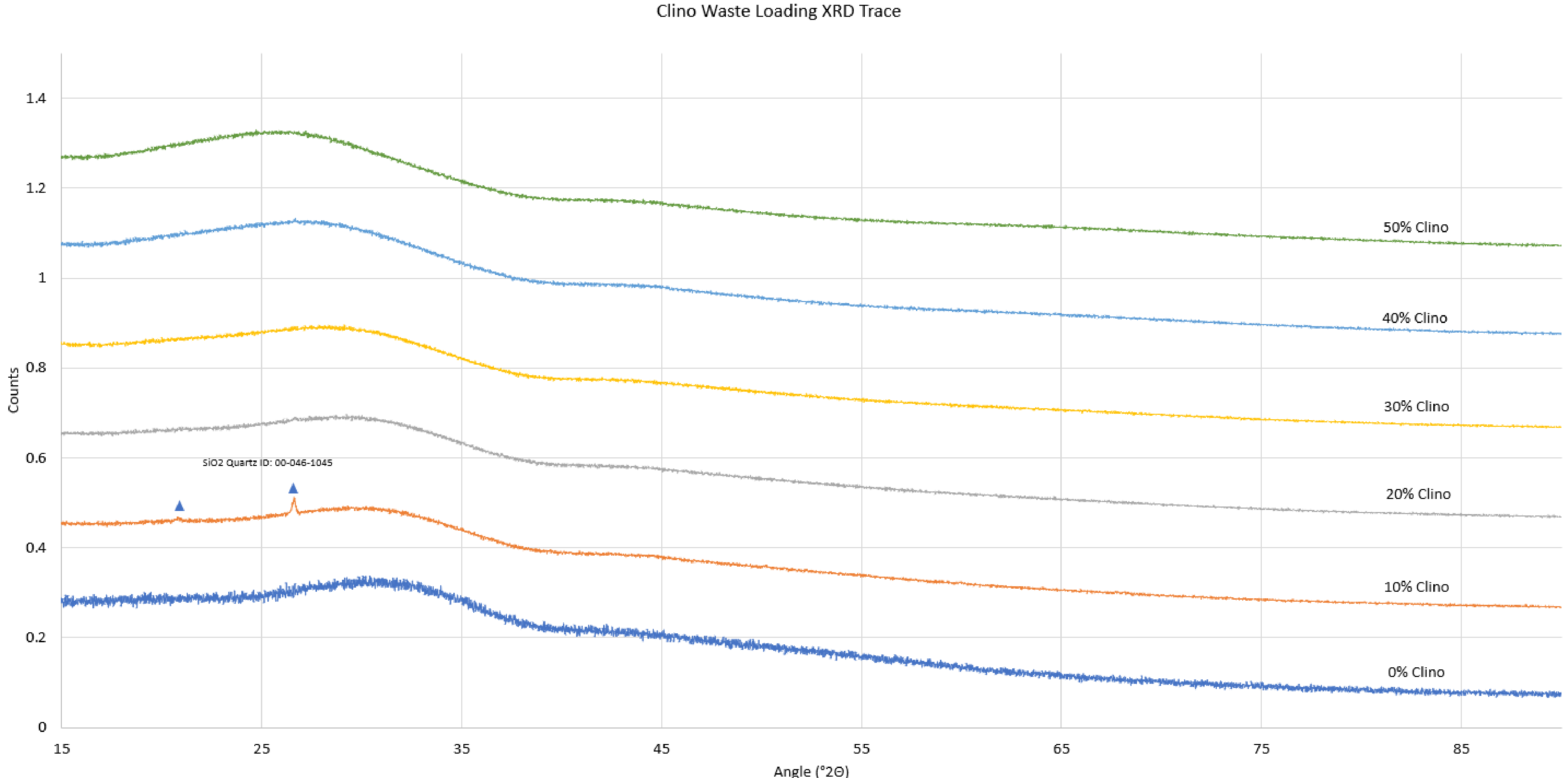

Transformative Science and Engineering for Nuclear Decommissioning

Discussion: Waste Loading

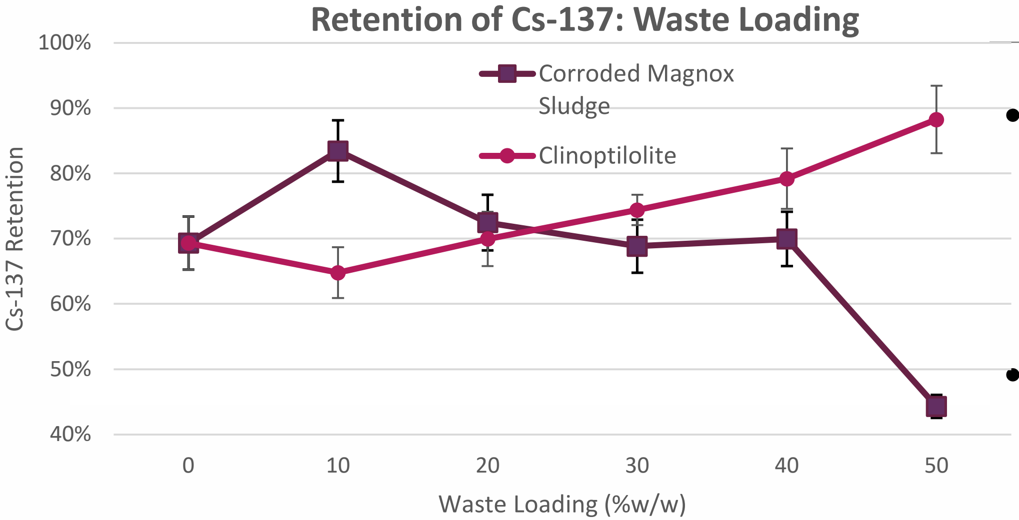

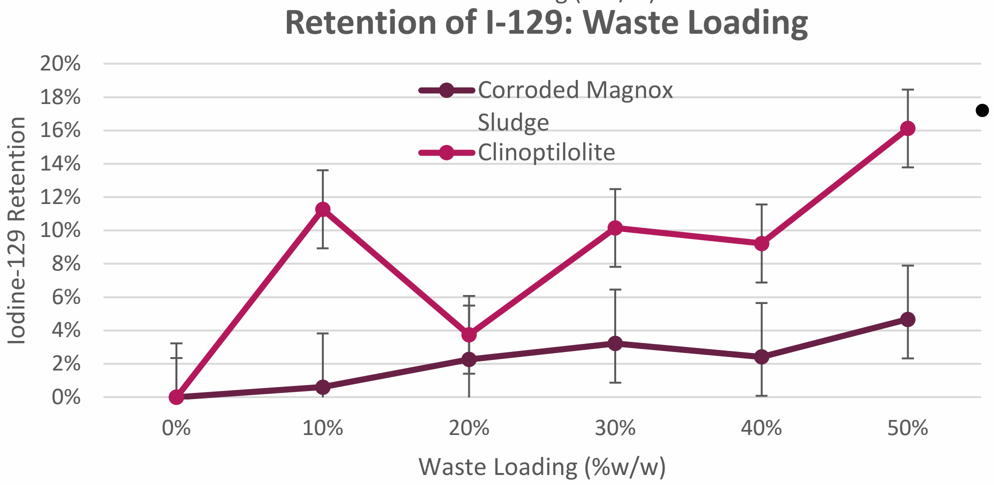

- Using pyrolysis adding the same concentration of each dopant we have been able to capture or retain **active** and inactive **caesium** and **iodine** in simulated wasteforms with **corroded Magnox sludge** and **clinoptilolite**
- Emissions reducing additives:
  - Carbon sources: Graphite, Xanthan gum, Starch
  - Glass formers and intermediates: SiO2, ZnO,
- Initial results show **waste loading** has a large effect on retention of active iodine 129 in the silica free CaZn glass systems studied
  - Clinoptilolite has a positive effect on retention for both I and Cs

Discussion: Carbon and Nitrogen

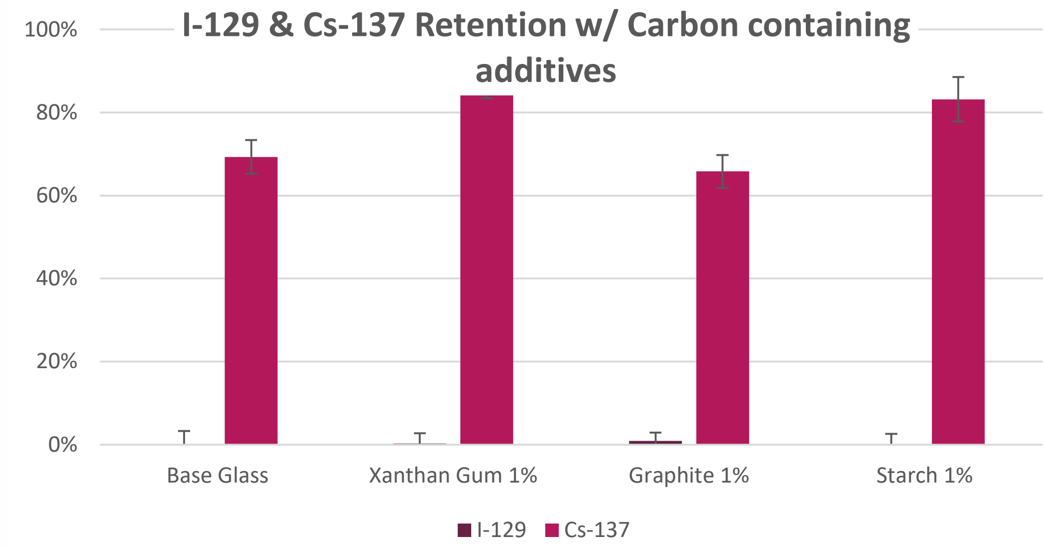

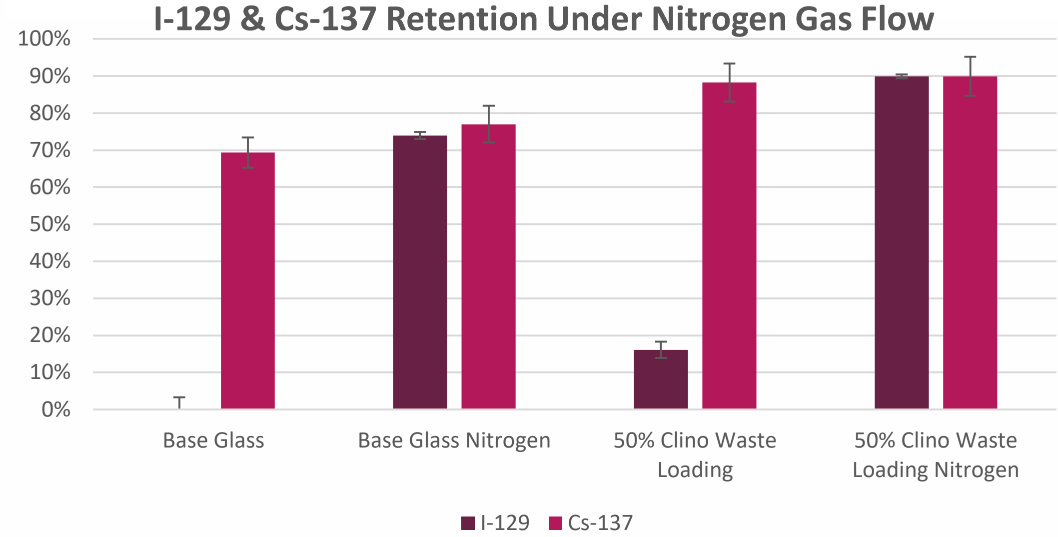

- Carbon containing additives had very **little effect** on **iodine retention** but a small change for **caesium** in the borate glass
  - Xanthan gum and Starch **positively** changed the retention by 17% and 14% respectively for Cs-137
  - Graphite had little effect for both radionuclides
- Atmosphere above the melt has a **large influence** on **iodine volatility** however less of an impact on **caesium**
  - Nitrogen gas flow over the melt **increased retention** of I-129 by up to 74% and Cs-137 by 8%

- Introduction
- High Temperature Glasses
- Low Temperature Glasses
- The Future

Temperature Dependance

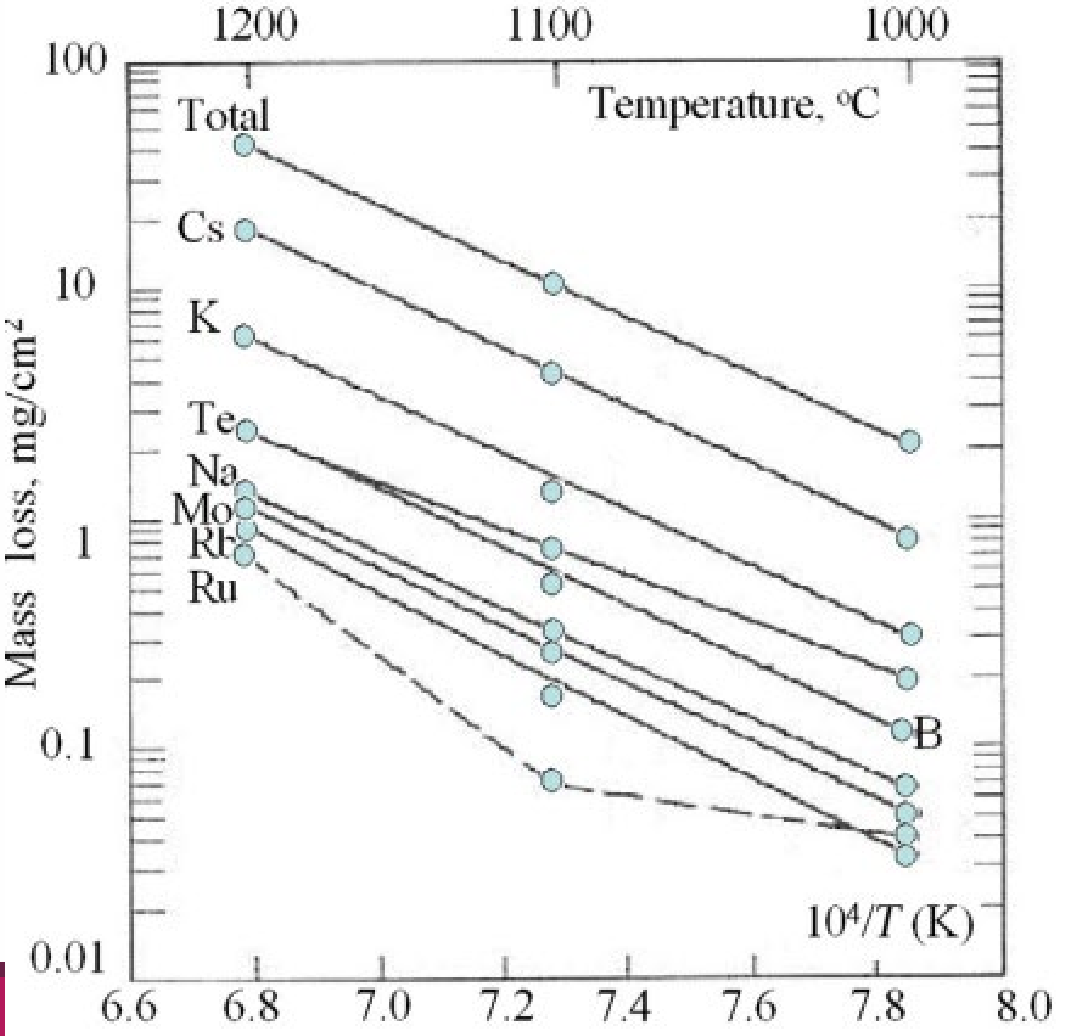

Ojovan M.I. (2019). Ref 5

Engagement Activities

- Higher activity waste thermal treatment (HAWTT) engagement event in West Cumbria, with presentations from Sheffield Hallam university, HAWTT team, NNL, Sellafield Ltd., Atkins and Cavendish Nuclear
  - Site visit to NNL Workington laboratory
  - Atkins facility walk around and robot dog demonstration
- Sheffield Hallam University <-> EXACT facility (Southampton University)
  - Seminar series promoting exchange of information between the two universities/institutions

Conclusion and Future Work

- Waste Glass Trials complete for Clino & CMS
  - @ 1150 °C
  - @ 950 °C
- Low temp. glass modifications, active Iodine
- Continue waste/glass modifications to reduce emissions and melting times/temperature
  - Eg. WL, Melting Temperature, Carbon sources, ZnO, carbonates -> Oxides
- EXACT facility Southampton experiments ongoing (active and inactive)
- Temperature Dependance on volatilisation of Cs, I and Cl

References

1. NDA. (2020). *The 2019 Inventory*. NDA Department for Business, Energy and Industrial Strategy. https://ukinventory.nda.gov.uk/the-2019-inventory/2019-uk-data/

2. Caurant, D. (2009). *Glasses, glass-ceramics and ceramics for immobilization of highly radioactive nuclear wastes*. Nova Science Publishers, Inc.

3. Kim, D., & Kruger, A. A. (2018). Volatile species of technetium and rhenium during waste vitrification. Journal of Non-Crystalline Solids, 481(October 2017), 41–50. https://doi.org/10.1016/j.jnoncrysol.2017.10.013

4. Cassingham, N. J., Corkhill, C. L., Stennett, M. C., Hand, R. J., & Hyatt, N. C. (2016). Alteration layer formation of Ca- and Zn-oxide bearing alkali borosilicate glasses for immobilisation of UK high level waste: A vapour hydration study. Journal of Nuclear Materials, 479, 639–646. https://doi.org/10.1016/j.jnucmat.2016.06.009

5. Ojovan, M. I., Lee, W. E., 38; Kalmykov, S. N. (2019). Chapter 19 - Immobilisation of Radioactive Wastes in Glass. An Introduction to Nuclear Waste Immobilisation (pp. 319–368). https://doi.org/https://doi.org/10.1016/B978-0-08-102702-8.00019-4

TRANSCEND

Transformative Science and Engineering for Nuclear Decommissioning

Thank you

NNUF
National Nuclear User Facility

Sheffield Hallam University

NATIONAL NUCLEAR LABORATORY

NDA
Nuclear Decommissioning Authority

Special Thanks to
Richard March
Frances Burrell
Andy Cundy
Tony Bell
Alex Scrimshire

alex.h.stone@student.shu.ac.uk

Transformative Science and Engineering for Nuclear Decommissioning

Comparison of the patterns for DIC in an in-situ SCC experiment

Kuo Yuan, University of Bristol

Ronald Clark, National Nuclear Laboratory

Mahmoud Mostafavi, University of Bristol

Transcend Annual Meeting

2nd Nov 2022

Introduction

Aim: To develop a new small punch test (SPT) setup for spent AGR cladding with surrogate material (thermally sensitised 304 stainless steel) that can initiate SCC (stress corrosion cracking) of stainless steel in a short period time with DIC (Digital image correlation) observation.

In this presentation, two patterns for DIC will be compared for the special corrosive environment.

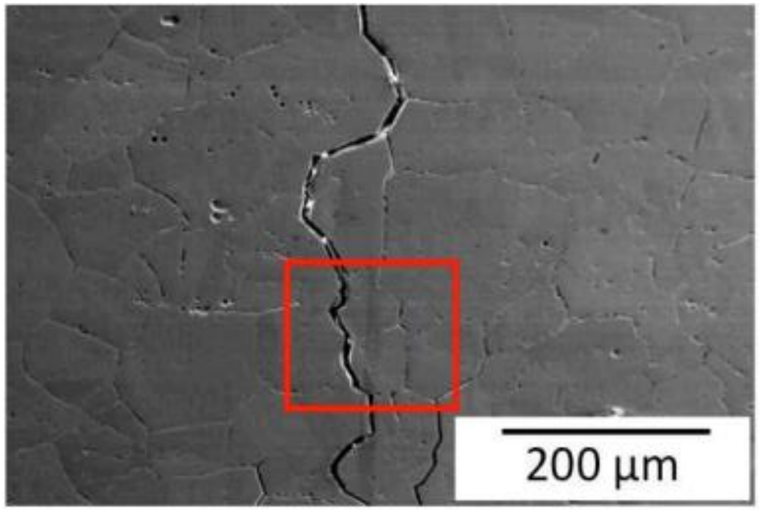

Fig. 1. SEM image of a stress corrosion crack; the crack initiation site is highlighted*

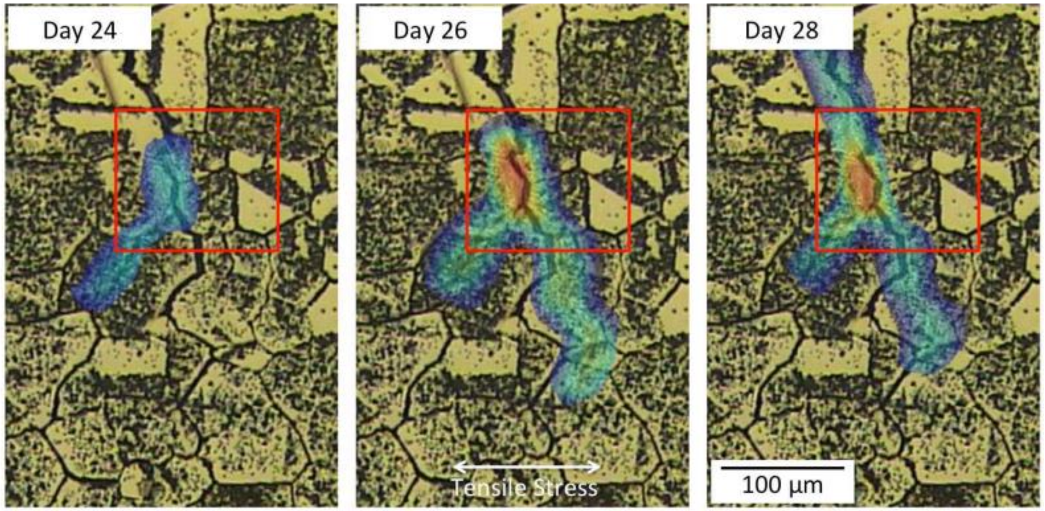

Fig. 2. DIC strain mapping of the development of a crack*

Background:

A SPT setup has been designed and built to allow the SPT held at a constant load while a loop of heated corrosive solution (1000 ppm sodium thiosulphate) is circulated around the sample for accelerating the initiation of SCC. A mirror is placed below the sample to allow DIC observation.

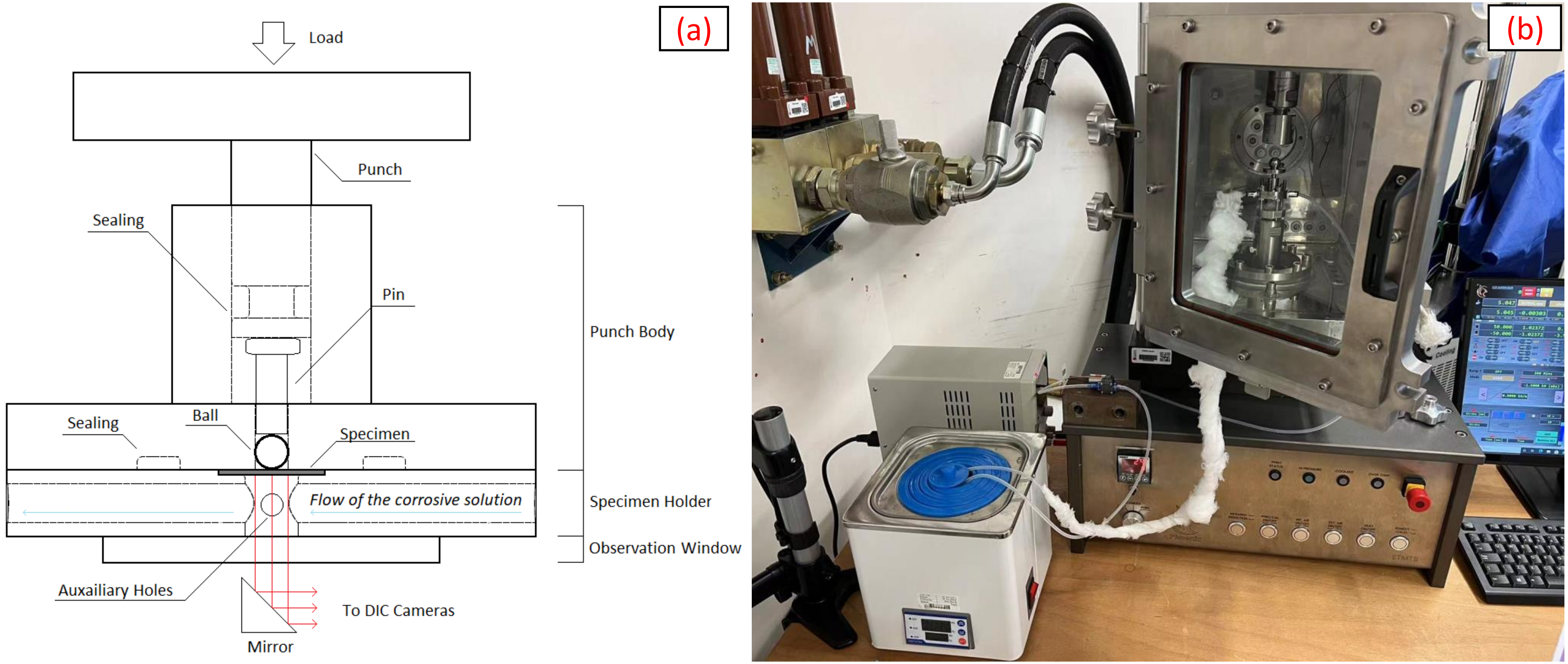

Fig. 3. (a) Schematic of the new SPT rig, (b) the loop system of the corrosion SPT

Background:

A trial test was conducted without DIC to prove that the new setup can successfully initiate SCC. 1000 ppm sodium thiosulphate solution heated at 60 °C was circulated in the loop, and a constant load of 1.5 kN was applied. After 113 hours, several SCCs were observed on the surface of the SPT sample.

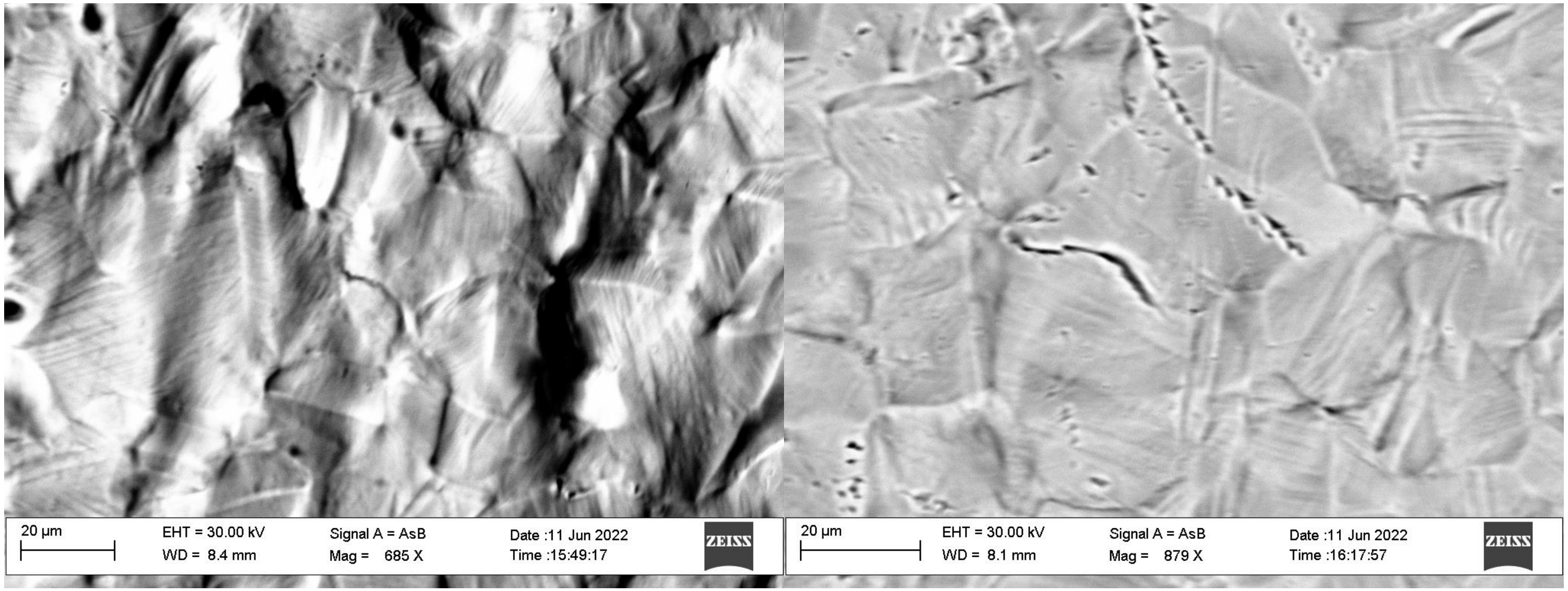

Fig. 4. Stress corrosion cracks observed on the small punch test sample

DIC

LaVision stereo micro DIC will be used for the experiments that allows observation from 2.4x to 30x with a field of view from 96 mm to 7.7 mm.

Two 5 MP cameras are attached to the microscope to capture images and a LED ring light is used to illuminate the observed aera.

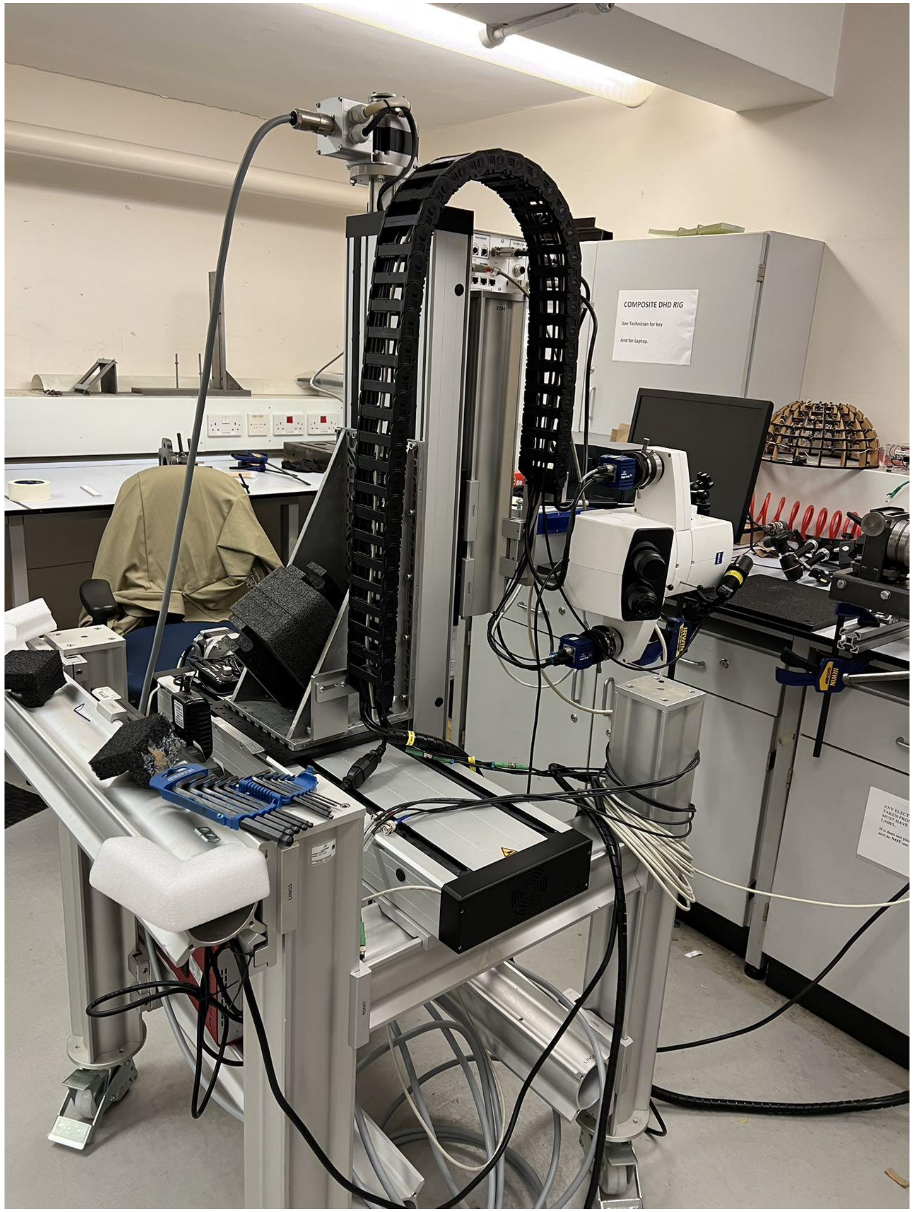

Fig. 5. LaVision stereo micro DIC

Pattern Preparation

Due to the corrosive environment, two patterns for DIC are compared:

Both the samples were electro polished in 92% acetic acid and 8% perchloric acid at 42v for 60s*to give a fine surface.

- Painted: black dots painted by an airbrush with high temperature primer
- Electro etched: in a 92% acetic acid and 8% perchloric acid solution at 13v for 20s*

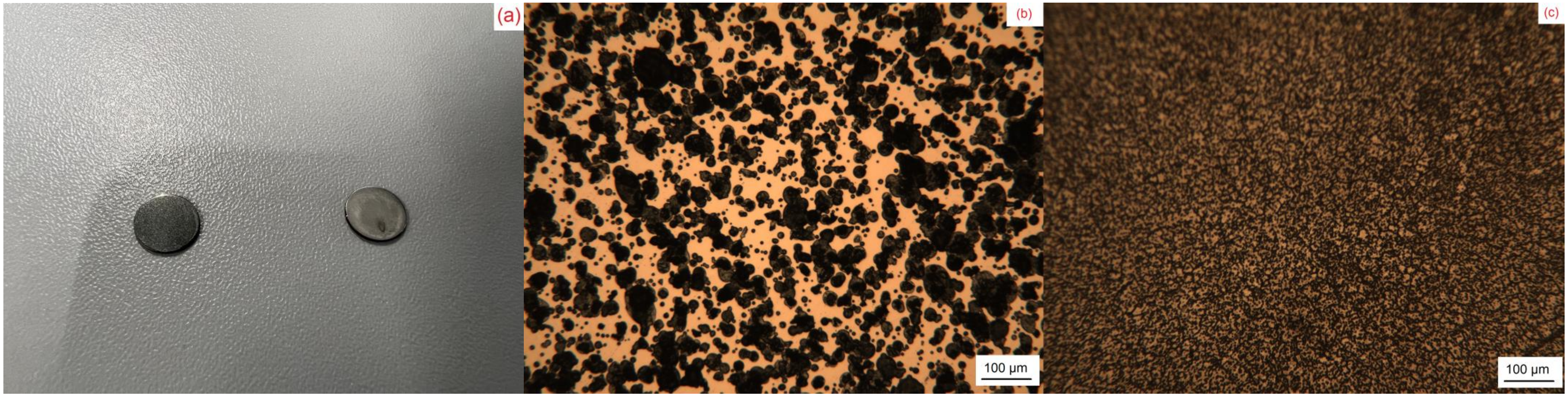

Fig. 6. (a) painted (left) and etched (right) SPT samples, (b) painted pattern, (c) etched pattern

Initial Correlation

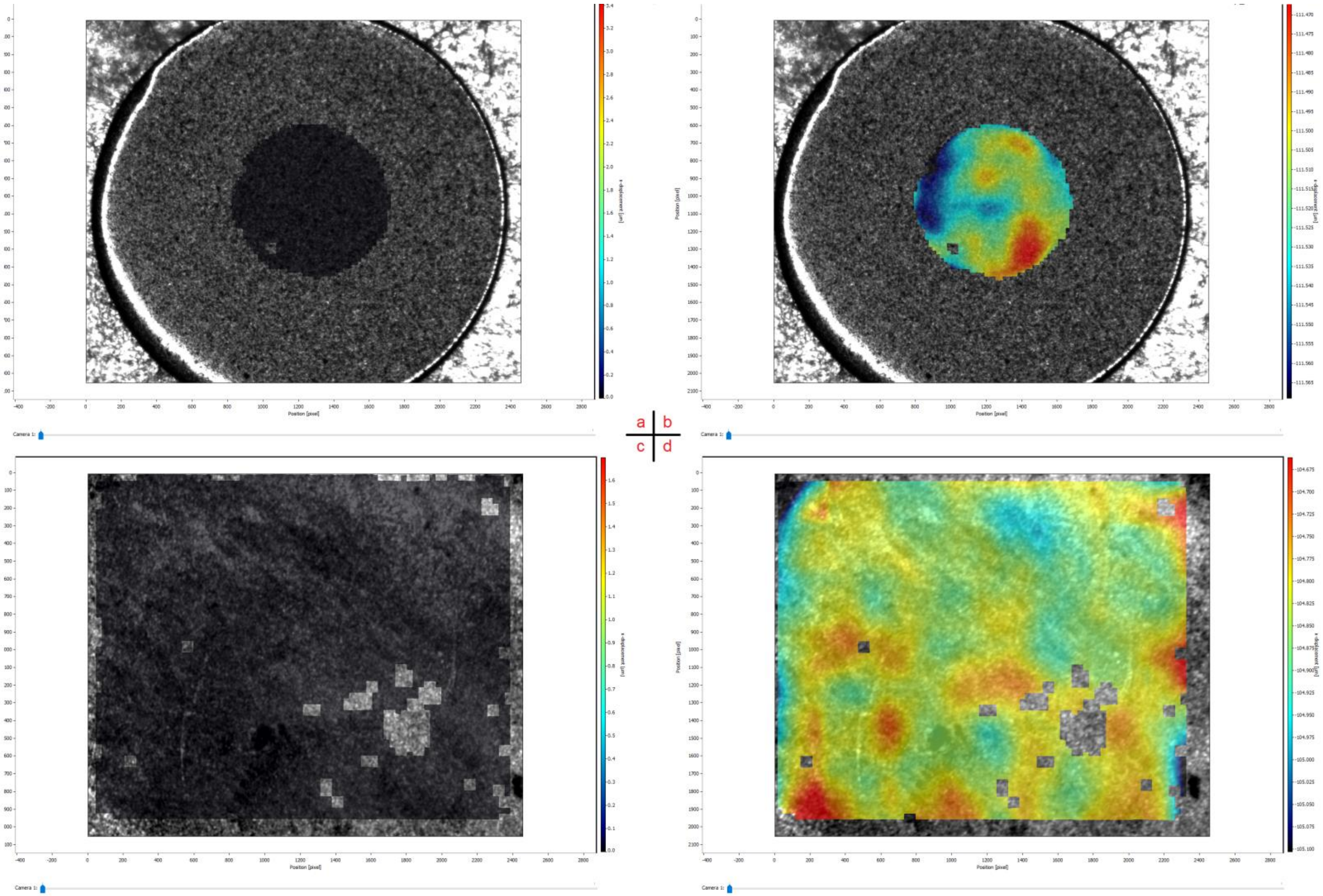

Fig. 7. DIC images of rigid body movement test of (a),(b) painted sample and (c), (d) etched sample

Rigid body movement tests to validate the correlation by moving the DIC camera 100µm horizontally.

Both samples were correlated, but the etched sample had more missing points and the higher error of 38.9 µs than that of the painted sample, which is only 9.168 µs.

Corrosion test

To test the durability of the patterns and the effect of the patterns on the corrosion process in a short period of time, two self-loading tensile rigs were used.

The tensile samples were prepared the same two ways and loaded in the rigs and immersed in the same corrosive environment for 105 hours.

Fig. 8. small tensile rig with etched tensile sample

Painted Sample Surface

After the corrosion tensile test, no cracking was observed on the painted sample. But the surface were heavily corroded by pitting near the paint spots.

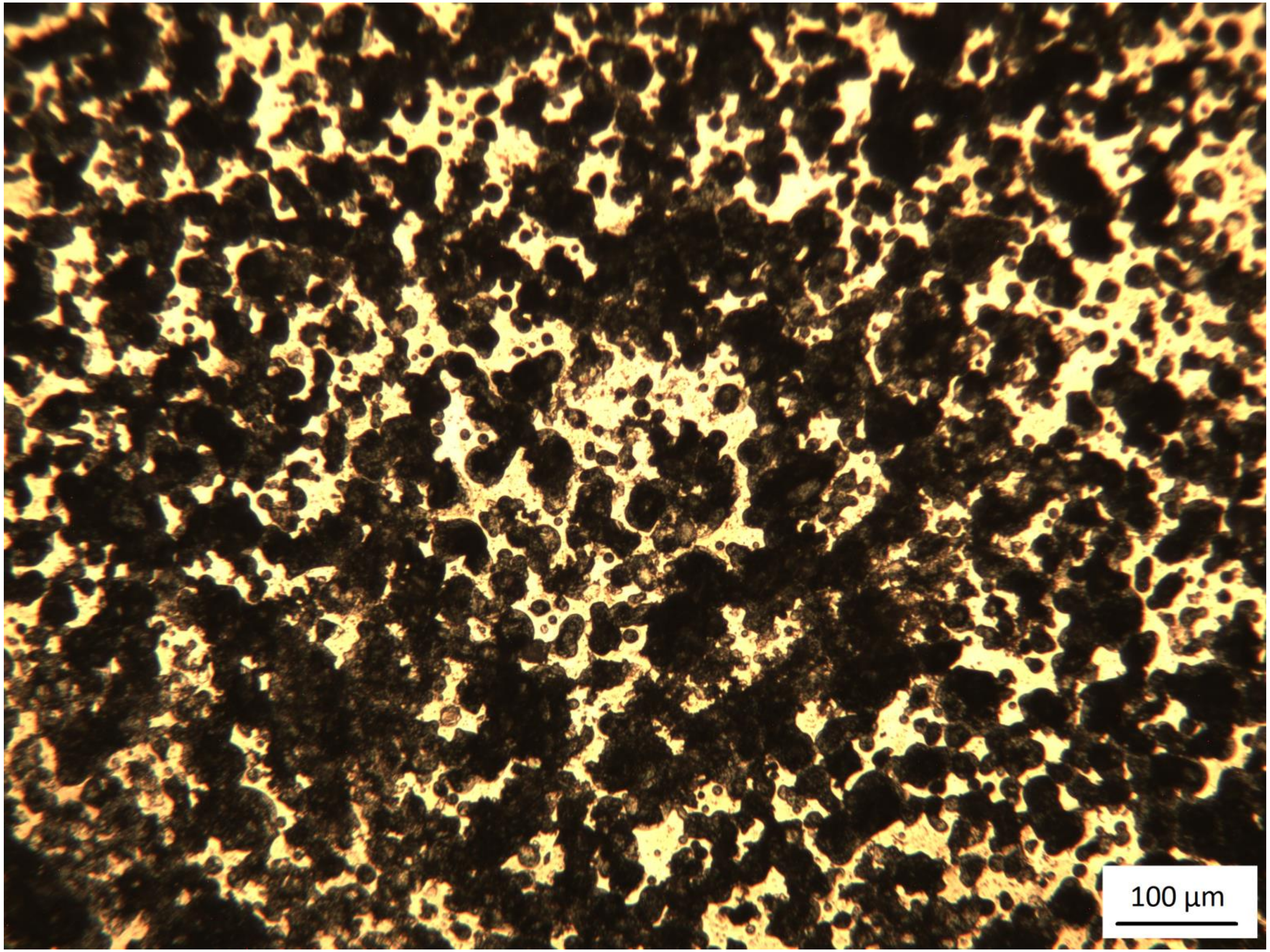

Fig. 9. surface of the painted tensile sample after the corrosion experiment

Etched Sample Surface

Although grain boundaries were more corroded, no intergranular SCC was observed. Overall, the pattern features remained intact.

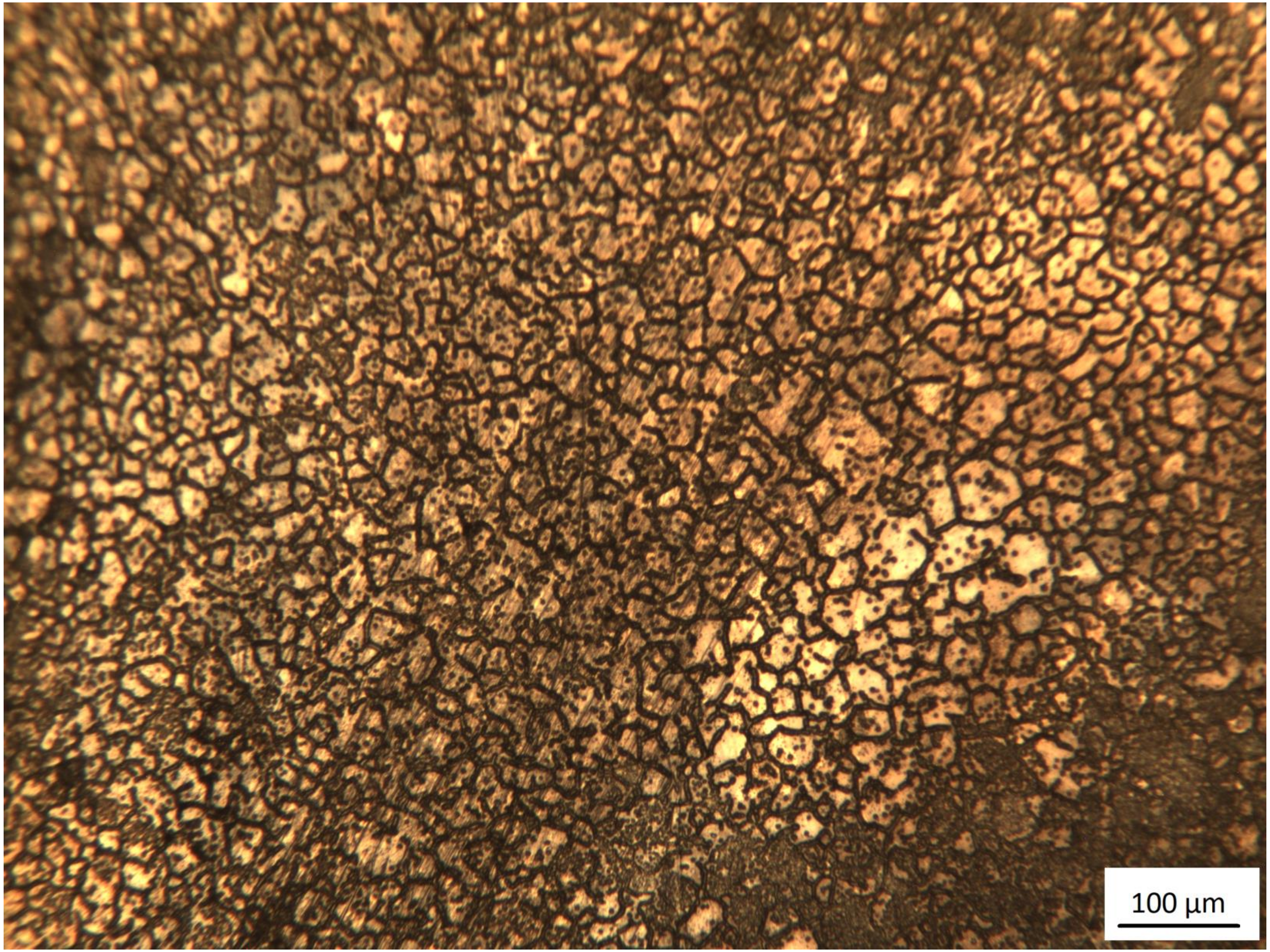

Fig. 10. surface of the etched tensile sample after the corrosion experiment

Correlation on Painted Sample

Although the surface was successfully correlated in DIC, many missing spots are showing due to the pits and the error had risen from 9 µs to 84 µs.

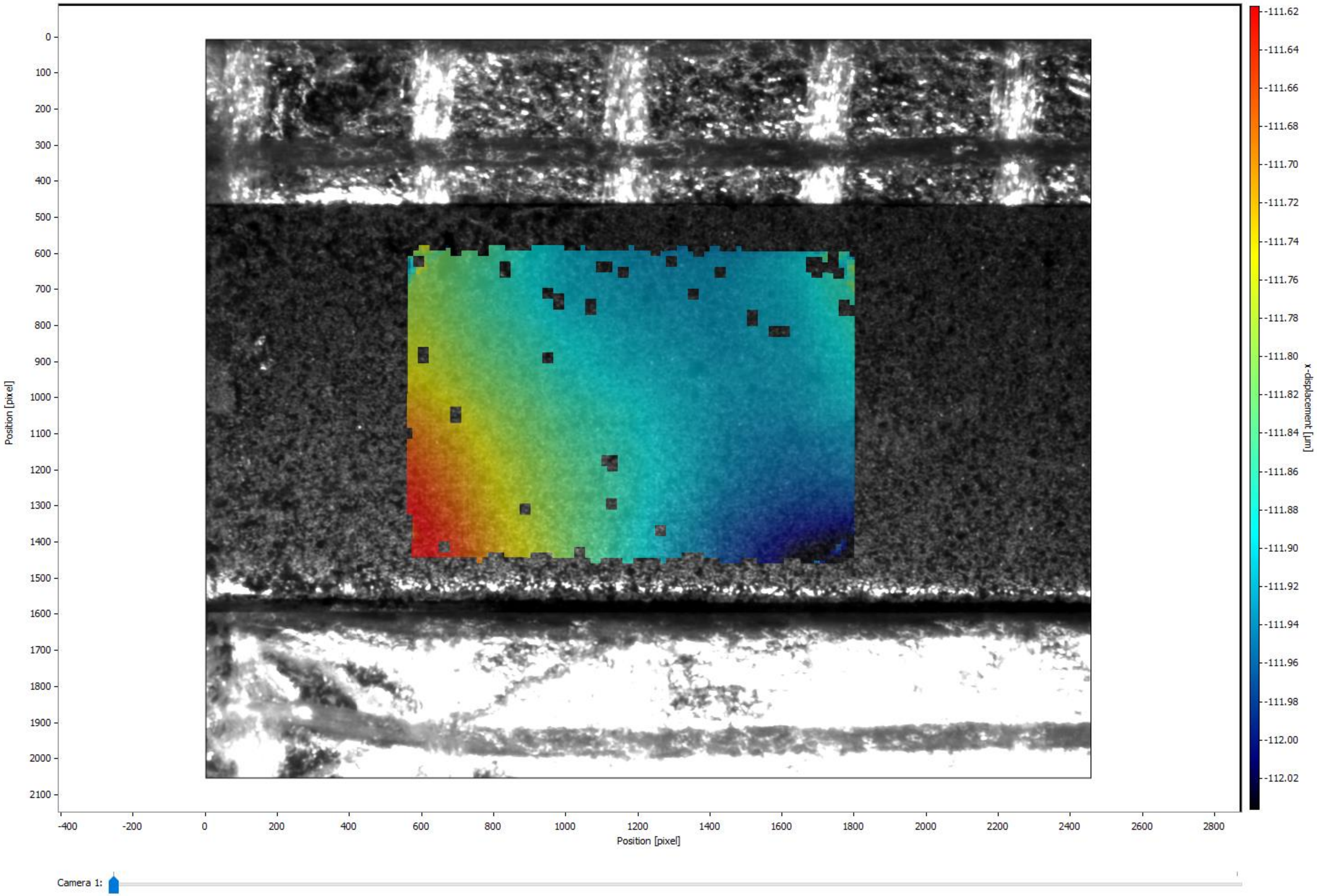

Fig. 11. DIC images of rigid body movement test of the painted sample

Correlation on Etched Sample

The surface was successfully correlated in DIC, and only few missing spots are showing on the images. However, the images are showing layered correlation. The error had risen from 39 µs to 85 µs.

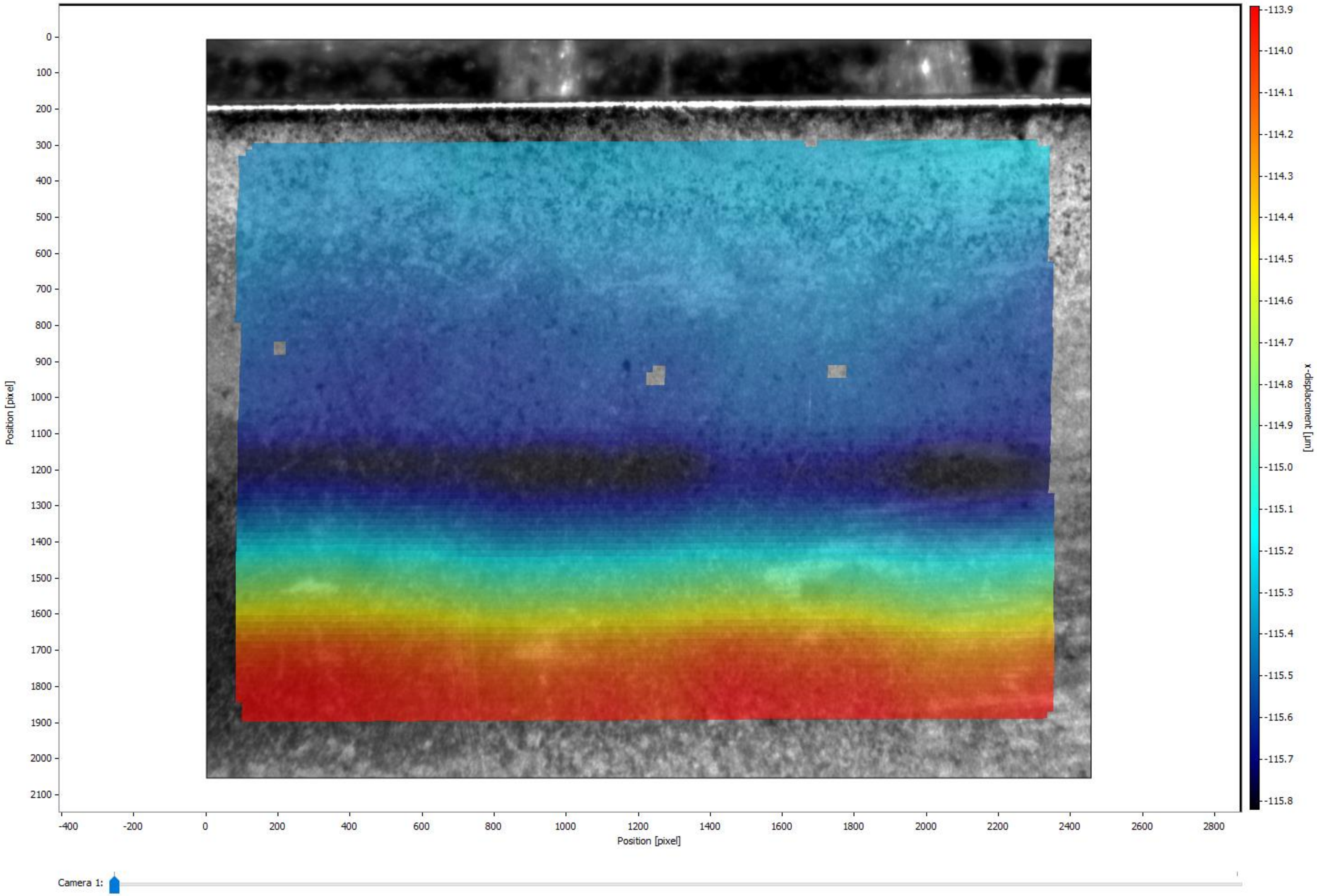

Fig. 12. DIC images of rigid body movement test of the etched sample

Conclusions and Plans

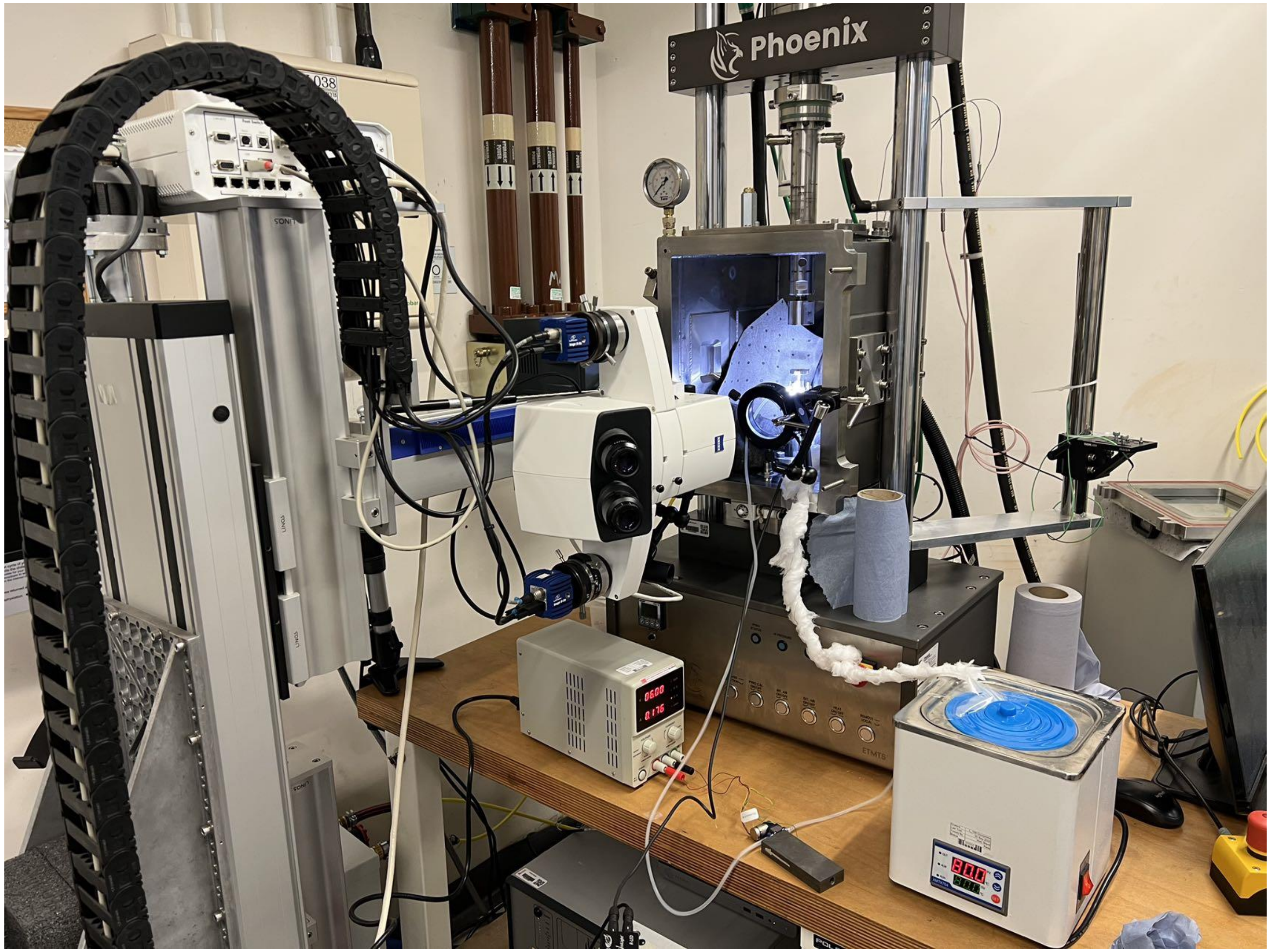

Fig. 13. Micro DIC setup on SPT

Two patterns for DIC in a corrosive environment have been compared: painting and etching.

Although, the painted surface had better correlation before corrosion, the surface was heavily corraded in the corrosive environment. Therefore, etching will be used as the preferred method for patterning in the DIC of SPT.

Similar correlation will be done in the SPT to see the effect of fluid on DIC.

TRANSCEND

Transformative Science and Engineering for Nuclear Decommissioning

Thank you

Reference:

*Stratulat, A., Duff, J., Marrow, J. (2014), Grain boundary structure and intergranular stress corrosion crack initiation in high temperature water of a thermally sensitised austenitic stainless steel, observed in situ, *Corrosion Science*, 85, 428-435

k.yuan@bristol.ac.uk

University of BRISTOL

NATIONAL NUCLEAR LABORATORY